

Dissertation  
submitted to the  
Combined Faculty of Natural Sciences and Mathematics  
of the Ruperto Carola University Heidelberg, Germany  
for the degree of  
Doctor of Natural Sciences

Presented by  
M. Sc. Anja Lena Herrmann  
born in: Rothenburg o.d.T.  
Oral examination: 24 November 2021



# **Anti-Tumorigenic Effects of the Iron Chelator Ciclopirox in HPV-Positive Cancer Cells**

Referees: Prof. Dr. Britta Brügger  
Prof. Dr. Felix Hoppe-Seyler



## Table of Contents

<b>Table of Contents</b>	<b>I</b>
<b>Summary</b>	<b>V</b>
<b>Zusammenfassung</b>	<b>VII</b>
<b>Acknowledgements</b>	<b>IX</b>
<b>Publications and Presentations</b>	<b>XI</b>
<b>1. Introduction</b>	<b>3</b>
1.1 Human papillomaviruses	3
1.1.1 The biology of HPV	3
1.1.2 HPV and cancer	5
1.1.3 Prevention and therapy of HPV-induced cancers	7
1.2 Iron	8
1.2.1 Iron metabolism	9
1.2.2 Iron and cancer	11
1.2.3 Iron chelators as potential chemotherapeutics	12
1.2.4 The iron chelator ciclopirox	14
1.3 Notch signaling pathway	15
1.4 Senescence and apoptosis	16
1.4.1 Senescence	17
1.4.2 Apoptosis	18
1.5 Cellular energy metabolism	19
1.5.1 Glycolysis	20
1.5.2 Oxidative phosphorylation	21
1.5.3 Metformin and other metabolic cancer drugs	22
1.6 Research objectives	25
<b>2. Results</b>	<b>29</b>
2.1 Proteome analyses of CPX-treated cells	29
2.2 CPX regulates cellular energy metabolism	31
2.2.1 Increased glucose levels partially revert anti-tumorigenic effects of CPX	33
2.2.2 Effect of glycolysis inhibition on the glucose-mediated apoptosis protection	38
2.3 Insights into senescence and apoptosis induction by CPX	39
2.3.1 CPX-induced senescence is irreversible	39
2.3.2 CPX-dependent regulation of factors involved in senescence and apoptosis	42

2.3.3	Comparison of CPX with other OXPHOS inhibitors	46
2.3.4	Comparison of CPX with other iron chelators	49
2.4	CPX regulates Notch signaling	51
2.5	Influence of HPV-status and tumor-status on CPX efficacy	54
2.5.1	Effect of CPX in HPV-positive vs. HPV-negative cell lines	54
2.5.2	Effect of CPX in keratinocytes vs. keratinocytes expressing E6/E7	55
2.5.3	Effect of CPX in primary cells	57
2.6	Combination therapies with CPX	58
2.6.1	CPX synergizes with radiation	58
2.6.2	CPX cooperates with cisplatin	59
2.6.3	CPX synergizes with glycolysis inhibitors	60
<b>3.</b>	<b>Discussion</b>	<b>65</b>
3.1	Mechanistic insights into the anti-tumorigenic effects of CPX	65
3.2	Glucose dependence of CPX	68
3.3	Induction of senescence and apoptosis by CPX	71
3.4	Tumor specificity of CPX	77
3.5	CPX in combination therapies	79
3.6	Clinical aspects	81
3.7	Conclusions	83
<b>4.</b>	<b>Materials and Methods</b>	<b>87</b>
4.1	Reagents and materials	87
4.2	Cell-based methods and assays	87
4.2.1	Cultivation of cells	87
4.2.2	Cryopreservation of cells	88
4.2.3	Generation of mCherry and mKate2 expressing cell lines	88
4.2.4	3-Dimensional cell culture	89
4.2.5	Transfection of synthetic siRNAs	89
4.2.6	Treatment of cells with chemotherapeutics	90
4.2.7	Irradiation of cells	91
4.2.8	Live-cell imaging	91
4.2.9	TUNEL assay	92
4.2.10	Senescence assay	93
4.2.11	Colony formation assay	93
4.2.12	Clonogenic assay	93
4.2.13	Glucose measurements	94
4.3	Protein-based methods	94

4.3.1	Harvest of cells and protein extraction	94
4.3.2	SDS-PAGE and western blot	95
4.3.3	Immunodetection of Proteins	96
4.3.4	Proteome analysis via TMT-MS	97
4.4	RNA-based methods	98
4.4.1	RNA isolation	98
4.4.2	Reverse transcription	98
4.4.3	Quantitative real-time PCR	98
4.5	Combination Index (CI) analyses	99
4.6	Statistical analyses	99
<b>Appendix</b>		<b>103</b>
	Supplemental data	103
	List of figures	104
	List of tables	105
	Abbreviations	106
	Units and prefixes	109
	References	110



## Summary

Oncogenic human papillomaviruses (HPVs) account for 5% of the total cancer incidence, being causal agents of cervical, other anogenital and oropharyngeal cancers. Innovative treatment options for HPV-induced cancers are thus urgently required. Metabolic alterations constitute one of the hallmarks of cancer, suggesting metabolic modulators such as iron chelators as a promising strategy for cancer therapy. In line with this, the iron chelating antifungal drug ciclopirox (CPX) showed promising anti-tumorigenic effects in numerous preclinical tumor models, including cervical cancer cells. In HPV-positive tumor cells, CPX suppresses expression of the viral *E6/E7* oncogenes and induces senescence or apoptosis. This thesis aimed to delineate the mechanisms underlying these anti-tumorigenic effects in cervical cancer cells and more specifically to gain insights into the determinants governing the switch from senescence to apoptosis.

By analyzing data from a comprehensive proteome screen of CPX-treated HPV16-positive tumor cells potential pathways involved in its anti-tumorigenic capacity were identified, including the induction of tumor-suppressive Notch signaling and deregulation of the cellular energy metabolism. The latter effect could be corroborated by demonstrating that CPX represses factors involved in oxidative phosphorylation (OXPHOS), accompanied by an upregulation of glycolysis related proteins. Consequently, the anti-tumorigenic effects of CPX were strongly glucose-dependent in that limited glucose availability facilitated the induction of apoptosis, while increased glucose supply prevented CPX-mediated cell death – a regulation shared by established OXPHOS inhibitors such as the anti-diabetic drug metformin. Instead, under glucose-replete conditions CPX-treated cells underwent senescence, which was not observed for metformin and other OXPHOS inhibitors, but for other iron chelators. Moreover, it was shown that viral *E6/E7* repression by CPX, metformin and other OXPHOS inhibitors is prevented by increasing glucose supply, indicating a vulnerability of HPV-oncogene expression to energy depletion. Additionally, experiments in *E6/E7* expressing normal keratinocytes point towards a sensitizing role of the viral oncogenes towards CPX-treatment. Finally, it was demonstrated that CPX synergistically enhances the growth-suppressing effects of radiotherapy, cisplatin and glycolysis inhibitors in HPV-positive cancer cells.

Collectively, the present study reveals a profound glucose-dependence of the anti-tumorigenic effects exerted by CPX and links its capacity to induce senescence or apoptosis to its dual role as an iron chelator and OXPHOS inhibitor, respectively. These results provide novel insights into the regulation of critical tumor-suppressive pathways in cervical cancer cells, illuminate the anti-proliferative activities of CPX and may facilitate the development of rational combination therapies comprised of CPX and glycolytic inhibitors to induce metabolic synthetic lethality in HPV-positive tumor cells.



## Zusammenfassung

Onkogene humane Papillomviren (HPVs) sind verantwortlich für 5% der Krebsinzidenz und verursachen neben Gebärmutterhalskrebs weitere Karzinome im Anogenitalbereich sowie im Oropharynx. Innovative Behandlungsmöglichkeiten für HPV-positive Tumore werden dringend benötigt. Da Veränderungen des Zellstoffwechsels eines der zentralen Merkmale von Krebszellen darstellen, könnten metabolische Modulatoren rationale Behandlungsmöglichkeiten bieten. So weisen zahlreiche präklinische Untersuchungen auf das therapeutische Potential des Eisenchelators Ciclopirox (CPX) in verschiedenen Tumormodellen hin, unter anderem auch in Zervixkarzinomzellen. In HPV-positiven Tumorzellen unterdrückt CPX die Expression der viralen *E6*- und *E7*-Onkogene und induziert Seneszenz oder Apoptose. Das Ziel der vorliegenden Arbeit war es, die dieser Regulation zugrundeliegenden Mechanismen aufzuklären und Erkenntnisse zu den Faktoren zu erlangen, welche die Entscheidung von Zervixkarzinomzellen zwischen Seneszenz und Apoptose bestimmen.

Die Analyse von Proteomdaten CPX-behandelter HPV16-positiver Tumorzellen ermöglichte es, zelluläre Prozesse zu identifizieren, welche eine Rolle für die Wachstumshemmung durch CPX spielen könnten. Unter anderem wurde gezeigt, dass CPX den Tumorsuppressor Notch aktiviert und den zellulären Energiestoffwechsel dereguliert. Letzteres äußerte sich unter anderem in der Hemmung von Faktoren, welche in der oxidativen Phosphorylierung (OXPHOS) involviert sind, bei gleichzeitiger Induktion von glykolytischen Faktoren. Entsprechend zeigte sich, dass der Effekt von CPX stark glukoseabhängig ist – niedrige Glukosekonzentrationen begünstigten die Induktion von Apoptose, während hohe Glukosekonzentrationen den Zelltod verhinderten. Stattdessen resultierte eine Behandlung mit CPX unter höherem Glukoseangebot in der Induktion von Seneszenz. Andere OXPHOS-Inhibitoren, z.B. das Antidiabetikum Metformin, führten ebenfalls zu einem glukoseabhängigen Zelltod, konnten jedoch keine Seneszenz auslösen. Hingegen induzierten andere Eisenchelatoren – wie CPX – Seneszenz und bei Glukosemangel Apoptose. Auch die Repression der viralen *E6/E7*-Onkogene durch CPX, Metformin oder andere OXPHOS-Inhibitoren wurde durch eine gesteigerte Glukosekonzentration verhindert, was auf eine Abhängigkeit der HPV-Onkogene vom zellulären Energiestatus hindeutet. Zusätzlich weisen Experimente in *E6/E7*-exprimierenden immortalisierten Keratinozyten darauf hin, dass die HPV-Onkogene Zellen für eine CPX-Behandlung sensibilisieren. Schließlich wurde in Kombinationsbehandlungen gezeigt, dass CPX die wachstumshemmenden Effekte von Radiotherapie, Cisplatin und Glykolyse-Inhibitoren synergistisch verstärkt.

Zusammenfassend deckt die präsentierte Arbeit eine starke Glukoseabhängigkeit der anti-tumorigenen Effekte von CPX auf und führt die Induktion von Apoptose oder Seneszenz auf die Bifunktionalität von CPX als OXPHOS-Inhibitor und Eisenchelator zurück. Diese Ergebnisse geben

Einblicke in die Regulation wichtiger tumorsuppressiver Signalwege in Zervixkarzinomzellen, beleuchten die wachstumshemmenden Effekte von CPX und könnten als Basis für die Entwicklung rationaler Kombinationstherapien von CPX mit Glykolyse-Inhibitoren dienen, welche in HPV-positiven Tumorzellen synthetisch letal wirken.

## Acknowledgements

In first place I want to thank Prof. Dr. Felix Hoppe-Seyler for giving me the opportunity to join his group and conduct my dissertation in his lab. Thank you for your constant support and guidance, for providing novel ideas and for being more optimistic than me at times. Likewise I want to thank Prof. Dr. Karin Hoppe-Seyler for her support, for the help on all experimental problems and for always adding a fresh view on my topic.

Further, I want to express my gratitude to Prof. Dr. Britta Brügger for evaluating my thesis as a first referee and being a valuable member of my TAC meetings. Likewise I want to thank Dr. Marco Binder for joining my thesis committee and for his helpful comments in my TAC meetings. I also want to acknowledge Prof. Dr. Peter Angel for being a member of my thesis committee.

Furthermore, I want to thank everyone who scientifically contributed to this thesis. I am grateful to Bianca Kuhn and Prof. Dr. Jeroen Krijgsveld for the collaboration on performing mass spectrometry analyses and help on interpreting the results. I also wish to thank Dr. Damir Kronic from the DKFZ light microscopy core facility for saving me a lot of work with his ImageJ Macros. Further, I am grateful to Barbara Leuchs for the collaboration on glucose measurements and to Dr. Ruwen Yang from the group of Prof. Dr. Frank Rösl for providing us her NOK cell lines.

A very special thanks goes to our 'iron lady' Julia Braun, who let me join and later gave over to me the ciclopirox project. Likewise I am grateful to Tobias Strobel who I had the pleasure to supervise for his master thesis and who at least partly continues the CPX legacy. I very much appreciate the help and technical expertise of Angela Holzer, Claudia Lohrey and Julia Bulkescher, thank you for your patience answering countless questions and for the experimental help especially towards the end of my thesis. A huge "thank you" goes to all past and present members of F065, namely Svenja Adrian, Felicitas Bossler, Julia Braun, Julia Bulkescher, Antonia Däschle, Kristin Frensemeier, Nora Heber, Angela Holzer, Bianca Kuhn, Claudia Lohrey, Julia Mändl, Katharina Siebenkäs, Tobias Strobel, Maria Weber and Dongyun Yang. Every one of you contributed to the warm and colloquial atmosphere in the group, which I appreciated a lot. Thanks for all the good times we had in and outside the lab. I also am grateful to Thomas Holz not only for his patience and help in all IT matters, but also for interesting discussions and conversations in our coffee breaks.

I further wish to thank my friends for sharing with me all ups and downs of (PhD) life. Importantly, I want to thank my family, especially my parents – thank you for your love and support at all times. Last but not least I am deeply grateful to Gabriel for celebrating the good times with me and making the bad times easier – thanks for your support and understanding!



## Publications and Presentations

### Publications

Hoppe-Seyler K, Bossler F, Braun JA, **Herrmann AL**, Hoppe-Seyler F. The HPV E6/E7 Oncogenes: Key Factors for Viral Carcinogenesis and Therapeutic Targets. (Review). *Trends Microbiol.* (IF 2020: 17.1); 2018; 26(2):158-168.

Braun JA, **Herrmann AL**, Blase JI, Frensemeier K, Bulkescher J, Scheffner M, Galy B, Hoppe-Seyler K, Hoppe-Seyler F. Effects of the Antifungal Agent Ciclopirox in HPV-Positive Cancer Cells: Repression of Viral E6/E7 Oncogene Expression and Induction of Senescence and Apoptosis. *Int J Cancer.* (IF 2020: 7.4); 2020; 146(2):461-474.

Hoppe-Seyler K\*, **Herrmann AL\***, Däschle A, Kuhn BJ, Strobel TD, Lohrey C, Bulkescher J, Krijgsveld J, Hoppe-Seyler, F. Treatment of HPV-Positive Cancer Cells with Metformin Blocks Viral E6/E7 Oncogene Expression but Enables Evasion from Cellular Senescence. *Int J Cancer.* (IF 2020: 7.4); 2021; 149: 1137– 1149. (\* joint first authors)

**Herrmann AL**, Kuhn BJ, Holzer A, Krijgsveld J, Hoppe-Seyler K, Hoppe-Seyler F. Delineating the Switch Between Senescence and Apoptosis in Cervical Cancer Cells Under Ciclopirox Treatment. Manuscript under review.

### Patent application

Hoppe-Seyler F., Hoppe-Seyler K, Strobel TD, **Herrmann AL**. Treatment of STAT3 related diseases by iron chelators, International Patent, Publication Number WO 2021/078937 A1. 2021.

### Presentations

**Herrmann AL**, Braun JA, Kuhn BJ, Krijgsveld J, Hoppe-Seyler K, Hoppe-Seyler F. Anti-Tumorigenic Effects of the Iron Chelator Ciclopirox in HPV-Positive Cancer Cells. 14<sup>th</sup> Charles Rodolphe Brupbacher Symposium, 30.01. – 01.02.2019, Zurich, Switzerland. Poster Presentation.

**Herrmann AL**, Braun JA, Kuhn BJ, Krijgsveld J, Hoppe-Seyler K, Hoppe-Seyler F. Anti-Tumorigenic Effects of the Iron Chelator Ciclopirox in HPV-Positive Cancer Cells. 1<sup>st</sup> German Cancer Research Congress. 04. – 05.02.2019, Heidelberg, Germany. Poster Presentation.

**Herrmann AL**, Braun JA, Hoppe-Seyler K, Hoppe-Seyler F. Ironing out HPV – Anti-Tumorigenic Effects of Iron Chelation in HPV-Positive Cancer Cells. Retreat of the DKFZ Research Program Infection, Inflammation and Cancer. 25.–27.03.2019, Schöntal, Germany. Oral presentation.

**Herrmann AL**, Braun JA, Kuhn BJ, Krijgsveld J, Hoppe-Seyler K, Hoppe-Seyler F. Anti-Tumorigenic Effects of the Iron Chelator Ciclopirox in HPV-Positive Cancer Cells. Helmholtz International Graduate School for Cancer Research PhD Poster Presentation. 20.11.2020, Heidelberg, Germany. Poster Presentation.



***CHAPTER 1***  
***INTRODUCTION***



## 1. Introduction

### 1.1 Human papillomaviruses

Cancer is one of the leading causes of death worldwide, with incidence and mortality starkly rising. In 2020, 19.3 million new cases were detected and almost 10 million deaths could be attributed to cancer.<sup>1</sup> Over the years numerous factors which can be associated with a higher risk for the development of tumors have been identified, making cancer to some extent a preventable disease. Next to lifestyle factors like obesity and the consumption of tobacco or alcohol, also environmental factors such as the exposure to ultraviolet or ionizing radiation or to chemical and biological carcinogens are important risk factors for cancer.<sup>2, 3</sup> Moreover, infectious agents are estimated to be responsible for around 15% of new cancer cases, with particularly high incidences in low and middle income countries.<sup>4</sup> The International Agency for Research on Cancer (IARC) classifies 11 pathogens as group 1 carcinogens, which either act directly carcinogenic or indirectly by inducing inflammation or enabling immune-suppression.<sup>5</sup> Four pathogens alone, namely hepatitis B and C, helicobacter pylori and human papillomavirus (HPV), account for 92% of the cancer cases related to infectious agents.<sup>6</sup>

#### 1.1.1 The biology of HPV

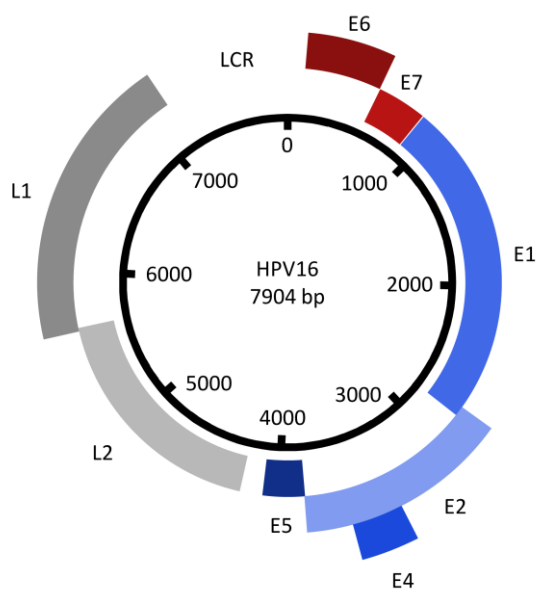


**Figure 1| Genome organization of HPV16.** E: early genes; L: late genes; LCR: long control region. Figure adopted from Herrmann, 2018.

HPVs are small non-enveloped DNA viruses with a circular double-stranded genome, which belong to the taxonomic family of *Papillomaviridae*. The HPV genome consists of approximately 8000 base pairs, which can be divided in an early (E), a late (L) and a long control region (LCR) (Figure 1). The presence of multiple promoters and alternative splicing sites allow expression of a relatively high number of proteins from this comparatively small genome. The early region consists of six open reading frames, encoding for the non-structural proteins E1, E2, E4, E5, E6 and E7, whose functions will shortly be described in the following. Early in the viral lifecycle the virus-specific DNA helicase E1

is recruited to the LCR of the viral episome by E2, enabling association with the cellular DNA polymerase and initiation of viral gene replication.<sup>7, 8</sup> E2 furthermore is a key transcriptional regulator of HPV and controls expression of the other viral genes.<sup>7</sup> Also the protein E5 which only is expressed in alpha-HPVs is important in the early infection phase. E5 promotes cell proliferation and is involved in immune evasion and can thus be regarded as a viral oncoprotein.<sup>9</sup>

However, in later phases of infection E5 is not essential anymore, thus the E5 ORF often is deleted in advanced cervical cancers.<sup>10</sup> In contrast, E4 plays a crucial role in the final stages of the HPV life cycle and is expressed in terminally differentiated keratinocytes, where it supports genome amplification and assembly and assists with virus escape from the epithelial surface.<sup>11</sup> E6 and E7, finally, are the major viral oncoproteins, which have transformative activity and induce cell immortalization.<sup>12</sup> Because of their outstanding importance they will be described in more detail below. The late region encodes for the structural major (L1) and minor (L2) viral capsid proteins, which are expressed at the final stages of infection. The LCR, finally, does not code for proteins but contains elements regulating genome transcription and replication.

HPVs like all papillomaviruses are characterized by a strict tropism for squamous epithelia, and thus exclusively infect keratinocytes of skin and mucosa.<sup>13</sup> In order to successfully complete replication, HPVs need to establish a long-term persistent infection, as their life-cycle is tightly coupled to the differentiation and migration of their host cells towards the epithelial surface (Figure 2). Initial infection generally requires (micro-)wounding of the epithelial tissue, which facilitates access of the virus to the basal lamina, where HPV can attach to heparin sulfate proteoglycans (HSPGs).<sup>14</sup> This interaction induces a conformational change of the capsid, allowing L2 cleavage by furin protease. The following internalization of HPVs is, in comparison to other viruses, an exceptionally slow process and the exact pathway is still not completely understood.<sup>15</sup> A reason why HPV exclusively infects cells in the basal layer might be that the viral DNA can enter the host cell nucleus only during mitosis.<sup>16</sup> Therefore productive infection requires cells actively progressing through the cell cycle, which is not the case in the upper, differentiated layers. In the beginning, viral copy numbers are rather low and only in later infection phases in the upper

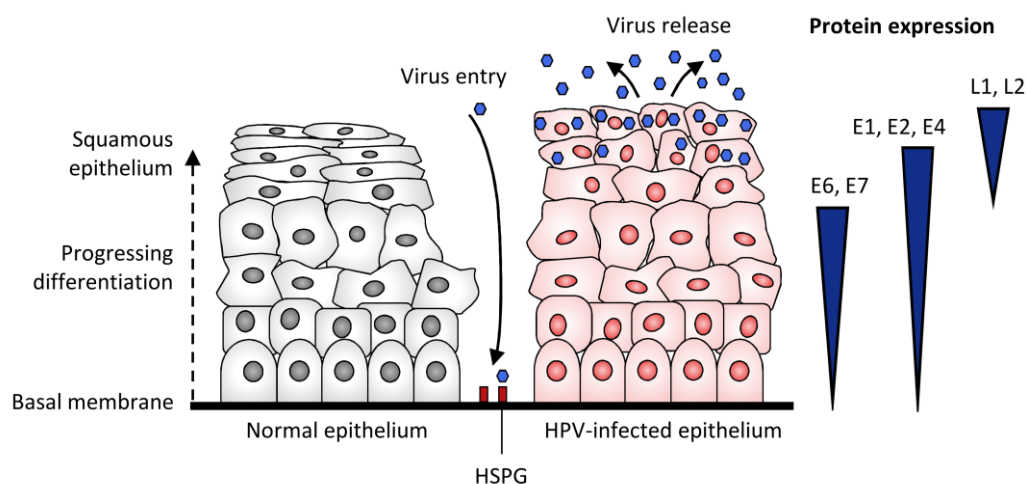


**Figure 2 | HPV life cycle.** HPVs access the basal lamina via microwounds in the epithelium. Upon HSPG attachment they are internalized and can establish a persistent infection. As the infected cells differentiate through the epithelium, first early and then late viral genes are activated. In the surface layer of the epithelium new virions are assembled and released. HSPG, heparin sulfate proteoglycan. Figure adapted from Herrmann, 2018.

epithelial layers viral DNA is replicated at high numbers. While infected epithelial cells differentiate and migrate upwards through the squamous epithelium, viral gene expression changes from expression of early to late genes. Finally, completing the viral life cycle, new virions are assembled and subsequently released in the upper layers of the epidermis or mucosa.

### 1.1.2 HPV and cancer

Infections with HPV can cause various epithelial diseases. While so-called low-risk HPVs mainly cause benign lesions like warts, HPV types classified as high-risk can facilitate the development of anogenital and oropharyngeal cancers. In total, around 4.5% of cancer cases worldwide can be attributed to HPV infection, which corresponded to 690,000 cases in 2018.<sup>4</sup> The causative role of HPV has been most extensively characterized for cervical cancers, which are almost exclusively caused by infections with high-risk HPVs.<sup>17</sup> With approximately 570,000 cases and 311,000 deaths in 2018, cervical cancer is the fourth most common cancer in women, with a disproportionately high incidence in middle to low income countries.<sup>18</sup> Next to cervical cancer, also a subset of other anogenital, as well as head and neck cancers are associated with HPV infection (Figure 3).<sup>4</sup> Out of the 15 types of HPV which have been classified as carcinogenic, HPV type 16 and 18 are responsible for 70% of cervical cancers.<sup>19</sup>

While the infection with high-risk HPVs is a prerequisite for the development of cervical cancer, it is not sufficient and only a minority of infected individuals will be diagnosed with cancer at some point. Instead, ca. 90% of HPV infections in the cervix are cleared by the immune system in the first months after infection.<sup>20</sup> If the infection persists over the course of 5-10 years, high-risk HPVs can induce the development of precancerous lesions called cervical intraepithelial neoplasias stage 1 to 3 (CIN1-3), which can finally progress to cancer. Interestingly, this often is accompanied by integration of the episomal viral DNA into the host genome which commonly results in loss of

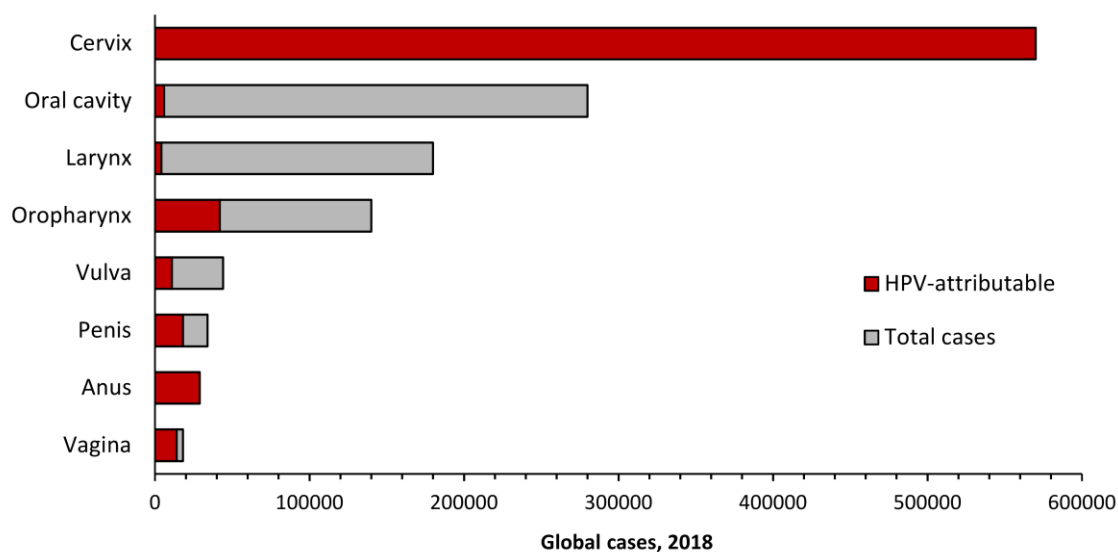
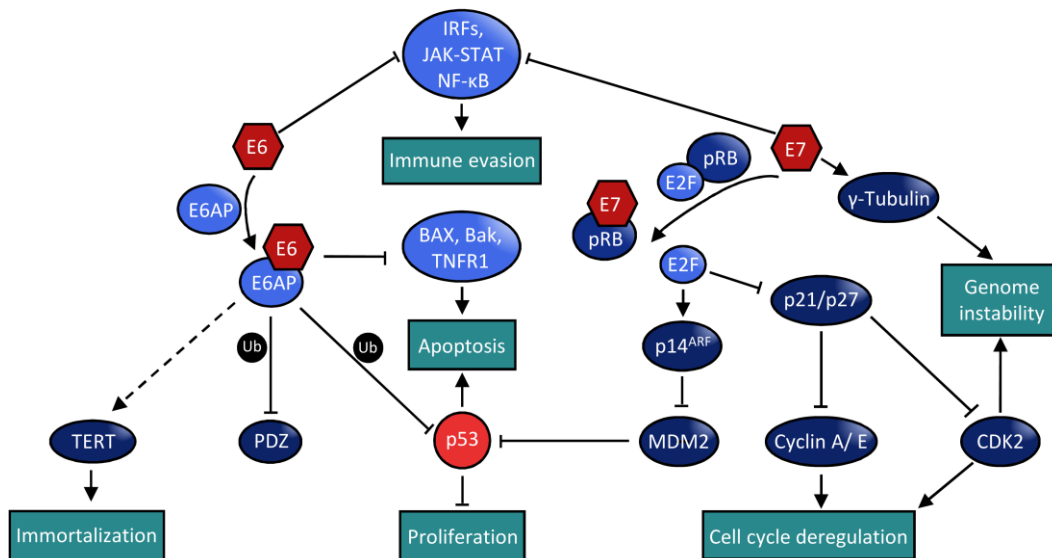


Figure 3 | Cancer cases attributable to HPV in 2018. Data from Globocan 2018.

E2 expression and a subsequent increase of E6/E7 expression.<sup>21</sup> The additional factors which determine if an infection will be cleared by the immune system or will progress into cancer are still not fully elucidated. Possible determinants in this context are the HPV type, the efficacy of cellular immune response and genome instability, which e.g. can be facilitated by E6 and E7.<sup>22</sup>

The HPV oncoproteins E6 and E7 are pivotal factors mediating the transformative activities of HPV and their persistent expression is required for maintaining the malignant phenotype of HPV-positive cancer cells.<sup>10, 23</sup> Both E6 and E7 are transcribed as polycistronic transcripts from a common promoter in the LCR. While the E6 and E7 oncoproteins do not exert any known enzymatic activity, they interact with and regulate a plethora of cellular proteins and processes (see Figure 4 for an incomplete overview). The small, ca. 185 amino acid long HPV E6 protein exerts most of its effects by inducing proteasomal degradation of cellular proteins through forming trimeric complexes with the cellular ubiquitin ligase E6-associated protein (E6-AP).<sup>24</sup> The most important E6 target for HPV-induced carcinogenesis is the tumor suppressor p53.<sup>25</sup> E6-mediated degradation of p53 enables the evasion of cellular checkpoints to ensure continuous cell proliferation and helps to block apoptosis. Furthermore, E6 oncoproteins from high-risk HPVs feature a PDZ-binding motif at their C-terminus, which facilitates binding to and degradation of numerous cellular PDZ-domain containing proteins.<sup>26</sup> Additionally, E6 was shown to inhibit apoptosis via p53-independent mechanisms by inducing degradation of pro-apoptotic proteins like Bax and Bak and inhibiting tumor necrosis factor receptor 1 (TNFR1).<sup>27-29</sup> Moreover, high-risk HPV E6 proteins activate expression of telomerase reverse transcriptase (TERT), which is essential for the immortalization of HPV-infected cells.<sup>30</sup>



**Figure 4 | Overview of cellular interaction partners of HPV E6 and E7.** The E6 and E7 oncoproteins interact with numerous cellular proteins and contribute to oncogenic transformation. Among others, they facilitate immortalization of the infected cell, contribute to immune evasion and inhibition of apoptosis, induce genomic instability and lead to cell cycle deregulation and enhanced proliferation.

HPV E7 is a small, approximately 100 amino acid long protein. Similar to E6, E7 can target numerous cellular substrate for proteasome-mediated degradation via a cullin-2 ubiquitin-ligase complex.<sup>31</sup> The most prominent targets of E7-mediated degradation are the pocket proteins pRb (Retinoblastoma protein), p107 and p130.<sup>32</sup> In healthy, non-infected cells pRb negatively regulates the cell cycle by complexing E2F transcription factors and thus inhibits transition to S-phase. In HPV-infected cells, in contrast, binding of E7 to pRb facilitates the release of E2F, which then promotes transcription of cyclin E, cyclin A and p16<sup>INK4A</sup> and consequently enables progression to S-phase, bypassing the G1/S transition checkpoint.<sup>33</sup> Furthermore, E7 inhibits cyclin-dependent kinase (CDK) inhibitors like p21<sup>Cip1/Waf1</sup> and p27<sup>Kip1</sup> and by binding to pocket proteins, disrupts the DREAM (dimerization partner, Rb-like, E2F and MuvB) complex, which further promotes cell cycle progression.<sup>34, 35</sup> Interestingly, E7 also causes an increase of p53 protein levels, which however is counteracted for by the action of E6, as described above.<sup>36</sup> As a further mechanism promoting carcinogenesis, both E6 and E7 have been reported to contribute to immune evasion. The viral oncoproteins interfere for example with activation of JAK-STAT signaling, reduce activity of NF-κB signaling, hinder induction of interferon regulatory factors (IRFs) and inhibit the cytosolic DNA sensor STING.<sup>37</sup> Moreover, E6 and E7 facilitate genomic instability via different mechanisms<sup>38, 39</sup> and both oncoproteins have been shown to induce chromosomal alterations<sup>40</sup>. Furthermore, E7 interacts with γ-tubulin, leading to centriole amplification.<sup>22, 41 22, 4122, 41</sup> The high genomic instability of HPV-infected cells might contribute to the acquisition of additional mutations, which can eventually lead to the development of cancer. Further processes influenced by E6/E7 include cell invasion, deregulation of cellular energetics, epigenetic regulation, angiogenesis and promotion of inflammation.<sup>42</sup>

Ablation of E6 expression by different means such RNAi or blocking peptides leads to efficient induction of apoptosis, while simultaneous suppression of E6 and E7 leads to rapid induction of senescence.<sup>23, 43-45</sup> This makes the viral *E6/E7* oncogenes promising targets for the therapeutic intervention in HPV-induced cancers. Attempts underwent in this direction so far include the use of small molecule inhibitors, RNA interference, inhibitory peptides or immunotherapeutic approaches.<sup>46</sup>

### **1.1.3 Prevention and therapy of HPV-induced cancers**

Prevention is better than cure – while cervical cancer in early stages is comparably well treatable, it is preferable to act in time and prevent either the progression of lesions to neoplasms (secondary prevention) or even better to prevent infection with high-risk HPVs upfront (primary prevention). A big advance in this respect has been made by establishing effective screening programs, which starkly reduced mortality by cervical cancer. For a long time the gold standard for screening was the Pap test (named after its inventor George Papanicolaou), which is now more

and more being replaced by or complemented with more sensitive and specific methods like liquid-based cytology and testing for HPV DNA/RNA.<sup>47</sup>

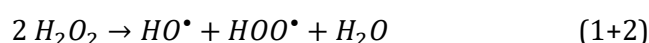
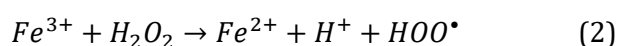
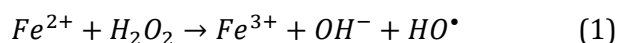
A further major step in the fight against cervical and other HPV-associated cancers was the development of effective vaccines targeting high-risk HPV types. Currently, three vaccines are commercially available, which all are based on virus-like particles (VLPs) and consist of inactivated, recombinant HPV capsid proteins. While Cervarix® (GlaxoSmithKline) only protects against the two most common high-risk HPV types 16 and 18, Gardasil® (MSD Vaccins) additionally offers protection against type 6 and 11, and the newest vaccine, Gardasil® 9 (MSD Vaccins) protects against nine types (6, 11, 16, 18, 31, 33, 45, 52 and 58). These prophylactic vaccines have proven extremely efficient at preventing infection with HPVs and development of pre-neoplastic lesions.<sup>48, 49</sup> Thus HPV vaccinations have become routine for pre-adolescents in many countries. In Germany the Robert Koch Institute (RKI) recommends the vaccination for 9-14 year old girls and since 2018 also for boys of the same age. While in countries with high vaccination rates, HPV incidence is decreasing, the vaccination coverage in less developed countries is still insufficient.<sup>50</sup> A further issue regarding these vaccines is that they only act in a prophylactic manner and are not effective against already persisting HPV-infections. Thus, intense research is ongoing on the development of therapeutic vaccines which target E6 and E7.<sup>51</sup>

Therapeutic options for cervical cancer depend mainly on the stage of disease. Precancerous lesions will usually be removed surgically, while in advanced stages radical hysterectomy will be complemented with adjuvant radiotherapy or concurrent chemo-radiotherapy.<sup>52</sup> The standard chemotherapy for treatment of cervical cancers are primarily platinum-based drugs like cisplatin, but can also include the nucleoside analog gemcitabine or further drugs like the angiogenesis inhibitor bevacizumab, the mitotic inhibitor paclitaxel or combinations thereof.<sup>53</sup> Moreover, also immunotherapeutic approaches showed promising results and the PD-1 (programmed cell death 1) inhibitor pembrolizumab has been approved by the FDA for use in advanced cervical carcinoma.<sup>54</sup>

### **1.2 Iron**

Iron is an essential micronutrient for almost all organisms, acting as crucial cofactor for a plethora of cellular processes. In most cases, iron exerts its functions being incorporated in hemes or in iron sulfur (Fe-S) clusters. The human body contains 2-4 g of iron, of which around 2.5 mg per day are required for the synthesis of hemoglobin to replenish erythrocytes.<sup>55, 56</sup> Other iron-dependent processes include DNA synthesis and repair, since certain DNA polymerases and helicases require iron for their enzymatic activity.<sup>57</sup> Furthermore, ribonucleotide reductase (RR), the enzyme catalyzing the conversion of ribonucleoside di- or triphosphates (rNDPs/rNTPs) into deoxyribonucleoside di- or triphosphates (dNDPs/dNTPs) requires iron to stabilize the catalytically

active tyrosyl radical.<sup>58</sup> Iron also is crucial for further processes including cellular respiration (see 1.5), epigenetic regulation or oxygen metabolism. In most of these processes iron functions as electron acceptor and donor in redox reactions, switching between its ferric ( $\text{Fe}^{3+}$ ) and ferrous ( $\text{Fe}^{2+}$ ) states. This transition metal property, however, also is the reason behind the toxic effects that iron can exert. Namely, iron salts catalyze the Fenton reaction<sup>59</sup>, which results in the production of reactive oxygen species (ROS) that can be toxic to the cell and are linked to carcinogenesis:



### 1.2.1 Iron metabolism

Since iron plays both essential and toxic roles in the organism, its levels have to be delicately balanced and thus are tightly regulated both on a systemic and cellular level. Systemically, iron levels are primarily controlled on the level of intestinal absorption via duodenal enterocytes and by mobilization of iron from storage tissues such as macrophages and the liver. Interestingly, there is no defined pathway for the excretion of iron. As iron is very efficiently recycled in the body e.g. via phagocytosis of erythrocytes, only 1-2 mg are excreted per day which have to be replenished by dietary iron.<sup>56</sup> If there is a systemic excess of iron it is mainly stored in the liver, bound to the iron storage protein ferritin. Systemic iron metabolism is mainly regulated by the small hepatic peptide hormone hepcidin (also known as Hamp1 or Leap1).<sup>60</sup> Hepcidin controls saturation of transferrin with iron by inducing degradation of the iron exporter ferroportin (FPN1), which leads to a decrease of iron release from storage tissues.<sup>61</sup> Hepcidin itself is regulated by a wide range of external and internal stimuli. While an increase in iron levels and inflammatory signals positively regulate hepcidin, increased erythropoietic demand and hypoxia reduce hepcidin levels.<sup>62</sup>

Also on cellular level, iron metabolism is a finely orchestrated process (see overview in Figure 5). In order to maintain circulating iron in a soluble form, it is bound to transferrin, a glycoprotein possessing two high-affinity binding sites for ferric iron. Diferric transferrin can form a complex with the transferrin receptor (TfR1, in specialized cells also TfR2), which is expressed on the plasma membrane of most cells.<sup>63</sup> This complex is then internalized via clathrin-dependent endocytosis and upon acidification of the endosome undergoes conformational changes which triggers the release of iron. In the endosome, ferric iron is reduced by metalloreductases of the six transmembrane epithelial antigen of prostate (STEAP) family and subsequently the divalent metal transporter 1 (DMT1) transports the ferrous iron into the cytosol, where it feeds into the labile

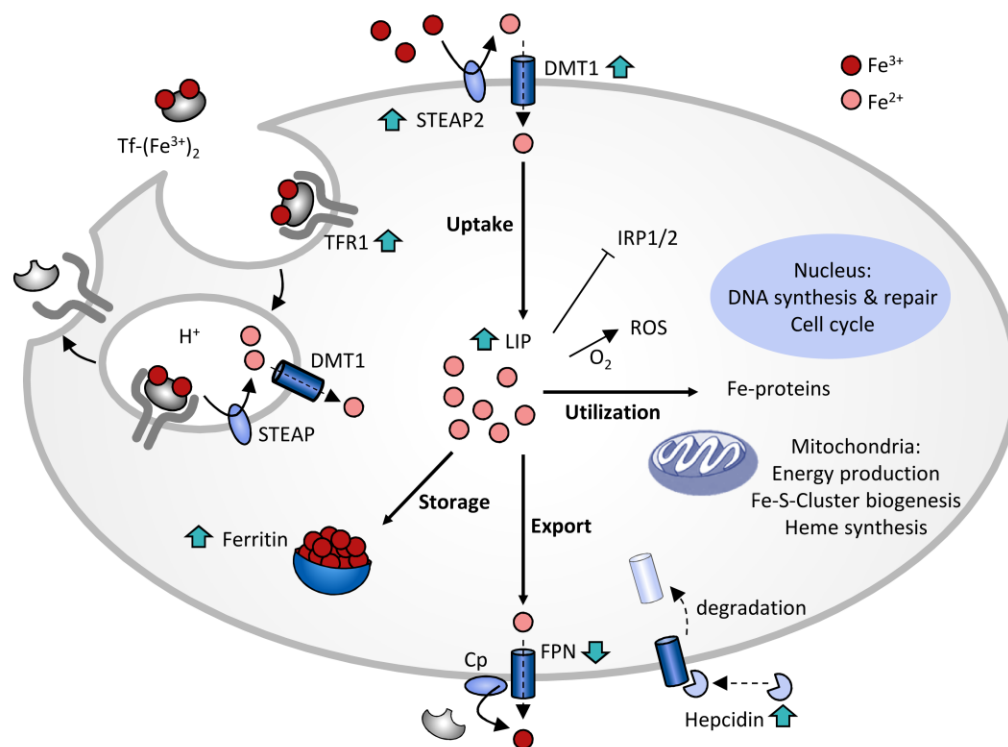


**Figure 5| Cellular iron metabolism.** Diferric transferrin binds to TfR, the complex is endocytosed and upon acidification of the endosome, ferric iron (dark red) is released. After reduction by STEAP, DMT1 transports the ferrous iron (light red) into the cytosol, where it feeds into the LIP. Iron can be directly utilized in cytosolic proteins, in the nucleus or in mitochondria. Excess iron is stored bound to ferritin or exported from the cells by FPN1. Iron levels are regulated by hepcidin, which induces FPN degradation via the IRE/IRP system. Cancer cells deregulate iron metabolism by changing expression of numerous proteins, as marked by turquoise arrows. Cp, ceruloplasmin; DMT1, divalent metal transporter 1; FPN, ferroportin; IRP1/2, iron regulatory protein 1/2; LIP, labile iron pool; ROS, reactive oxygen species; Tf, transferrin; TfR1, transferrin receptor 1; STEAP, six transmembrane epithelial antigen of the prostate protein. Figure adapted from Herrmann, 2018.

iron pool (LIP). Alternatively to this transferrin cycle, DMT1 can also take up non-transferrin bound iron<sup>64</sup> and further transferrin-independent pathways for iron uptake exist, which however are less well characterized. Within the cytosol, iron can be directly utilized and be incorporated into cytosolic iron-containing proteins or it can be transported to the mitochondria, which are a center of iron homeostasis where synthesis of heme and Fe-S clusters takes place.<sup>65, 66</sup> A fraction of the labile iron also is transported into the nucleus, where it is essential for e.g. DNA synthesis. Excess iron is stored bound to ferritin, an iron-storage protein composed of 24 light and heavy chain subunits, which can contain up to 4500 iron atoms.<sup>67, 68</sup> In case of iron overload or increased systemic demand, iron can be exported from the cell via the membrane transporter FPN1 and is subsequently oxidized by the ferroxidases ceruloplasmin (Cp) or hephaestin to ferric iron, which again can be loaded onto transferrin.<sup>69, 70</sup>

As mentioned earlier, FPN1 is inhibited by hepcidin to ensure systemic iron homeostasis. Cellular iron homeostasis in contrast, is mainly controlled via the IRE-IRP system. The iron regulatory proteins 1 and 2 (IRP1/2) are able to sense cellular iron levels and to regulate expression of proteins involved in iron metabolism (Figure 6).<sup>71</sup> When cellular iron levels are high, both IRP1

and 2 are inactive. The multifunctional protein IRP1 then binds a 4Fe-4S cubane cluster and acts as cytosolic aconitase, a citric acid cycle enzyme which catalyzes the isomerization of citrate to isocitrate.<sup>72</sup> IRP2 interacts with the iron sensing F-box protein FBXL5 and is proteolytically degraded by the SCF E3 complex, when iron levels are high.<sup>73</sup> In contrast, under iron deplete conditions, IRP1 and 2 are active and by binding to iron responsive elements (IREs) regulate the expression of iron-dependent proteins. IREs are highly conserved *cis*-regulatory hairpin structures, which can be found in the 3' or 5' UTR of mRNAs coding for iron-regulated proteins such as ferritin or TfR. When IRP1/2 bind to single IREs localized in the 5' UTR, translation initiation is inhibited and thus protein synthesis is blocked.<sup>74</sup> Such single 5' UTR IREs are for example present in the mRNAs encoding for ferritin, FPN1 or mitochondrial aconitase, which are not needed when iron levels are low.<sup>75</sup> In contrast, when IRPs bind to multiple IREs present in the 3' UTR, endonucleolytic cleavage and subsequent degradation of these mRNAs is prevented. Such 3' IREs can be found for example in *TfR* or *DMT1* mRNAs.<sup>76</sup> Thus, when iron levels are low, more TfR is expressed and more iron is imported, while storage in ferritin and export via FPN1 are reduced.

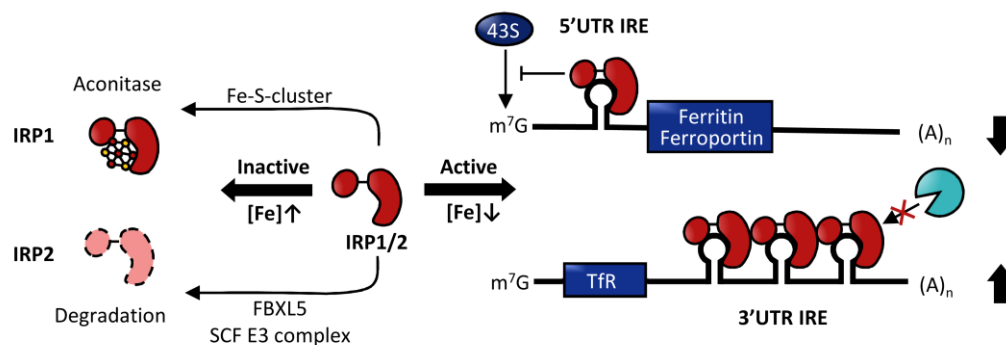


**Figure 6 | The regulatory IRE-IRP system.** In iron-replete cells, IRPs are inactive. IRP1 binds a cubane cluster and acts as aconitase, while IRP2 is degraded via the proteasome. Under iron deplete conditions, IRPs bind to IREs in the UTR of target gene mRNAs. Binding to 5' IREs blocks their translation, thus ferritin and ferroportin are downregulated. Binding to 3' IREs blocks degradation of the respective mRNAs, thus TfR is upregulated. Figure modified from Herrmann, 2018.

### 1.2.2 Iron and cancer

Epidemiological studies have provided clear evidence for a positive association between increased body iron levels and cancer.<sup>77,78</sup> Consistent with this, individuals living with hereditary hemochromatosis, a condition causing excessive iron overload, show an increased risk for hepatocellular and other carcinomas and also other iron overload disorders are associated with an increased cancer risk.<sup>79-81</sup> This carcinogenic effect of iron is likely mediated via direct and indirect mechanisms. On the one hand, non-transferrin bound iron can cause DNA damage indirectly due to the production of ROS via the Fenton reaction (see above).<sup>82</sup> Iron also can directly support cell proliferation through various routes. For example, ribonucleotide reductase, the enzyme catalyzing the rate-limiting step in DNA synthesis depends on iron for its catalytic

function and also cell cycle control and cellular energy generation are reliant on iron. Thus, it is not surprising that tumor cells have higher requirements for iron and deregulate several proteins to increase intracellular iron levels (see turquoise arrows in Figure 5). In order to enhance iron uptake, TfR is often overexpressed in cancers and could thus represent a potential target in cancer therapy.<sup>83, 84</sup> Also STEAP, DMT1 and lipocalin 2 (LCN2) are overexpressed in cancer cells, further stimulating iron uptake.<sup>85-88</sup> Additionally, tumor cells typically reduce iron storage via ferritin, which leads to an increase of intracellular available iron and stimulates proliferation.<sup>89</sup> Furthermore, cancer cells increase metabolically available iron by limiting iron efflux from the cell. To this end, levels of FPN1 are decreased either directly or via deregulation of hepcidin.<sup>90, 91</sup> Collectively, these cancer-associated alterations of the cellular iron metabolism lead to an increased intracellular iron availability, which allows tumor cells to maintain accelerated proliferation rates.

### 1.2.3 Iron chelators as potential chemotherapeutics

The increased dependence on iron makes cancer cells “iron addicted” and renders them more sensitive to the effects of iron depletion. Thus it is not surprising that compounds acting as iron chelators possess potential as cancer therapeutics. Chemically, iron chelators can be classified as bidentate, tridentate or hexadentate ligands, depending on how many of the six coordination sites of iron can be occupied by one molecule (Figure 7). Due to its chemical properties iron preferably binds to oxygen and nitrogen donor atoms of its ligands, but sometimes also sulfur functions as electron donor.

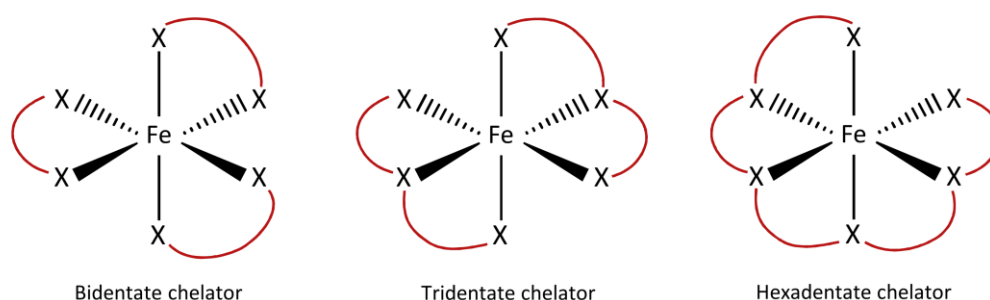


**Figure 7 | Iron coordination by chelators.** Iron chelators can be classified as bi-, tri- or hexadentate, depending on how many of the coordination sites of iron they occupy.

Some iron chelators have been in clinical use for a longer time. For instance deferasirox (DFX), deferoxamine (DFO, also desferrioxamine), and deferiprone (DFP) are used for the treatment of iron overload disorders such as  $\beta$ -thalassemia, hereditary hemochromatosis, sickle cell disease or myelodysplastic syndromes, while ciclopirox (CPX) is used to treat topical fungal infections.<sup>92, 93</sup> More recently, intense effort has been made in repurposing iron chelators for cancer therapy. Several structurally unrelated iron chelators have demonstrated antitumor activity in preclinical and partly also in clinical studies (see incomplete overview in Table 1).

**Table 1 | Overview of iron chelators with anti-tumorigenic potential.**

Chelator	Chemical name	Denticity	Studies	References
<b>Ciclopirox (CPX)</b>	6-Cyclohexyl-1-hydroxy-4-methyl-1H-pyridin-2-one	bidentate	preclinical, clinical	94-96
<b>Deferasirox (DFX)</b>	4-[3,5-Bis-(2-hydroxy-phenyl)-[1,2,4]triazol-1-yl]-benzoic acid	tridentate	preclinical, clinical	97, 98
<b>Deferoxamine (DFO)</b>	N-[5-[[4-[5-[acetyl(hydroxy)amino]pentylamino]-4-oxobutanoyl]-hydroxyamino]pentyl]-N'-(5-aminopentyl)-N'-hydroxybutanediamide	hexadentate	preclinical, clinical	99-101
<b>Dp44mT</b>	Di-pyridylketone thiosemicarbazone	tridentate	preclinical	102, 103
<b>Triapine (3-AP)</b>	3-aminopyridine-2-carboxaldehyde thiosemicarbazone	tridentate	preclinical, clinical	104-107
<b>V LX600</b>	6-Methyl-3-((2Z)-2-(1-(2-pyridinyl)ethylidene)hydrazino)-5H-[1,2,4]triazino[5,6-b]indole	tridentate	preclinical, clinical	108, 109

DFO was the first iron chelator which has been evaluated in regard of potential antitumor effects. While it has demonstrated *in vitro* activity against neuroblastoma and leukemia<sup>101, 110</sup>, its clinical use is limited due to its hydrophilicity. As DFO possesses a low membrane permeability it mostly chelates extracellular iron only and cannot be administered orally but only intravenously.<sup>111</sup> Furthermore, DFO is rapidly excreted and has a short plasma life, thus high doses are needed. DFX in contrast is highly cell permeable, which makes it a pharmacologically more favorable agent compared to DFO and was the first approved orally available iron chelator. It has shown profound anti-tumorigenic activities *in vitro*<sup>97, 112</sup> and could also be effective *in vivo*<sup>98</sup>. Also iron chelators from the thiosemicarbazone class, such as triapine (3-AP) and Dp44mT have potential as anti-tumorigenic agents.<sup>113</sup> 3-AP has proven effective in blood cancers, but not in solid tumors.<sup>104, 105</sup> Dp44mT is a demethylated derivative of 3-AP with a strongly increased potency and has shown good efficacy in animal studies.<sup>102</sup> Also new classes of iron chelator with improved properties are being developed, for example the iron chelator VLX600 was shown to be more potent in reducing tumor cell growth compared to established iron chelators.<sup>108</sup> However, a first clinical phase I study in refractory advanced solid tumors could not prove its efficacy.<sup>109</sup> In general, clinical studies found mild to moderate side effects for most iron chelators, with dose-limiting gastrointestinal toxicity and fatigue as primary symptoms.

The biological effects of iron chelators on tumor cells are complex and multifaceted. Numerous cellular pathways have been linked to their anti-tumorigenic actions. One important mechanism of action is the induction of cell cycle arrest via targeting RR, cyclin D, CDK2 and further cell cycle regulatory proteins.<sup>114</sup> Iron chelators also induce expression of N-myc downstream regulated gene 1 (NDRG1), which represses invasion and epithelial-mesenchymal transition (EMT) and could inhibit metastasis of cancers.<sup>115</sup> Also numerous signaling pathways, such as

PI3K/AKT/mTOR signaling, TGF- $\beta$  signaling and STAT3 signaling are modulated by iron chelation.<sup>116</sup>

### 1.2.4 The iron chelator ciclopirox

One possibility to improve safety and efficacy of iron chelators for cancer treatment is to use an alternative route of administration. Topical application in this respect could be advantageous as it reduces systemic side effects and enables treatment with higher drug doses. This could be an interesting approach for easily accessible cancers or pre-neoplasias situated in skin and mucosa, such as cervical cancers and CINs. Ciclopirox (CPX, IUPAC name 6-cyclohexyl-1-hydroxy-4-methyl-2(1H)-pyridone)) is a topically available bidentate iron chelator from the hydroxyl-pyridonone family (see structure in Figure 8A). CPX has a high affinity for polyvalent metal cations, it preferentially binds ferric iron but also binds to other divalent and trivalent metal ions such as Al<sup>3+</sup>, Zn<sup>2+</sup>, Mg<sup>2+</sup>, Ca<sup>2+</sup>, Cu<sup>2+</sup> and Mn<sup>2+</sup>.<sup>117, 118</sup> It is mainly used in the form of its olamine salt, which increases the water solubility but does not change its pharmacological properties.<sup>93</sup> The term CPX in the following will be used both for ciclopirox and ciclopirox olamine. CPX as a lipophilic molecule can penetrate the cell membrane and thus mainly chelates intracellular iron, which is in contrast to DFO and other iron chelators.<sup>118, 119</sup>

CPX has been used clinically since the early 1980s as a topical antifungal agent for the treatment of superficial mycoses of skin, mucosa and nails.<sup>93</sup> For this application, it is sold under many brand names and is available in numerous different formulations, e.g. as cream, suspension, gel, shampoo or nail lacquer.<sup>93</sup> The mechanism behind the antifungal action of CPX is not fully elucidated yet, but differs from other antimycotic agents and is probably related to its iron chelating properties.<sup>120</sup> Amongst others, CPX has been shown to target metabolic processes, induce ROS and inhibit DNA repair and cell division in yeast.<sup>121, 122</sup> More recently, CPX has gained considerable interest for the treatment of other disorders in humans, such as inflammatory and cardiovascular diseases, diabetes, acquired immune deficiency syndrome (AIDS) and cancer (reviewed in Shen and Huang, 2016<sup>123</sup>). The advantage of repurposing a drug for new medical uses lies in the drastically reduced development time and costs and the fact that such compounds already have undergone rigid safety evaluations.

During the last years, CPX was investigated in numerous types of cancer and has proven profound anti-tumorigenic effects.<sup>124</sup> Promising results could be shown in *in vitro* models of cervical cancer<sup>125</sup>, pancreatic cancer<sup>126</sup>, colorectal cancer<sup>127</sup>, neuroblastoma<sup>128</sup> and further cancer types. Also first animal trials showed its efficacy in acute myeloid leukemia and breast cancer.<sup>95, 96</sup> Finally, the first clinical trial using CPX as an anti-tumorigenic oral agent was started in 2009 in patients with relapsed or refractory hematologic malignancies.<sup>129</sup> Two out of 24 patients showed hematologic improvements and CPX was generally well tolerated, however gastrointestinal

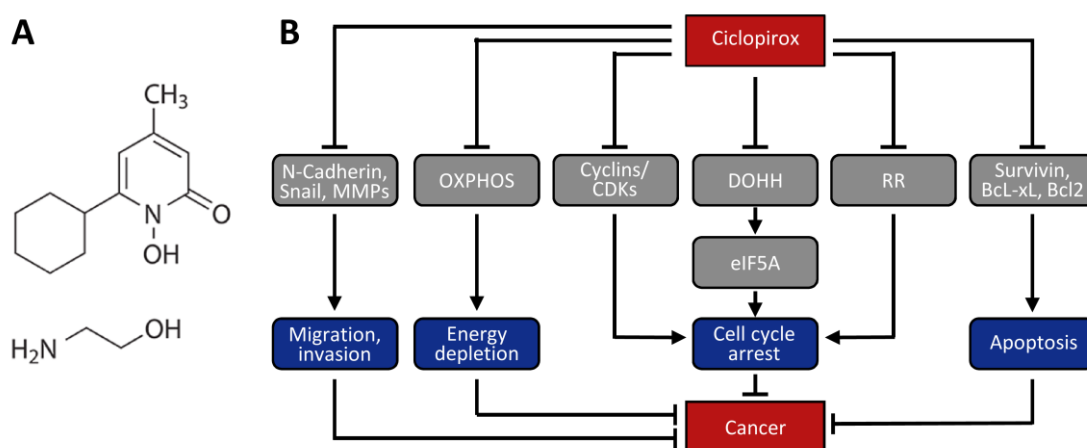


**Figure 8 | Anti-tumorigenic effects of ciclopirox. (A)** Chemical structure of ciclopirox olamine. **(B)** Cellular pathways and processes targeted by CPX that are relevant for its anti-tumorigenic effects.

toxicities limited the maximum dose and serum half-life was quite short with less than 6 h. More recently, clinical trials have been initiated in bladder cancer patients employing a parenterally applicable CPX derivate, which has improved pharmacological properties, with promising first results.<sup>130</sup>

Mechanistically, CPX targets multiple molecular pathways, which can mostly be attributed to the chelation of intracellular iron, see overview in Figure 8B. A main anti-tumorigenic effect is the repression of cell proliferation, e.g. by inhibition of RR.<sup>95</sup> CPX also induces cell cycle arrest in G1/S phase, mediated via downregulation of cyclins A, B1 and D, inhibition of CDK4 and 6 and downregulation of pRb.<sup>96, 127, 131</sup> Also inhibition of the iron-dependent enzyme deoxyhypusine hydroxylase (DOHH), which normally catalyzes hypusination of the eukaryotic translation initiation factor 5A (eIF5A) plays a role in CPX-mediated growth inhibition.<sup>132</sup> Furthermore, CPX induces apoptosis by inhibiting the anti-apoptotic proteins BCL-X<sub>L</sub>, BCL-2 and survivin.<sup>96, 126</sup> Another potential anti-tumorigenic mechanism is the inhibition of migration and invasion via downregulation of N-cadherin, matric metalloproteinases (MMPs) and Snail.<sup>133</sup> Additionally, the recently shown inhibition of mitochondrial oxidative phosphorylation (OXPHOS) by CPX might play a role in inhibiting tumor cell growth.<sup>108, 127</sup> Further anti-tumorigenic activities of CPX could include inhibition of Wnt signaling<sup>94, 131</sup> and histone demethylases<sup>128</sup>, induction of endoplasmatic reticulum (ER) stress<sup>127</sup> and autophagy<sup>134</sup>, and inhibition of mTOR signaling<sup>135</sup>.

### 1.3 Notch signaling pathway

A novel potential target of CPX, which was identified in the present thesis is Notch1. In mammals there are four Notch paralogs (Notch1-4), which are large transmembrane proteins and are at the core of an evolutionary conserved and ubiquitous intercellular communication pathway, which is implicated in regulatory processes including development, EMT, cell proliferation and apoptosis.<sup>136</sup> Furthermore, aberrant Notch signaling plays a role for several genetic diseases and

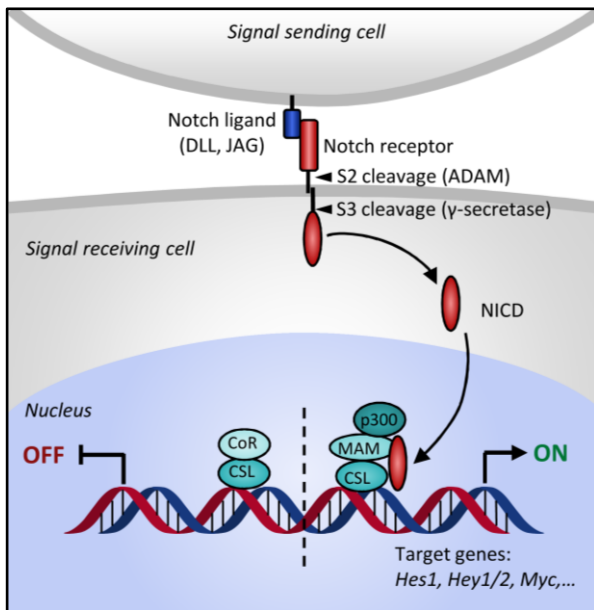


**Figure 9 | Notch signaling pathway.** Ligand binding induces cleavage of Notch receptor at S2 and S3. The liberated intracellular domain (NICD) travels to the nucleus where it with co-activators drives target gene transcription. NICD, Notch intracellular domain.

is of importance for different types of cancer.<sup>137</sup> Before the Notch receptor can be expressed at the cellular membrane, it undergoes several posttranslational modifications and is matured in the Golgi by cleavage at site 1 (S1) through a furin-like convertase.<sup>138</sup> The canonical Notch signaling pathway (as depicted in Figure 9) is activated upon binding of the Notch receptor to a ligand from a neighboring cell<sup>139</sup>, which leads to a conformational change of Notch, exposing a cleavage site (S2) for ADAM metalloproteases<sup>140</sup>. The resulting Notch extracellular truncation (NEXT) fragment can undergo a third proteolytic cleavage by the  $\gamma$ -secretase complex at site 3 (S3), which leads

to liberation of the Notch intracellular domain (NICD).<sup>141</sup> NICD then translocates to the nucleus, where it associates with the DNA-binding protein CSL (CBF1, Suppressor of Hairless, Lag1), the transcriptional coactivator Mastermind (MAM) and additional factors to transcriptionally activate target gene expression.<sup>139</sup>

Recent studies found mutations in Notch genes in numerous types of cancers<sup>142</sup> and both hyper- and hypo-activation of the Notch signaling pathway have been implicated with cancer. Thus it depends on context and cell type if Notch acts as tumor suppressor or as oncogene.<sup>143, 144</sup> In some cancers like T-cell acute lymphoblastic leukemia (T-ALL) and triple-negative breast cancer Notch1 activates oncogenic *Myc* signaling<sup>145</sup> and enhances the PI3K-Akt pathway<sup>146</sup>. Moreover, there is evidence for Notch acting as a promoter of metastasis/EMT<sup>147, 148</sup> and chemotherapy resistance<sup>149</sup>. In contrast, a tumor-suppressive role for Notch was identified for example in squamous cell carcinomas (SCCs), which often feature loss-of-function mutations of Notch signaling components.<sup>150</sup>

#### 1.4 Senescence and apoptosis

Recent work from our group showed that CPX acts anti-tumorigenic in cervical cancer cells and blocks proliferation of HPV-positive cells by inducing cellular senescence and apoptosis.<sup>125</sup> While apoptosis is known as programmed cell death, senescence is typically defined as a permanent growth arrest, where cells maintain their metabolic activity.<sup>151, 152</sup> Both senescence and apoptosis can occur in response to different stressors and both possibly evolved as anti-tumorigenic

mechanisms to hinder damaged cells from further proliferation.<sup>153</sup> Surprisingly, the knowledge about what determines if a certain stressor preferably induces senescence or apoptosis is still relatively sparse.

### **1.4.1 Senescence**

Normal, non-transformed cells do not proliferate indefinitely, instead after a limited number of divisions they adapt a permanent state of cell cycle arrest, in which they are still metabolically active but do not divide anymore. This phenomenon was first described in 1961 by Leonard Hayflick and Paul Moorhead and coined cellular senescence.<sup>151</sup> From an evolutionary perspective senescence probably developed as a safeguard mechanism, protecting the body from cancer induction by arresting damaged cells. However, with prolonged life span senescence also has harmful effects as it contributes to aging.<sup>154</sup> Most disadvantageous effects of senescence are caused because senescent cells secrete a mixture of inflammatory cytokines, growth factors and proteases, collectively termed the senescence-associated secretory phenotype (SASP).<sup>155, 156</sup> These secreted proteins alter the tissue microenvironment and, in a paracrine manner, promote processes such as cell proliferation or cell motility and thus can exert pro-tumorigenic effects.<sup>155</sup> Senescence can occur either as a response to acute stress, such as DNA damage, oxidative stress or oncogene activation (premature senescence), or as a consequence of continuous passaging of cells or aging (telomere-initiated senescence).<sup>157</sup> Telomeres are special nucleoprotein structures protecting the ends of chromosomes.<sup>158</sup> Human cells usually have telomeres of 5-15 kb length. Because standard DNA polymerases are unable to fully replicate DNA ends, normal, mortal cells (not expressing telomerase) lose 50-200 bp of telomeric DNA during each cell cycle.<sup>159</sup> Eventually, one or more telomeres become too short which triggers a DNA damage response (DDR) to which cells react by inducing senescence.<sup>160</sup> Also DNA damage caused by other stressors such as chemotherapeutic drugs or radiation can initiate senescence in tumor cells which makes senescence a desired outcome for cancer therapy.<sup>161, 162</sup> Other possible inducers of senescence are mitochondrial malfunction, leading to excessive ROS production, oncogene activation or activation of tumor suppressors.<sup>163, 164</sup>

Different stressors activate different pathways leading ultimately to the induction of senescence (see overview in Figure 10). These pathways are often interconnected and activated in parallel. The two main pathways, however, are the p53-p21 and the p16-pRb tumor suppressor pathways.<sup>165</sup> Cellular stress leads to p53 activation, which induces the CDK inhibitor p21, causing cell cycle arrest partly via activating pRb.<sup>166, 167</sup> Active, hypo-phosphorylated pRb then binds to E2F proteins and thus inhibits cell cycle progression.<sup>168</sup> pRb can also be activated by the CDK inhibitor p16 (INK4A), which is expressed from the *CDKN2A* locus, together with p14 (ARF). In contrast to p21, the mechanisms leading to p16 induction are still not well understood.<sup>169</sup> The p53

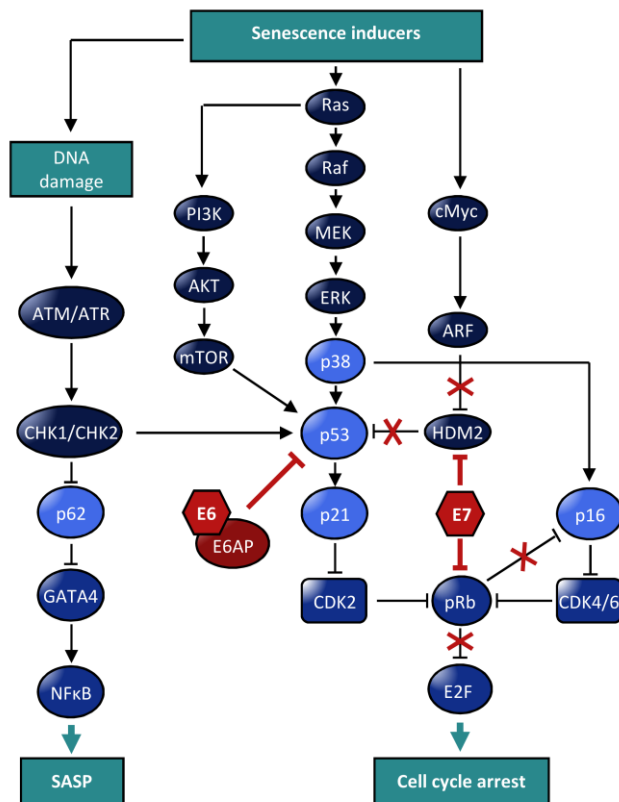


**Figure 10| Molecular pathways involved in senescence induction and how they are altered by HPV E6/E7.** For more details, please see text.

turn activates NF- $\kappa$ B, which has a crucial role in initiating the SASP. Also increased ROS production can trigger a senescence response by activation of p16 and p53 via p38.<sup>174, 175</sup> Furthermore, many oncogenes induce senescence via p16, for example oncogenic forms of proteins in the Ras signaling pathway.<sup>171, 176, 177</sup>

Notably, in HPV-positive tumor cells the viral oncoproteins E6 and E7 effect several of the pathways involved in senescence. Firstly, E7 inactivates pRb, thereby releasing E2F, which leads to uncontrolled cell cycle progression.<sup>32</sup> pRb inactivation also results in an overexpression of p16, which is thus often used as a diagnostic marker for HPV-infection.<sup>178, 179</sup> Secondly, in HPV-positive cells p53 is not repressed via ARF and HDM2 but by a unique pathway via E6 and E6AP.<sup>180</sup> Therefore, E6/E7 repression in HPV-positive tumor cells leads to effective induction of senescence by activating the p53 and pRb pathways<sup>181, 182</sup> with p21 playing a major role in this process<sup>183</sup>.

### 1.4.2 Apoptosis

Unlike senescence, apoptosis does not induce an inflammatory response and might thus be the preferable way of inactivating cancer cells. Apoptosis is a form of programmed cell death and as such is a highly orchestrated process leading to the orderly removal of damaged cells.<sup>184</sup>

and p16 pathways are connected, but can also independently induce senescence. There is even the possibility to induce senescence independent of both of these pathways.<sup>170, 171</sup>

A main inducer of senescence is DNA damage eliciting a prolonged DDR. DNA damage is detected by a variety of sensor proteins, which induce activation of the upstream protein kinases ataxia telangiectasia mutated (ATM) and ATM and Rad-3 related (ATR).<sup>172</sup> Downstream protein kinases like checkpoint kinase 1 and 2 (CHK1/2) propagate the signal and activate the p53 arm of senescence. These kinases also lead to stabilization of the transcription factor GATA4, which is under normal conditions degraded via p62-mediated autophagy.<sup>173</sup> GATA4 in

Morphologically, apoptosis is characterized by cell shrinkage, chromatin condensation, plasma membrane blebbing, extracellular exposure of phosphatidylserine and DNA fragmentation.<sup>184</sup> Apoptosis can be triggered by various internal and external signals, such as genotoxic stress or death-inducing ligands. There are two major cellular signaling pathways through which apoptosis is executed, the intrinsic and the extrinsic pathway. These pathways are interconnected and both culminate in the activation of caspases, specialized cysteine-aspartic proteases that execute the apoptotic program by cleaving a set of effector proteins.<sup>185</sup> Caspase targets involve apoptotic factors, structural proteins, DNA repair proteins and cell cycle related factors.<sup>186</sup>

The intrinsic pathway of apoptosis is triggered by cellular stresses such as DNA damage, metabolic stress or microtubule damage. Stress sensors like p53 or AKT activate BH3 proteins, which stimulate the death agonists BAK and BAX.<sup>187</sup> Activation of these proteins promotes mitochondrial outer membrane permeability (MOMP), allowing release of cytochrome c and Smac/DIABLO (second mitochondria derived activator of caspases/direct IAP binding protein with low PI).<sup>188</sup> Cytochrome c then induces a conformational change in Apaf-1, allowing its oligomerization to form the apoptosome.<sup>189</sup> This complex cleaves and activates the initiator caspase-9, which in turn cleaves and activates the effector caspases-3 and -7.<sup>185</sup>

The extrinsic pathway of apoptosis is initiated via death receptors, such as Fas, TNFR1/2 and death receptors 4 and 5 (DR4/5) upon binding of extracellular death ligands like FasL, TNF and TNF-related apoptosis-inducing ligand (TRAIL).<sup>186</sup> This interaction leads to the recruitment of adaptor proteins such as Fas-associated protein with death domain (FADD) and initiator caspase-8 to facilitate formation of the death-inducing signaling complex (DISC).<sup>190</sup> In some cells, activated caspase-8 then directly induces activation of the effector caspases-3 and -7. In other cells, caspase-8 stimulates activation of the BH3 only protein BID, which then activates the intrinsic apoptotic pathway via BAX and BAK, leading to activation of effector caspases through the mitochondrial pathway.<sup>191</sup>

Apoptosis often is deregulated in tumor cells and evasion of apoptosis is one of the hallmarks of cancer.<sup>192</sup> Many anticancer treatments, including chemo- and radiotherapy aim to trigger apoptosis in cancer cells, e.g. by inducing DNA damage, and a multitude of approaches to directly activate the apoptotic pathway are in development.<sup>193</sup>

### **1.5 Cellular energy metabolism**

Multiple cellular processes contribute to the generation of energy, which is needed in anabolic processes to synthesize biomolecules, perform mechanical work and actively transport molecules. Larger molecules such as carbohydrates, fatty acids and amino acids are first broken down to smaller units, such as monosaccharides, which then can feed into energy producing pathways. The

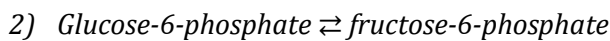
major ATP-generating pathways are glycolysis and oxidative phosphorylation (OXPHOS), which will be described in detail below.

### 1.5.1 Glycolysis

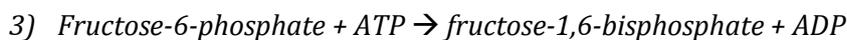
During glycolysis glucose and other monosaccharides are catabolized to pyruvate and the released energy is stored in the form of ATP and NADH. Glycolysis can be divided into two phases: in the preparatory phase energy in the form of 2 molecules ATP is invested, while in the pay-off phase 4 molecules ATP and 2 molecules NADH are produced. Thus, the net yield of glycolysis is 2 ATP and 2 NADH, which means most of the energy of glucose is still bound in pyruvate and only released in the second and third steps of respiration – the citric acid cycle and oxidative phosphorylation. Glycolysis consists of the following ten sequential reactions<sup>194</sup>:



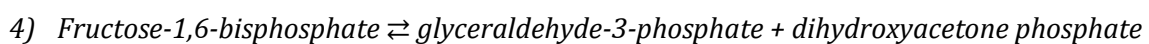
In the first step, hexokinase (HK) phosphorylates glucose by using 1 molecule ATP. This reaction is irreversible and serves to activate glucose and fix it in the cell.



Glucose-6-phosphate isomerase (GPI) catalyzes the reversible isomerization of glucose-6-phosphate to fructose-6-phosphate.



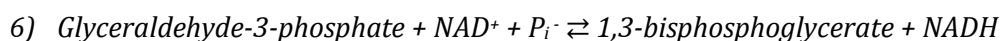
In a second priming reaction fructose-6-phosphate is phosphorylated using another molecule of ATP. This reaction is catalyzed by phosphofructokinase-1 (PFK-1), an enzyme underlying a complex allosteric regulation, allowing it to react to the cells energetic status.



Fructose-1,6-bisphosphate is cleaved into two different triose phosphates by aldolase.



The enzyme triose phosphate isomerase catalyzes the interconversion of the both triose phosphates as only glyceraldehyde-3-phosphate (GA-3P) can enter the next glycolytic step.



In the first reaction of the pay-off phase, GA-3P is oxidized by GA-3P dehydrogenase to 1,3-bisphosphoglycerate (1,3-BP). 1 molecule NADH is generated per molecule GA-3P.



The enzyme phosphoglycerate kinase transfers the phosphoryl group from 1,3-BP to ADP and 1 molecule ATP per molecule 1,3-BP is built.



Phosphoglycerate mutase then promotes the reversible shift of the phosphoryl group between C-2 and C-3 of the glycerate.

9)  $2\text{-Phosphoglycerate} \rightleftharpoons \text{phosphoenolpyruvate} + \text{H}_2\text{O}$

In the penultimate step, enolase catalyzes the removal of one molecule water from 2-phosphoglycerate and phosphoenolpyruvate (PEP) is produced.

10)  $\text{Phosphoenolpyruvate} + \text{ADP} \rightarrow \text{pyruvate} + \text{ATP}$

Finally, pyruvate kinase catalyzes the transfer of the phosphoryl group from PEP to ADP, again yielding one molecule ATP per molecule PEP and producing pyruvate as the end product of glycolysis.

The generated pyruvate can be reduced to lactate in order to replenish  $\text{NAD}^+$  from NADH, which is mainly the case under hypoxic conditions, but also common in (normoxic) cancer cells. Anaerobic glycolysis only utilizes about 5% of the energy contained in glucose, however, it is considerably faster than OXPHOS.<sup>195</sup> Alternatively, pyruvate can be oxidized to acetyl CoA which is fueled into the tricarboxylic acid (TCA) cycle (also citric acid cycle or Krebs cycle). In the TCA cycle, pyruvate is completely oxidized to  $\text{CO}_2$  and  $\text{O}_2$ , producing a greater amount of energy in the form of ATP and reduction equivalents. The electron carriers produced during glycolysis and TCA cycle can subsequently be oxidized in the mitochondrial respiratory chain, which releases energy that is ultimately stored in ATP (see next chapter). The formation of glucose-6-phosphate by hexokinase is also the starting point of the pentose phosphate pathway (PPP), which runs in parallel to glycolysis and produces NADPH and pentose phosphates needed for the synthesis of nucleic acids and several co-enzymes.<sup>196</sup>

### 1.5.2 Oxidative phosphorylation

Oxidative phosphorylation is the last step of cellular respiration, taking place in the mitochondria. Electrons from NADH and  $\text{FADH}_2$ , which were produced during glycolysis and the TCA cycle are used to generate energy in the form of ATP. In a series of redox reactions these electrons are transported along the respiratory complexes I to IV of the mitochondrial electron transport chain (ETC), with oxygen serving as final electron acceptor (see scheme in Figure 11).<sup>194</sup>

Complex I is comprised of the enzyme NADH dehydrogenase, which catalyzes the exergonic transfer of two electrons from NADH to ubiquinone via flavin mononucleotide (FMN) and seven Fe-S centers. During this reaction, four protons are transported from the matrix to the intermembrane space in an endergonic reaction. Alternatively, electrons can enter the ETC through complex II, where succinate dehydrogenase transfers two electrons donated from  $\text{FADH}_2$  to ubiquinone via flavin adenine dinucleotide (FAD) and Fe-S centers. Ubiquinol (the reduced form of ubiquinone) carries the electrons from complex I and II to complex III, the ubiquinone cytochrome *c* oxidoreductase. Electrons are then transferred to cytochrome *c* which is again coupled to the vectorial transport of four protons per electron pair from the matrix to the

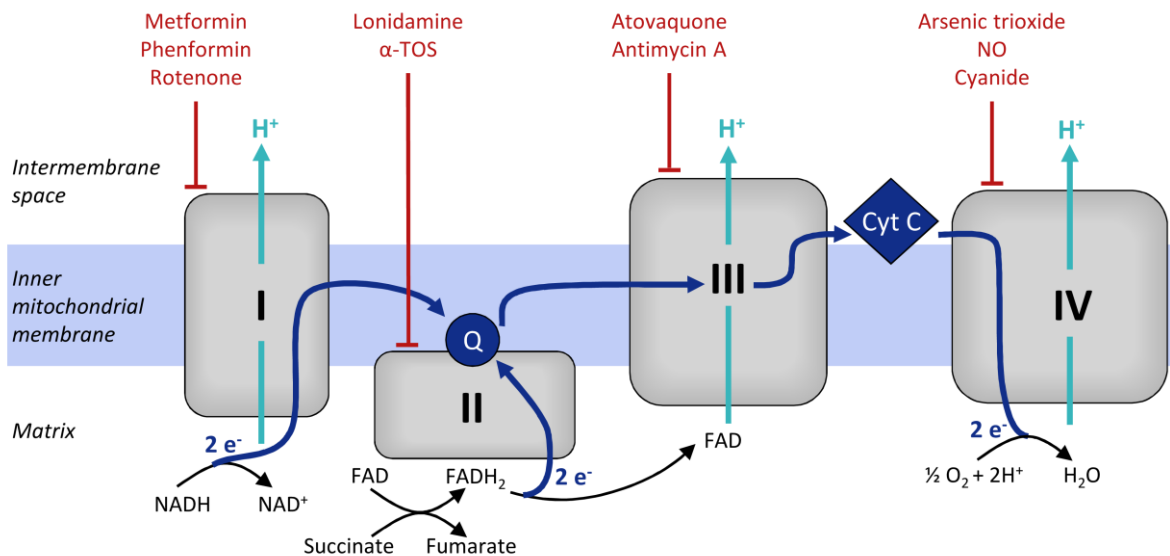


**Figure 11| The mitochondrial electron transport chain.** Electrons from NADH or FADH<sub>2</sub> are transported via a series of electron transporters through the OXPHOS complexes I to IV with oxygen serving as final electron acceptor (dark blue path). Simultaneously, protons are pumped from the mitochondrial matrix to the intermembrane space (turquoise paths), building up an electrochemical gradient. Inhibitors of the respective OXPHOS complexes are shown in red. α-TOS, α-tocopherol; NO, nitric oxide; Q, ubiquinone; Cyt C, cytochrome c.

intermembrane space. Electron transfer takes place in a sequential manner via the so-called Q-cycle, which involves cytochrome *b* and a 2Fe-2S cluster. Finally, in complex IV, cytochrome oxidase transfers the electrons from cytochrome *c* to molecular oxygen, which is reduced to water. Next to the two protons needed to reduce  $\frac{1}{2} \text{O}_2$  to H<sub>2</sub>O, two further protons are transported through the membrane in this step.

As a net reaction, two electrons from NADH are transferred to  $\frac{1}{2}$  molecule O<sub>2</sub>, yielding NAD<sup>+</sup> and one molecule H<sub>2</sub>O. The energy of this exergonic reaction is converted to proton-motive force by pumping 10 protons per NADH or 6 protons per FADH<sub>2</sub> through the membrane, building up a proton gradient. This electrochemical energy is then used by the enzyme ATP synthase (also termed OXPHOS complex V), which can synthesize one molecule ATP per four protons. The maximum yield that can be generated from one mole of glucose via glycolysis, TCA cycle and OXPHOS is 32 moles ATP.

### 1.5.3 Metformin and other metabolic cancer drugs

The metabolism of tumor cells profoundly differs from that of non-transformed cells, allowing them to sustain high proliferation rates and resist apoptosis.<sup>197</sup> Already in 1928, the German biochemist Otto Warburg observed that tumor cells perform glycolysis at a much higher rate than healthy cells, even in the presence of oxygen.<sup>198</sup> This is in contrast to normal cells, where oxygen inhibits glycolytic flux, a phenomenon known as “Pasteur effect”.<sup>199</sup> One explanation for this increased glycolysis rate is that cancer cells often grow under hypoxic conditions, forcing them to adapt to this hostile microenvironment by switching to an anaerobic metabolism.<sup>200</sup> However, this

does not explain why also under oxygen-replete conditions aerobic glycolysis is preferred by tumor cells. An alternative explanation which is broadly accepted in cancer research is that tumor cells use certain metabolites and intermediates of the glycolytic and PPP pathways as precursors for anabolic pathways, like synthesis of nucleic acids, lipids and amino acids, which compensates for the poor energetic balance of glycolysis.<sup>201,202</sup>

Following Warburg's initial theory<sup>198</sup> it was assumed for a long time that most cancer cells have impaired mitochondria, explaining their preference for glycolytic energy production accompanied by downregulation of OXPHOS. However, there is growing evidence that in most tumor cells mitochondria are functional and OXPHOS contributes similarly to ATP generation in cancer cells as in healthy cells.<sup>203</sup> In several cancers OXPHOS even seems to be upregulated<sup>204</sup> and is often only limited by oxygen supply but not functionally impaired<sup>205</sup>. Therefore, targeting mitochondrial metabolism emerges as a promising option for cancer therapy at least for a subset of tumors.<sup>206</sup> The OXPHOS complexes can be inhibited with classical mitochondrial poisons, such as rotenone (complex I), antimycin A (complex III), cyanide (complex IV) or oligomycin (complex V), but there also are numerous inhibitors possessing clinical potential which currently are under investigation *in vitro* and *in vivo*.<sup>207</sup>

A particularly interesting compound with anti-tumorigenic potential is the biguanide metformin (Figure 12A), which is clinically used for the first line treatment of type 2 diabetes. Metformin decreases blood glucose levels mainly by reducing hepatic glucose production.<sup>208</sup> In addition to its antidiabetic effects, metformin was more recently recognized as a potential anticancer therapeutic and numerous studies have demonstrated its preventive or therapeutic potential in diverse cancer entities.<sup>209</sup> This anti-tumorigenic effect is primarily caused by inhibition of mitochondrial complex I, which leads to an inhibition of OXPHOS and thus an increased AMP:ATP ratio, which activates the energy sensor AMP-activated kinase (AMPK) via liver kinase B1 (LKB1) (see overview in Figure 12B).<sup>208</sup> AMPK controls many metabolic processes and inhibits e.g. fatty acid synthesis and gluconeogenesis, thus reducing glucose production.<sup>210</sup> A major target of AMPK is mammalian target of rapamycin complex I (mTORC1), which can also be inhibited by metformin

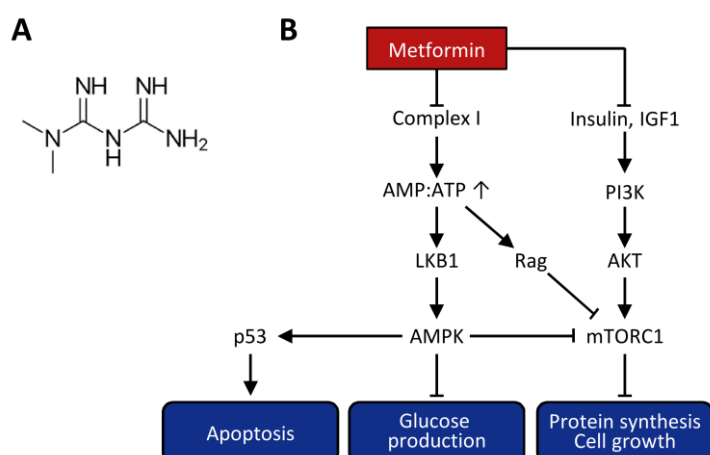


**Figure 12| Anti-tumorigenic effects of metformin.** (A) Chemical structure of metformin. (B) Metformin primarily exerts anti-tumorigenic potential by inhibiting OXPHOS complex I, leading to reduced cellular ATP levels and activation of AMPK, which reduces glucose production. AMPK can also activate p53, contributing to apoptosis induction. Furthermore, Metformin inhibits mTORC1 in an AMPK-dependent or independent manner, thus repressing protein synthesis and cell growth.

in an AMPK-independent manner via inhibition of the PI3K-AKT signaling pathway<sup>211</sup> or repression of Rag GTPases<sup>212</sup>. Thus, mTORC1 is a key target of metformin in respect to its anti-tumorigenic effects, its inhibition leading to impaired protein synthesis and reduced cell growth. Apart from mTORC1, AMPK can phosphorylate and activate p53 which can exert further anti-proliferative and pro-apoptotic effects.<sup>213</sup> Indirectly, also the reduction of glucose and insulin levels by metformin might contribute to suppressing tumor growth. In cervical cancer, the effect of metformin is still under debate. While it was shown to reduce mortality in diabetic cervical cancer patients<sup>214</sup>, another study could not identify such effects of metformin<sup>215</sup>.

Besides metformin several other OXPHOS inhibitors possess potential for chemotherapy (see Figure 11). For example, BAY89-2243, IACS-010759 and ME-344 are high affinity complex I inhibitors, which are still under development.<sup>207</sup> Few compounds target complex II, the most promising probably is  $\alpha$ -tocopherol ( $\alpha$ -TOS), a vitamin E analogue.<sup>216</sup> Complex III can be targeted for example with the antimalarial drug atovaquone which has shown efficacy in preclinical studies<sup>217</sup>, and complex IV is inhibited by arsenic trioxide, an FDA approved drug for the treatment of acute promyelocytic leukemia that was reported to reduce hypoxia and sensitize cells to radiation.<sup>218, 219</sup>

Alternatively, also other metabolic pathways such as PPP or glycolysis may be targeted for cancer therapy. One glycolysis inhibitor studied in this context is 2-deoxy-D-glucose (2-DG), which is phosphorylated by hexokinase, producing 2-deoxyglucose-6-phosphate, which cannot be metabolized further and thus competitively inhibits hexokinase.<sup>220</sup> Other drugs targeting HK are 3-bromopyruvate and lonidamine, which also inhibits OXPHOS complex II but could not demonstrate sufficient efficacy in clinical trials.<sup>221</sup> While some glycolysis inhibitors showed promising results in preclinical trials, they turned out to be toxic when used in higher concentrations and thus their clinical success has been limited.<sup>222-224</sup> However, as part of combination therapies these compounds might still be a promising option as they were shown to sensitize tumor cells to chemo- and radiotherapy.<sup>225, 226</sup>

## 1.6 Research objectives

The iron chelator ciclopirox is an antimycotic drug, which has shown promising anti-tumorigenic potential in multiple tumor types and thus is under discussion of being repurposed for cancer therapy. Previous work from our group could demonstrate that iron depletion exerts profound anti-tumorigenic effects in HPV-positive cervical cancer cells in that it efficiently downregulates the viral *E6/E7* oncogenes and strongly represses cell proliferation.<sup>125, 227</sup> Interestingly, after shorter treatment periods CPX mainly induces senescence, while prolonged treatment results in induction of apoptosis.

The present study aims to gain insights into the mechanisms behind these anti-tumorigenic effects of CPX. In detail, the following aspects should be elucidated:

- (I) Which molecular pathways underlie the phenotypic responses of cervical cancer cells towards CPX?

Data from a proteome screen of CPX-treated HPV16-positive cervical cancer cells will be analyzed for potentially involved pathways and compared to proteome screens of hypoxic cells or cells treated with the metabolic drug metformin. A particular focus will be set on factors linked to the cellular energy metabolism. Further, it will be assessed if the Notch signaling pathway contributes to the anti-tumorigenic effects of CPX.

- (II) Which factors determine the switch between induction of senescence or apoptosis upon CPX treatment?

Since CPX may profoundly affect glucose metabolism, the influence of glucose concentrations on these different phenotypic outcomes will be elucidated. Moreover, the expression of factors impaired in senescence and apoptosis will be investigated and candidates regulating the therapeutic outcome will be identified. In this context, the effects of CPX will also be compared to those of established OXPHOS inhibitors such as metformin and to those of other iron chelators.

- (III) Can CPX enhance the effects of radio- and chemotherapy?

To this end, CPX treatment of cervical cancer cells will be combined with irradiation or cisplatin as well as with metabolic modulators. Subsequently, effects of the different drug combinations on cellular proliferation will be evaluated and analyzed for functional cooperativity.

Overall, this thesis aims to provide new insights into the anti-tumorigenic mechanisms of the iron chelator ciclopirox, which may serve as a basis for developing innovative treatment strategies for the therapy of HPV-induced neoplasias.



# ***CHAPTER 2***

## ***RESULTS***



## 2. Results

### 2.1 Proteome analyses of CPX-treated cells

Previous work from our group showed that the iron chelator ciclopirox exerts profound anti-tumorigenic effects in HPV-positive tumor cells, which include inhibition of cell proliferation, downregulation of the viral *E6/E7* oncogenes and induction of senescence or apoptosis.<sup>125, 227, 228</sup> Furthermore, a growing body of literature has investigated CPX in different preclinical tumor models and demonstrated that it exerts anti-tumorigenic effects in a broad range of cancer entities.<sup>95, 126, 128, 131, 229</sup> With the aim to gain more insights into these anti-tumorigenic mechanisms exerted by CPX, comprehensive proteome analyses were conducted<sup>227</sup>, comparing the global protein expression of HPV16-positive SiHa cells treated with CPX or EtOH as solvent control under normoxic (21% O<sub>2</sub>) or hypoxic (1% O<sub>2</sub>) conditions. Under normoxia, 5919 proteins were detected in total, out of which 301 were significantly downregulated ( $\log_2$  fold change,  $\log_2\text{FC} \leq -1$ ,  $p$ -value  $\leq 0.01$ ) while 91 were significantly upregulated ( $\log_2\text{FC} \geq 1$ ,  $p$ -value  $\leq 0.01$ ) by CPX treatment (Figure 13A). This relatively high number of differentially regulated proteins is in accordance with a growing body of literature, highlighting a variety of cellular processes and pathways that are influenced by CPX. In Figure 13B a heat map is depicted which contains a selection of factors associated with cancer and metabolism that were identified in the proteome analyses and their regulation by CPX both under normoxia and hypoxia. Furthermore, for comparison also proteome analyses of cells treated with metformin<sup>230</sup>, an OXPHOS inhibitor and antitumor agent (see 1.5.3), were included.

As can be expected for an iron chelator, CPX regulates the protein levels of a number of factors involved in iron metabolism. Furthermore, several of the hits might be of interest for the anti-tumorigenic activities, as they are involved in relevant processes like cell proliferation and migration, in apoptosis and senescence, in energy metabolism or in therapy resistance.

Strikingly, many proteins are regulated similarly by CPX treatment and under hypoxia. This suggests that the expression is modulated via hypoxia inducible factor 1 $\alpha$  (HIF-1 $\alpha$ ), which is also upregulated by CPX and other iron chelators.<sup>117</sup> CPX treatment under hypoxic conditions results in a similar but less pronounced regulation than under normoxia, consistent with the observation that CPX exerts a decreased efficiency under hypoxia.<sup>228</sup> Furthermore, some factors are regulated similarly by metformin treatment as by CPX treatment, which could point to a role of OXPHOS inhibition in regulation of these proteins.

In order to validate the results from proteomics by an independent method, protein expression of several hits was assessed by immunoblot in both HeLa and SiHa cells after 8, 24 or 48 h of CPX treatment (Figure 14).

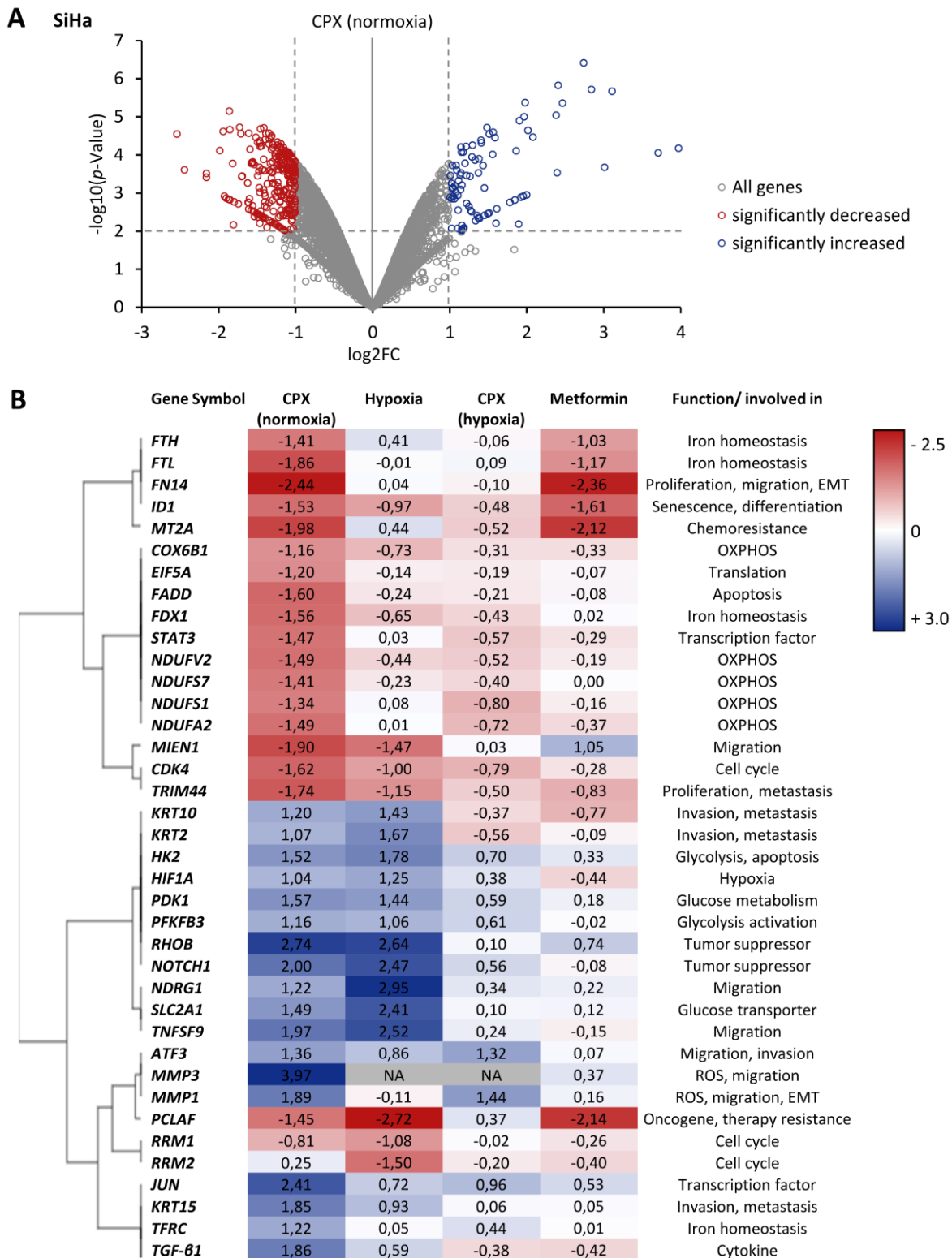


**Figure 13 | Proteome analyses of differentially expressed proteins under CPX treatment. (A)** The proteome of SiHa cells treated with 10  $\mu$ M CPX for 48 h was compared to the proteome of solvent control (EtOH) treated cells via TMT-mass spectrometry (sample preparation was performed by Julia Braun, proteome analyses were performed by Bianca Kuhn). Log<sub>2</sub>-fold change (log<sub>2</sub>FC) values of all proteins detected in the screen are plotted against  $-\log_{10}(p\text{-Value})$ . Significantly decreased proteins (log<sub>2</sub>FC  $\leq$  1,  $p$ -value  $\leq$  0.01) are marked in red, significantly increased proteins (log<sub>2</sub>FC  $\geq$  1,  $p$ -value  $\leq$  0.01) are marked in blue. **(B)** Heat map comparing factors from the proteome analyses in (A) with further proteome analyses of SiHa cells cultured for 48 h under hypoxia (1% O<sub>2</sub>) with or without 10  $\mu$ M CPX and cells treated with 7.5 mM metformin for 24 h. Log<sub>2</sub>FC values of a selection of proteins of interest is depicted. Color scale is shown at the top. Missing values: NA, not available.

In general, all results from the screen could be confirmed both in HeLa and SiHa cells. The tumor suppressor RhoB (Ras homolog family member B) is upregulated upon CPX treatment, as is the iron-regulated growth and metastasis suppressor NDRG1. In contrast, CPX downregulates the TWEAK (tumor necrosis factor like weak inducer of apoptosis)-receptor Fn14 (Fibroblast growth factor-inducible 14), a protein involved in numerous tumor-relevant processes like proliferation, migration and EMT. Also expression of the transcription factor STAT3 (signal transducer and activator of transcription 3) and ID1, a protein involved in growth and senescence control, is decreased after CPX treatment.

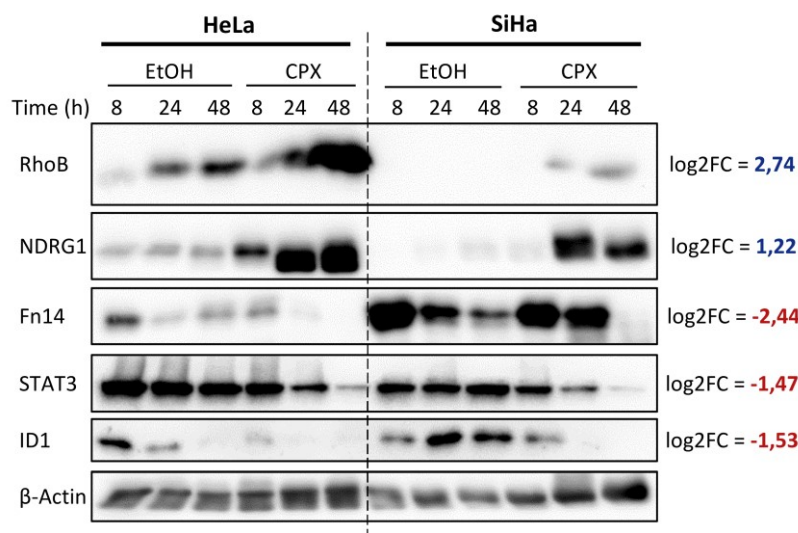


**Figure 14| Validation of proteomics hits.** Protein levels of CPX-regulated factors identified in the proteome screen were analysed by immunoblot in HeLa and SiHa cells treated with 10  $\mu$ M CPX or EtOH as solvent control for 8, 24 or 48 h. Log<sub>2</sub>FC values from the proteome analyses are given for comparison.  $\beta$ -Actin, representative loading control.

## 2.2 CPX regulates cellular energy metabolism

Next, the proteome data was analyzed via gene set enrichment analysis (GSEA) to identify cellular pathways which are differentially regulated under CPX treatment. As expected, CPX was found to influence a wide variety of processes. Among the strongest downregulated gene sets were processes like translation (initiation) and ribosome biogenesis, and also iron-sulfur cluster binding, nucleotide metabolism and mTOR signaling were downregulated by CPX, which fits to experimental observations made before in our and other groups. Many of the strongest upregulated gene sets include factors involved in the cellular response to hypoxia, consistent with the induction of HIF-1 $\alpha$  by CPX. Further interesting positively enriched gene sets are related to extracellular matrix organization, sumoylation or the DREAM pathway.

Moreover, it was found that under CPX treatment gene sets including proteins involved in oxidative phosphorylation are negatively enriched (e.g. "GO\_oxidative\_phosphorylation", Figure 15A, gene symbols and log<sub>2</sub>FC values in Table S1). This downregulation of OXPHOS is consistent with the fact that the mitochondrial respiratory complexes comprising the ETC are dependent on iron atoms as electron acceptors and donors.<sup>231</sup> Probably in order to compensate for the reduced energy production via OXPHOS, cells upregulate glycolysis upon CPX treatment, as indicated by

## Results

positive enrichment of glycolysis-related gene sets (e.g. “GO\_glycolytic\_process”, Figure 15A, gene symbols and log2FC values in Table S2). These findings are corroborated by immunoblot analyses, assessing the protein expression of several factors involved in OXPPOS or glycolysis (Figure 15B). Upon CPX treatment the expression levels of the OXPPOS enzymes NADH:Ubiquinone oxidoreductase core subunits S1 and S2 (NDUFS1, NDUFS2; OXPPOS complex I) and cytochrome c oxidase subunits 6B1 and 4 (COX6B1, COX4; OXPPOS complex IV) are decreased in HeLa and SiHa cells. Conversely, expression levels the glycolytic enzymes hexokinase I and II (HKI, HKII), phosphofructokinase (PFKP) and glucose-6-phosphate isomerase (GPI) are increased by CPX. Interestingly, in SiHa cells the upregulation of PFKP is not as pronounced as in HeLa cells and GPI even is initially downregulated and upregulated only after 72 h. This cell type dependence could be due to metabolic differences between the cell lines.

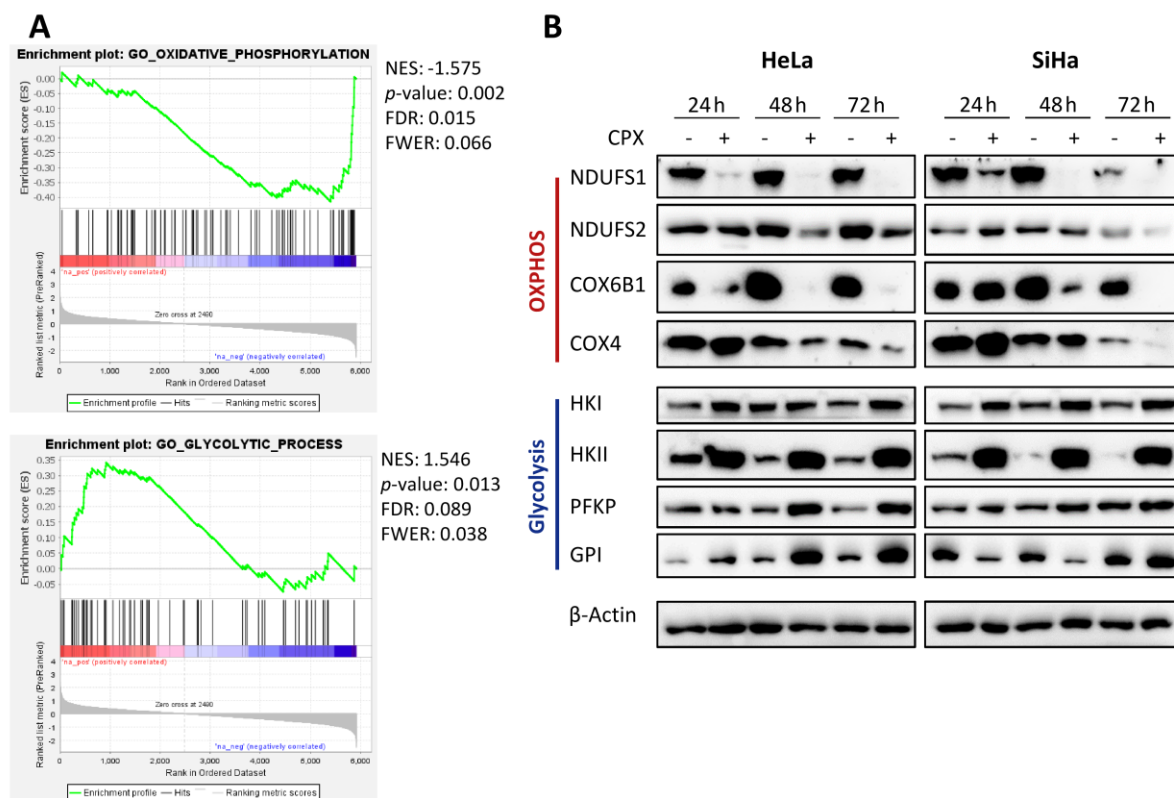


**Figure 15 | CPX upregulates factors involved in OXPPOS and downregulates factors involved in glycolysis. (A)** Data from the proteome screen in Figure 13 was analyzed via gene set enrichment analysis (GSEA). Enrichment plots of the gene sets “GO\_glycolytic\_process” and “GO\_oxidative\_phosphorylation” are shown. NES, normalized enrichment score; FDR, false discovery rate; F-WER, family-wise error rate. **(B)** Immunoblot analyses of HeLa or SiHa cells treated for 24, 48 or 72 h with 10 μM CPX (+) or EtOH (-) as solvent control. Protein levels of exemplary factors involved in OXPPOS or glycolysis were assessed. NDUFS1 and NDUFS2, NADH:Ubiquinone oxidoreductase core subunits S1 and S2; COX6B1 and COX4, cytochrome c oxidase subunits 6B1 and 4; HKI and HKII, hexokinase I and II; PFKP, phosphofructokinase, platelet isoform; GPI, glucose-6-phosphate isomerase; β-Actin, representative loading control.

These observations indicate that the anti-tumorigenic effects induced by CPX might (at least partly) be caused by OXPPOS inhibition and subsequent energy depletion, which cells aim to compensate with an increased glycolysis rate. To test if CPX upregulates glycolysis, glucose levels

were measured in the medium of HeLa cells treated with CPX or solvent control while cultured in medium containing either glucose levels physiological for human serum (1 g/L) or increased glucose levels (4.5 g/L) for 12, 24 or 48 h. The glucose measurements were performed in cooperation with Barbara Leuchs, DKFZ, Heidelberg. Surprisingly, there can be no difference detected and glucose levels decrease at a constant rate in treated and untreated cells (Figure 16A). However, when comparing the cell count which was determined in parallel, it can be observed that untreated cells continue proliferating, while the number of treated cells stays constant (Figure 16B). Thus under CPX treatment a lower number of cells consumes the same amount of glucose as a higher number of untreated cells. This becomes obvious when normalizing the consumed glucose to the cell number (Figure 16C). In light of these considerations CPX does indeed seem to enhance glycolytic rates.

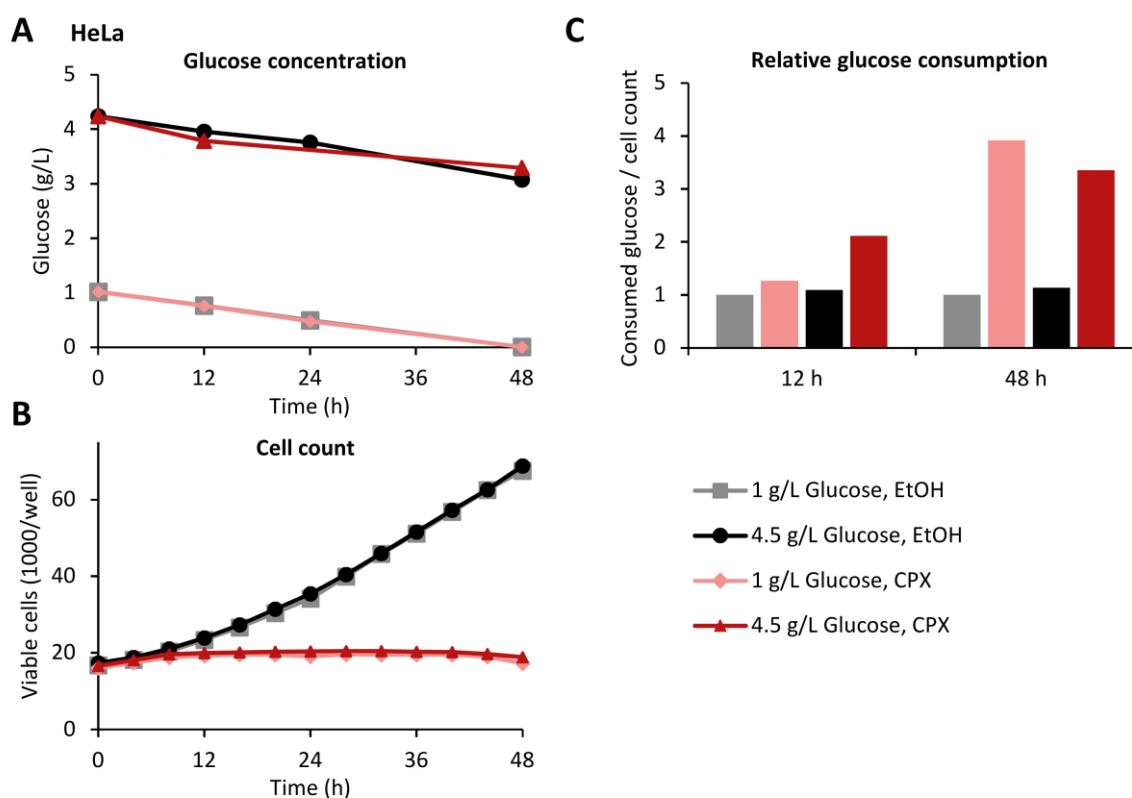


**Figure 16| CPX-treated cells exhibit an increased glucose consumption. (A)** HeLa mKate2 cells were treated with 10  $\mu$ M CPX or EtOH as solvent control in medium containing 1 g/L or 4.5 g/L glucose. After 12, 24 and 48 h glucose concentrations in the cell culture medium were measured using a Cedex Bio Analyzer. **(B)** In parallel to (A), cell counts were determined every 4 h via live-cell imaging. **(C)** Glucose consumption derived from (A) was normalized to cell counts from (B) to obtain the relative glucose consumption per cell.

### 2.2.1 Increased glucose levels partially revert anti-tumorigenic effects of CPX

The presented data indicates that CPX decreases energy production via OXPHOS, which the cells attempt to compensate for by increasing glycolysis. This raises the question if the CPX-induced effects are affected by differences in glucose supply. To test this, cells were treated with CPX in medium containing varying glucose concentrations. Standard cell culture medium containing

glucose levels of 1 g/L was compared to medium containing increased levels of glucose (4.5 g/L) or reduced levels of glucose (0.33 g/L) and to glucose deficient medium (0 g/L). Interestingly, it was found that increased glucose levels protect cells from the anti-tumorigenic effects induced by CPX. In immunoblot analyses, it could be shown that increasing glucose levels to 4.5 g/L counteracts both upregulation of the apoptosis marker cleaved PARP and downregulation of E7 protein levels by CPX (Figure 17A). Also at mRNA level increased glucose levels protect cells from CPX-mediated *E6/E7* downregulation (Figure 17B).

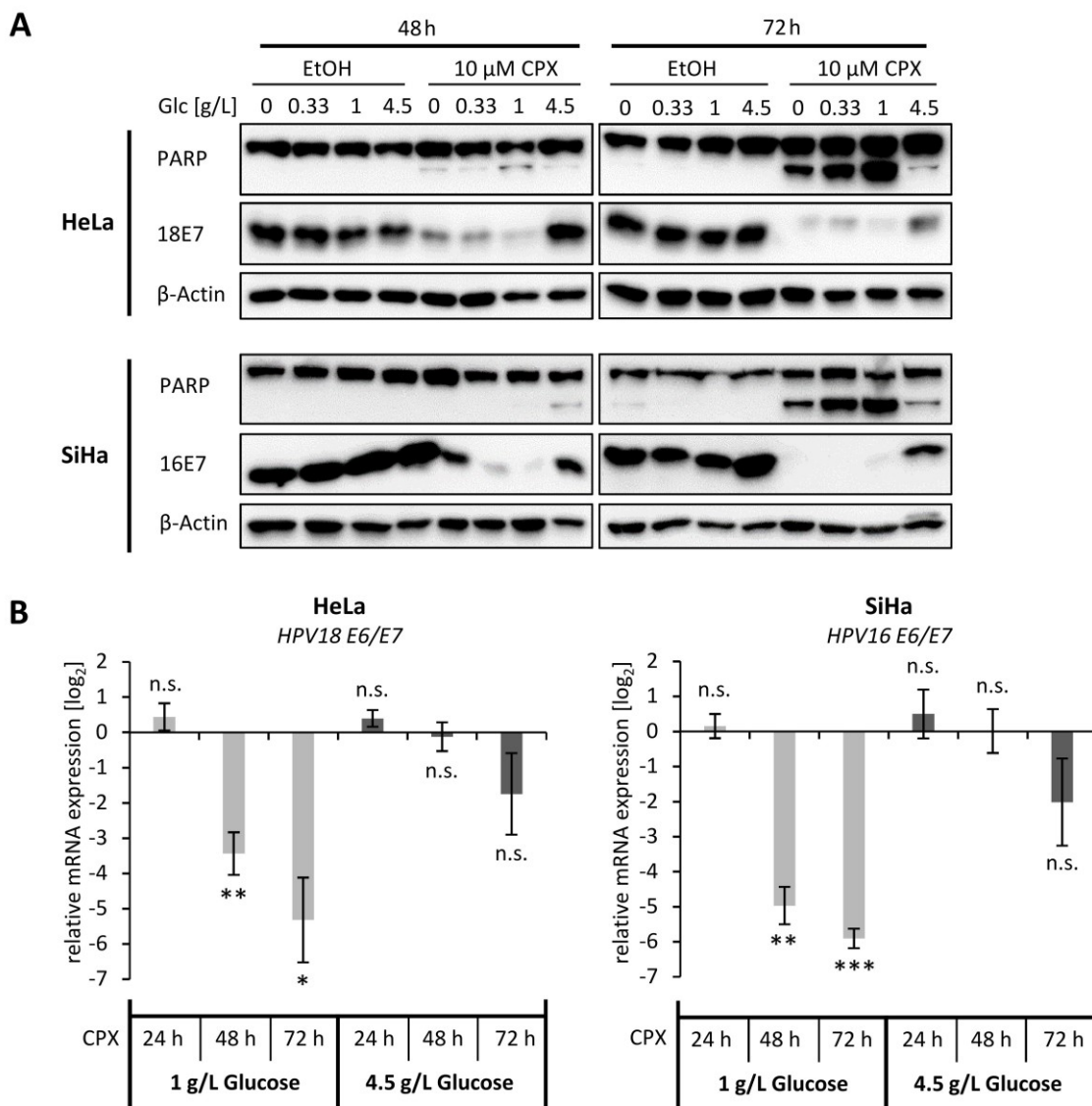


**Figure 17 | Increased glucose availability counteracts E6/E7 downregulation by CPX. (A)** Immunoblot analyses of PARP (upper bands), cleaved PARP (lower bands) and HPV18 or HPV16 E7 expression levels in HeLa or SiHa cells treated with 10  $\mu$ M CPX or solvent control (EtOH) for 48 or 72 h in the presence of the indicated amounts of glucose.  $\beta$ -Actin, loading control. Glc, glucose. **(B)** qRT-PCR analyses of *HPV18* or *HPV16 E6/E7* mRNA levels after treatment of HeLa or SiHa cells with 10  $\mu$ M CPX for 24, 48 or 72 h at 1 g/L or 4.5 g/L glucose in the medium. Expression levels were normalized to control cells for each time point and are depicted as  $\log_2$  fold changes. Error bars represent standard deviations of 3 independent experiments. Asterisks indicate statistically significant differences compared to EtOH-treated cells. n.s., non-significant; \* =  $p \leq 0.05$ ; \*\* =  $p \leq 0.01$ , \*\*\* =  $p \leq 0.001$ .

Decreased cleavage of PARP indicates that CPX-induced apoptosis can be counteracted by increasing glucose supply. In order to investigate this by an independent method, numbers of dead cells were determined in live-cell imaging experiments over a period of 144 h (Figure 18A). When cells were treated with CPX in medium containing 1 g/L glucose, cell death is induced after

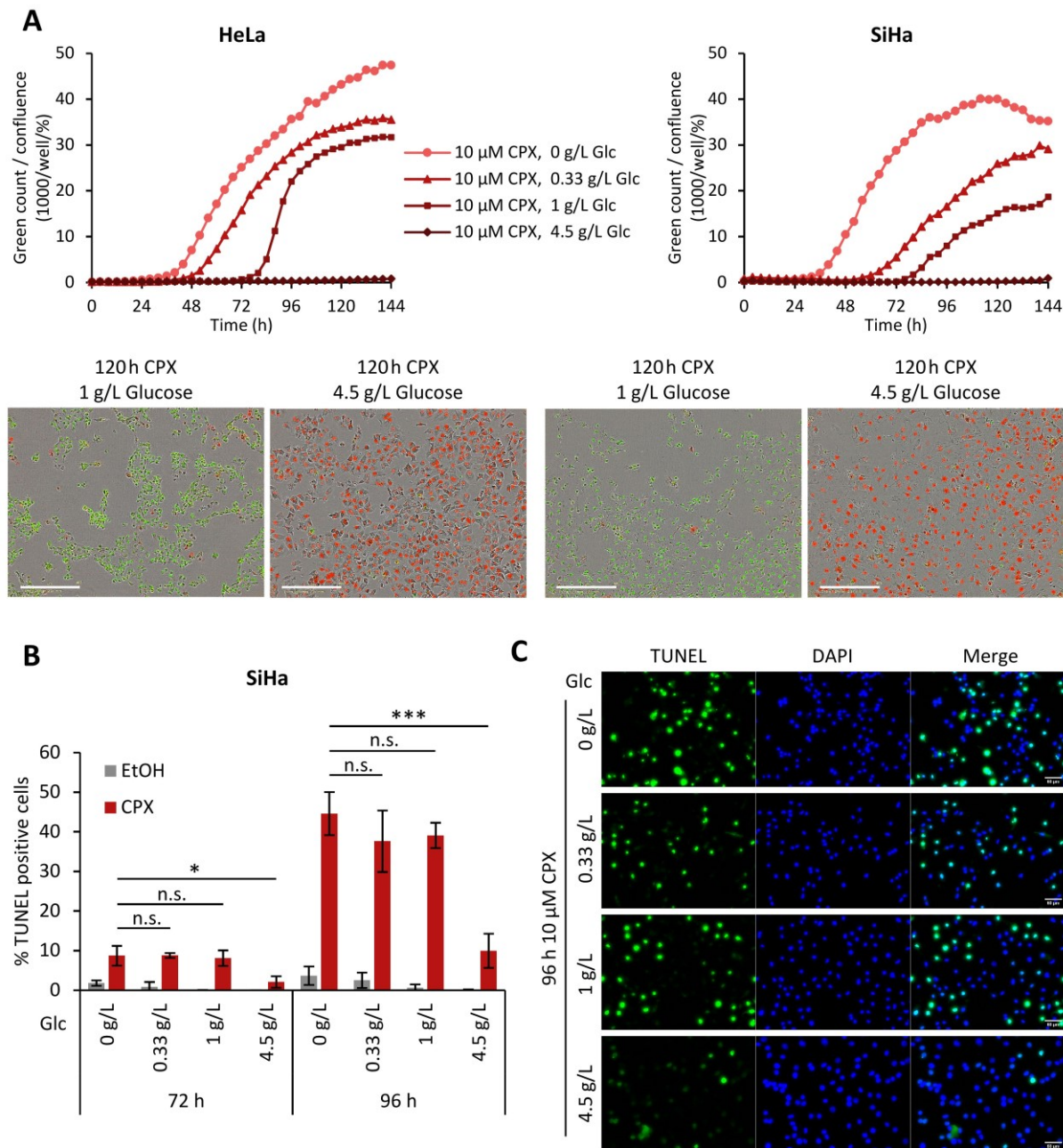


**Figure 18 | Increased glucose availability protects cells against CPX-induced apoptosis. (A)** For quantification of cell death, HeLa mKate2 or SiHa mKate2 cells were treated for 144 h with 10  $\mu$ M CPX under varying glucose levels in the presence of 100 nM IncuCyte<sup>®</sup> Cytotox Green Reagent. An image was acquired every 4 h and dead cells were quantified as green counts per well and normalized to the cell confluence in percent. Exemplary images after 120 h treatment are shown. Viable cells can be identified by red labeled nuclei, dead cells fluoresce green due to Cytotox activation. Scale bars: 400  $\mu$ m. **(B)** The percentage of TUNEL positive cells was determined in SiHa cells treated for 72 or 96 h with solvent control or 10  $\mu$ M CPX under the indicated glucose levels. Average values of three replicates are shown, error bars represent standard deviations. Asterisks indicate statistically significant differences between samples connected by horizontal lines. n.s., non-significant; \* =  $p \leq 0.05$ ; \*\*\* =  $p \leq 0.001$ . **(C)** Representative images of the TUNEL assays in (B), depicting cells after 96 h of CPX treatment. Scale bars: 50  $\mu$ m. Glc, glucose.

72-96 h, which can be completely prevented when cells are cultured in medium containing 4.5 g/L glucose. This is also demonstrated in exemplary images taken after 120 h: CPX-treated cells under 1 g/L glucose have lost membrane integrity and fluoresce green due to DNA binding of the Cytotox dye, while at the same time they have lost the red staining for viable cells. Under increased glucose concentrations (4.5 g/L) in contrast, cells remain viable as indicated by the red fluorescent nuclei and absence of green fluorescence. In line with this glucose dependency, reduced concentrations of glucose (0 g/L or 0.33 g/L) lead to an earlier and more pronounced induction of cell death by CPX. Finally, TUNEL assays detecting apoptosis-induced DNA strand breaks were performed in CPX-treated SiHa cells. Also the results from this assay support the previous finding that increased glucose levels counteract apoptosis induction by CPX since the number of TUNEL positive cells is strongly reduced under 4.5 g/L glucose (Figure 18B, C).

This poses the question which fate cells undergo instead of apoptosis when treated with CPX under glucose-replete conditions. Growth curves illustrating viable cell count reveal that cells treated with CPX at 4.5 g/L glucose do not proliferate anymore but instead cell numbers stay constant over several days (Figure 19A). In contrast, under lower glucose levels the number of viable cells decreases over time as cells die (please compare with Cytotox assays in Figure 18A). With colony formation assays (CFAs) the ability of single cells to grow into colonies after a specific treatment can be determined. When comparing colony formation capacity upon CPX treatment for 72 or 96 h under different glucose concentrations, no increased outgrowth of colonies could be observed under increased glucose levels (Figure 19B, upper panels). In SiHa cells there was even an increase in colony number under reduced glucose concentrations (0 and 0.33 g/L), while HeLa cells showed a non-linear dependency of colony formation capacity on glucose concentrations, with a minimum of colony outgrowth at 1 g/L.

Morphologically, CPX-treated cells cultured at 4.5 g/L glucose exhibit a typical senescent phenotype, with an enlarged and flattened shape and cytoplasmic extensions. Positive staining for the senescence marker senescence-associated  $\beta$ -galactosidase (SA- $\beta$ -gal) corroborates that CPX induces senescence under these experimental conditions after 48 (not shown), 72 or 96 h of treatment (Figure 19B, lower panels). Cells cultivated under lower glucose concentrations or in the absence of glucose (0 to 1 g/L glucose) also senesce in response to 48-72 h of CPX treatment, however after prolonged treatment they increasingly undergo apoptosis as demonstrated earlier. This is supported by the decreased number of surviving cells visible after 96 h of treatment. In strong contrast, cells cultured under glucose-replete conditions are protected from CPX-induced apoptosis and retain a senescent phenotype also after prolonged treatment.

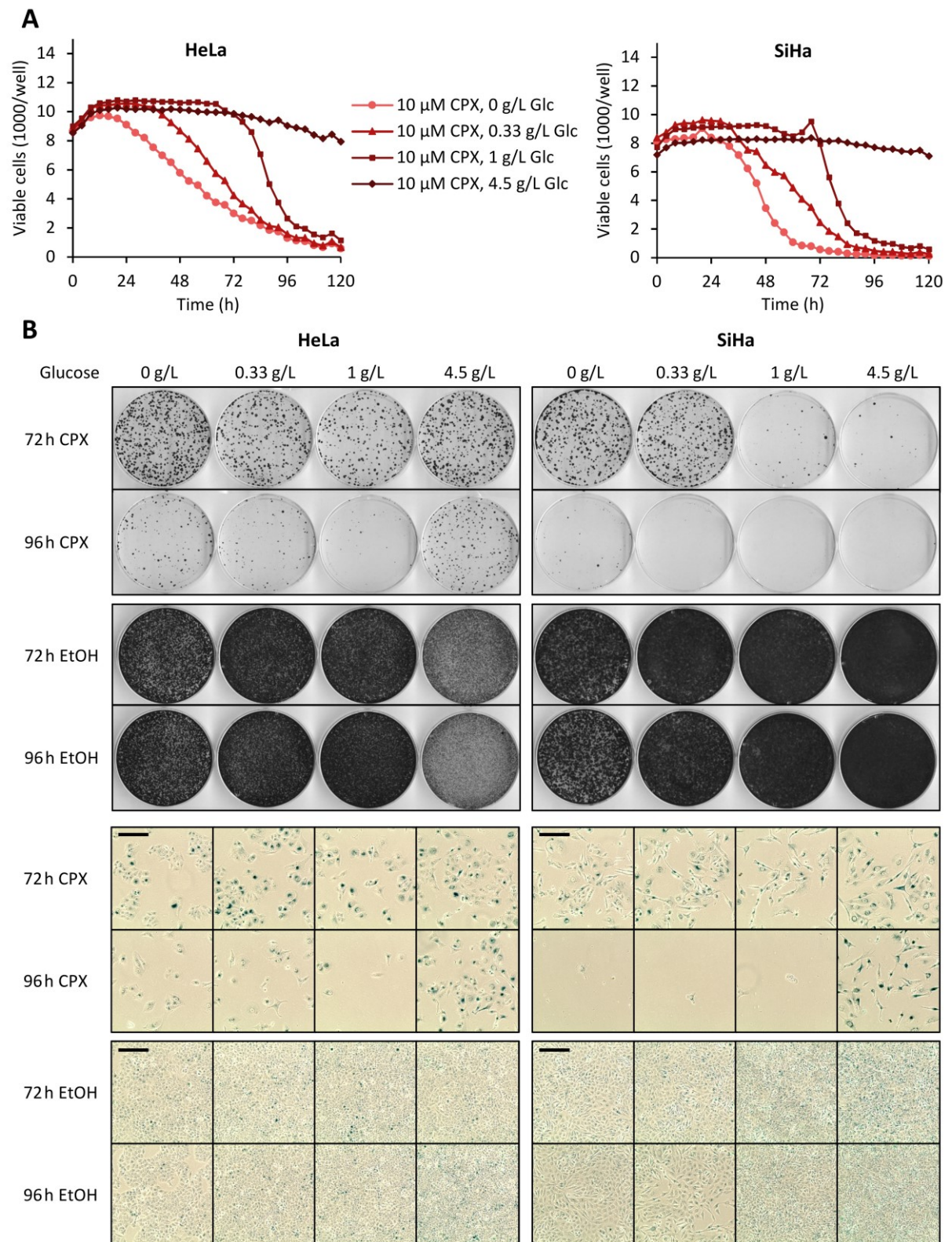


**Figure 19| Inhibition of cell proliferation by CPX is glucose-dependent. (A)** Growth curves of HeLa mKate2 or SiHa mKate2 cells that were treated with 10  $\mu$ M CPX under varying glucose concentrations. Every 4 h over the course of 120 h the number of viable cells was determined by counting red objects. **(B)** Colony formation assays (upper panels) or senescence assays (lower panels) of HeLa and SiHa cells treated with 10  $\mu$ M CPX or EtOH as solvent control for 72 or 96 h under the indicated glucose concentrations. Subsequently cells were split and grown in CPX-free medium containing 1 g/L glucose. Colony formation assays were fixed and stained after 12 days, SA- $\beta$ -gal assays were performed after 4 days. Sale bars: 200  $\mu$ m.

**2.2.2 Effect of glycolysis inhibition on the glucose-mediated apoptosis protection**

The data presented above indicates that increased levels of glucose can prevent CPX-induced apoptosis by allowing enhanced rates of glycolysis, which protects cells from death due to energy depletion. This would suggest that inhibition of glycolysis should revert the protective effect of increased glucose supply. To test this, glycolytic enzymes were downregulated via RNA interference while treating cells with CPX under 1 g/L or 4.5 g/L glucose. Downregulation of HKII, but not of PFKP or GPI restores sensitivity to CPX-induced apoptosis under 4.5 g/L glucose, as indicated by induction of the cleaved forms of PARP and caspase-9 (Figure 20A). Even

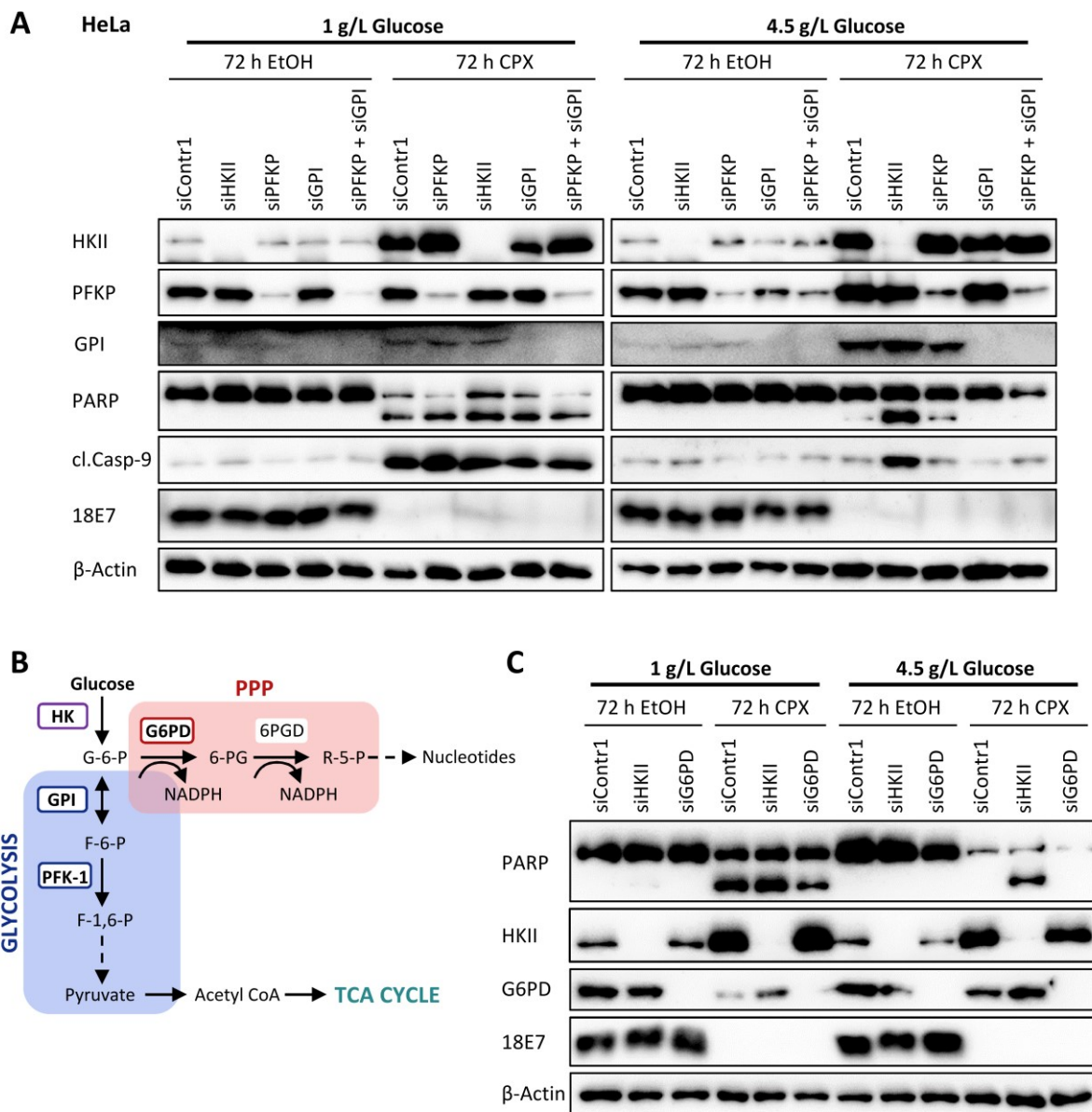


**Figure 20| Influence of glycolysis inhibition on the protective effects exerted by increased glucose levels. (A, C)** Immunoblot analyses of HeLa cells treated with CPX or EtOH for 72 h in medium containing 1 g/L or 4.5 g/L glucose under concomitant downregulation of the enzymes HKII, PFKP, GPI or G6PD with siRNA. cl. Casp-9, cleaved caspase-9. G6PD, glucose-6-phosphate dehydrogenase; β-Actin, representative loading control. **(B)** Schematic representation of the intersection of glycolysis and the pentose phosphate pathway (PPP). TCA cycle, tricarboxylic acid cycle.

simultaneous downregulation of both PFKP and GPI, which should inhibit glycolysis more efficiently cannot resemble the effect of HKII inhibition.

As seen in Figure 20B, HKII acts upstream of the intersection of glycolysis and the pentose phosphate pathway (PPP). Thus it was investigated if PPP inhibition would revert the protective effect of increased glucose levels by inhibiting glucose-6-phosphate-dehydrogenase (G6PD), the enzyme catalyzing the first and rate-limiting step of the PPP. However, also G6PD silencing could not reproduce the effect of HKII inhibition (Figure 20C). This suggests that the PPP is not relevant for the protective effect of increased glucose levels against CPX-induced apoptosis. Thus it remains to be elucidated what causes the discrepancy between inhibition of HKII and PFKP or GPI.

### **2.3 Insights into senescence and apoptosis induction by CPX**

While many established chemotherapeutic drugs induce apoptosis and/or senescence, only little is known about the factors determining this therapeutic outcome. The data presented above suggests glucose availability as a key determinant of this fate decision in CPX-treated cervical cancer cells. Thus, especially in regard of glucose dependence, it is of high interest to yield further insights on the one hand into CPX-induced senescence and on the other hand into the mechanisms governing the switch between senescence and apoptosis.

#### **2.3.1 CPX-induced senescence is irreversible**

Senescence is typically defined as a permanent growth arrest, however according to more recent results<sup>232</sup>, senescence rather can be regarded as a dynamic state and escape from senescence is possible. Furthermore, also diverse senescence-like states such as dormancy exist, which share many features with and are not always easy to discriminate from “real” senescence.

Therefore, to investigate if CPX-induced senescence is reversible, cells were released from treatment after 48 or 72 h and cell numbers were determined over several days via live-cell imaging. As can be seen in Figure 21A, cells treated with CPX for 72 h do not resume proliferation after release from treatment. In HeLa cells released from treatment after 48 h a minor amount of proliferation can be observed, indicating that after this treatment period not all cells are senescent yet, which is in accordance with the CFAs shown in Figure 19B. In SiHa cells also upon release after 48 h treatment no proliferation is observable, indicating a stable growth arrest. In contrast to CPX, the OXPHOS inhibitor metformin only induces a reversible growth arrest, allowing cells to resume proliferation as soon as they are released from treatment (Figure 21B).<sup>230</sup>

Thus, these results indicate that CPX-induced senescence is indeed irreversible, at least in the analyzed time frame.

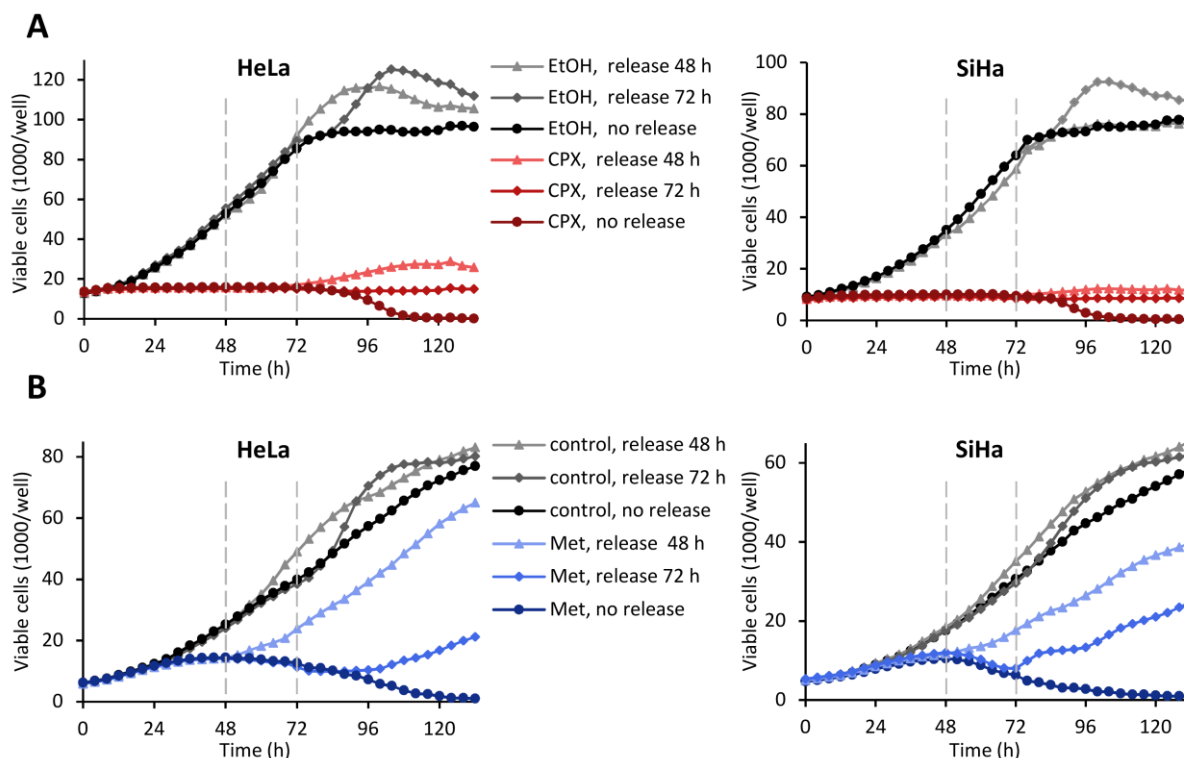


**Figure 21 | CPX induces an irreversible, metformin a reversible growth arrest.** Cell counts of HeLa and SiHa cells treated with 10  $\mu$ M CPX (A) or 2.5 mM metformin (Met) (B) were recorded over 132 h. Cells were either continuously cultured in medium containing drugs (red or blue circles) or released from treatment by changing to drug-free medium after 48 h (red or blue diamonds) or 72 h (red or blue triangles). The respective control cells were continuously grown in the absence of CPX or metformin, also with medium change after 48 h or 72 h, respectively. CPX treatment was performed at 1 g/L glucose, metformin treatment at 0.33 g/L glucose. Dashed vertical lines mark the time points for medium exchange after 48 h or 72 h. Figure (B) is modified from Hoppe-Seyler, Herrmann et al., 2021.

To further investigate release from CPX treatment, cells were treated with CPX for 72 h at 1 g/L or 4.5 g/L glucose and subsequently released from treatment for further 24-96 h (see scheme in Figure 22A). Positive staining for SA- $\beta$ -gal after 72 h of release confirms the induction of senescence (Figure 22B). Interestingly, many of the CPX-induced changes on protein expression are reversible upon release from treatment (Figure 22C). While cleaved PARP, indicative of apoptosis induction, is upregulated in cells harvested directly after 72 h CPX treatment at 1 g/L glucose, the cleaved product decreases after releasing the cells in CPX-free medium for 24-96 h. p53 and p21 are initially downregulated after treatment, but get strongly induced upon release from treatment, consistent with their important roles in senescence. Similarly, E7 downregulation is reversible on both protein level and mRNA level (Figure 22D). Increased glucose levels (4.5 g/L) mostly counteract the CPX-induced alterations on protein level, but also under these conditions the regulation of e.g. E7 or p21 upon release is similar as under 1 g/L glucose. These results show that certain proteins such as factors implicated in DNA damage repair are only regulated transiently upon CPX treatment, which is however sufficient to initiate downstream signaling cascades such as sustained p53-p21 signaling.

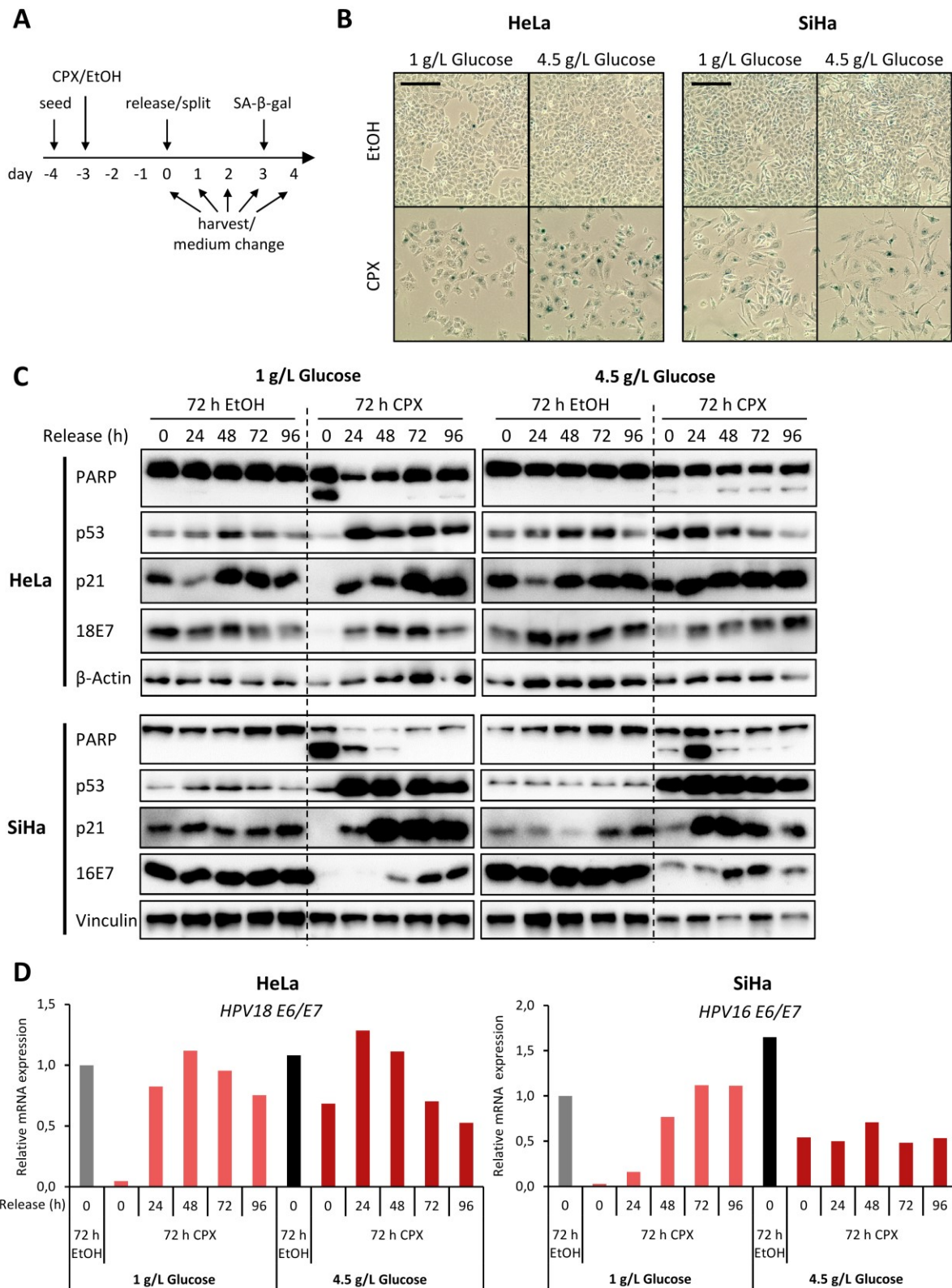


**Figure 22 | Release from CPX treatment.** (A) Scheme of the experimental setup: cells were treated with 10  $\mu$ M CPX for 72 h under in medium containing 1 g/L or 4.5 g/L glucose. Subsequently cells were released from treatment in CPX-free medium containing 1 g/L, which was renewed daily and harvested after 0-96 h. Alternatively, cells were split for senescence assays after treatment. (B) SA- $\beta$ -gal assays were performed after release for 72 h. Scale bars, 200  $\mu$ m. (C) Immunoblot analyses of (cleaved) PARP, p53, p21 and E7.  $\beta$ -Actin or Vinculin, representative loading controls. (D) Relative mRNA expression levels of *HPV18* or *HPV16 E6/E7* corresponding to the protein analyses in (C).

### 2.3.2 CPX-dependent regulation of factors involved in senescence and apoptosis

In order to gain deeper insights into CPX-induced senescence and apoptosis induction and the switch between these states, the regulation of potential senescence- and apoptosis-involved factors was investigated under 1 g/L and 4.5 g/L glucose. On protein level, glucose-dependent differences in the CPX-mediated regulation of several factors involved in senescence and/or apoptosis can be observed (Figure 23). In line with the results described in 2.2.1, apoptotic markers, such as cleaved PARP and cleaved caspase-9 are induced upon CPX treatment at 1 g/L glucose, but not at 4.5 g/L glucose. Similarly, also E7 downregulation is counteracted by increased levels of glucose. In contrast, markers of DNA damage such as the phosphorylated forms of p53 (P-Ser15) and RPA32 (P-Ser33) are upregulated by CPX independent of the glucose concentration. Also downregulation of p62 (SQSTM1), which is regarded as crucial step for SASP development<sup>173</sup>, occurs in a glucose-independent manner. In contrast, protein levels of p53, p21 and E2F1 are repressed upon CPX treatment at 1 g/L glucose, while increased glucose levels (4.5 g/L) counteract this downregulation. These three factors are involved in senescence (and apoptosis) regulation and thus could be interesting candidates for investigating their role in the glucose-dependent switch from senescence to apoptosis upon CPX treatment.

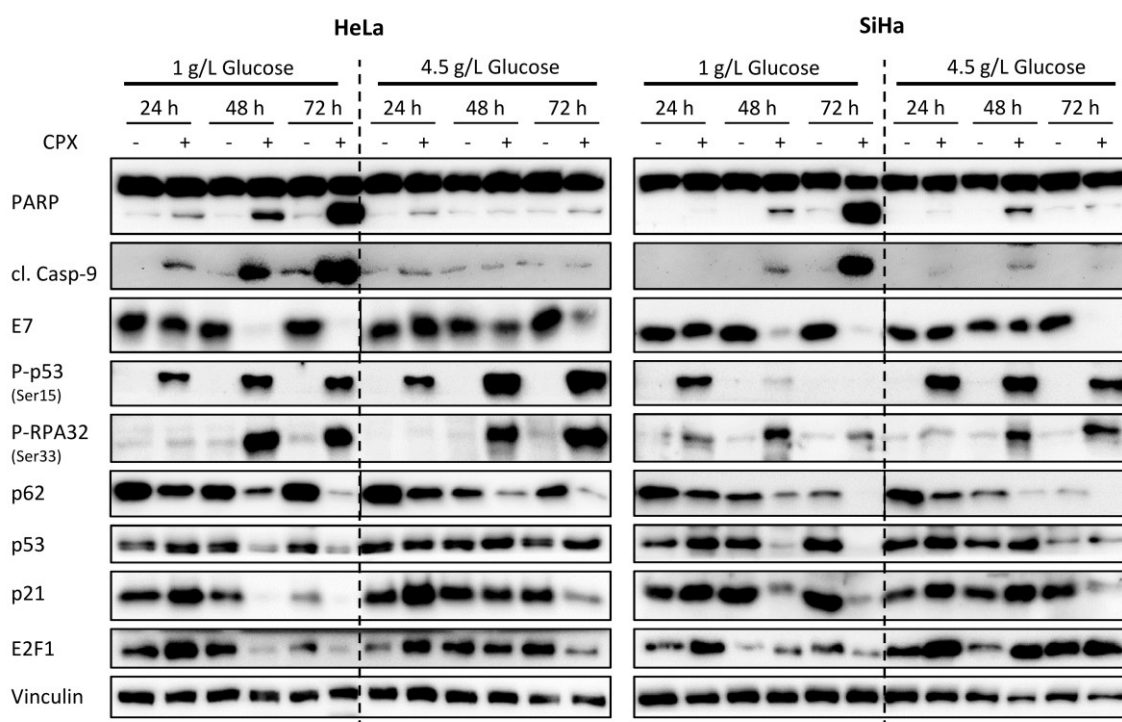


**Figure 23** | Regulation of senescence and apoptosis-related factors by CPX under different glucose conditions. Immunoblot analyses of HeLa or SiHa cells treated for 24, 48 or 72 h with 10  $\mu$ M CPX (+) or solvent control (-) in medium containing 1 g/L or 4.5 g/L glucose. cl. Casp-9, cleaved caspase-9. Vinculin, representative loading control.

Hence it was tested if silencing of either E2F1, p21 or p53 can push cells treated with CPX under increased glucose supply from a senescent towards a more apoptotic response. Knockdown of

neither of the factors did increase PARP cleavage compared to control siRNA, indicating that silencing of E2F1, p21 or p53 cannot re-sensitize cells to CPX-induced apoptosis under conditions of glucose abundance (Figure 24A).

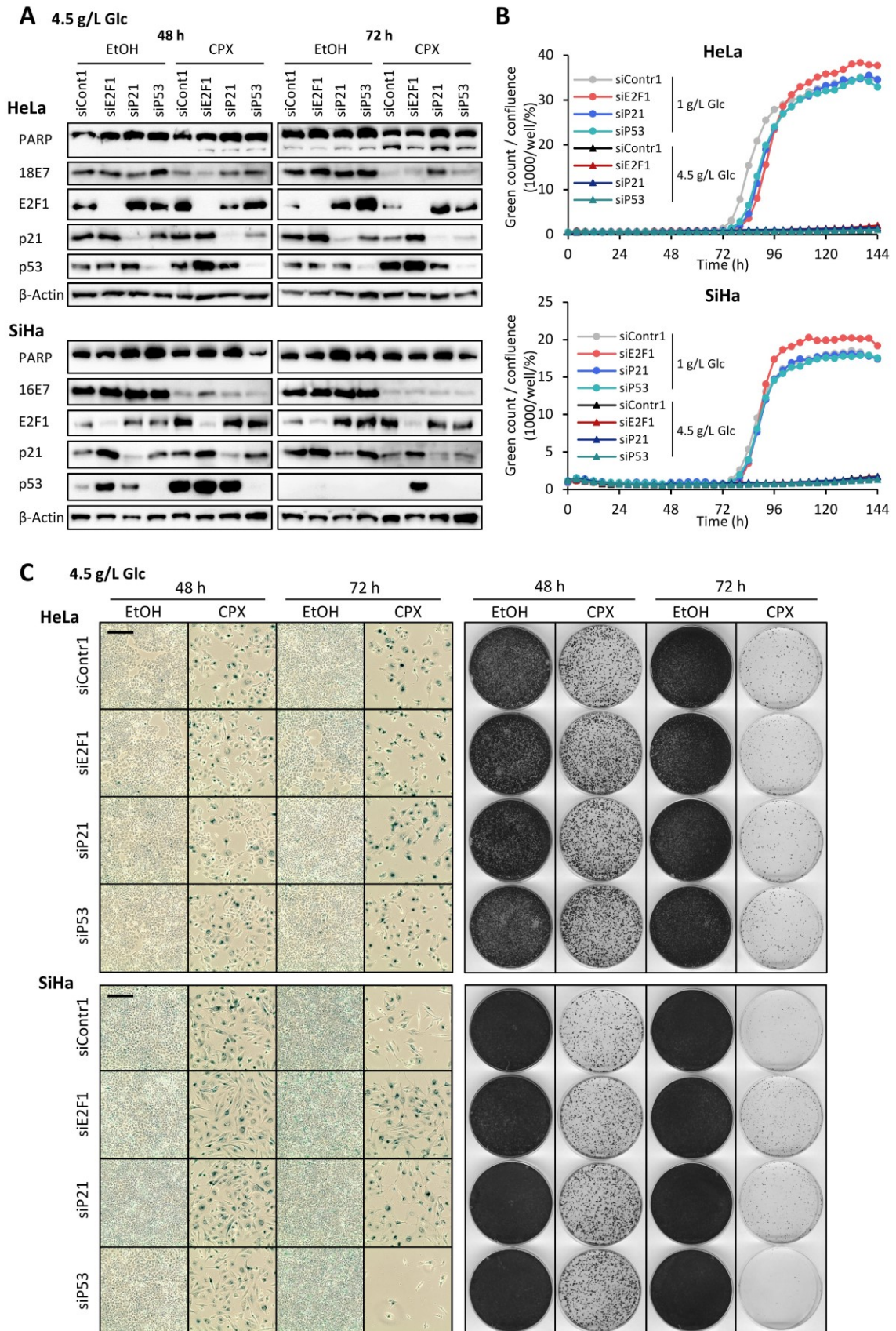


Figure 24 | (see legend on next page)

(see figure on previous page)

**Figure 24 | Influence of E2F1, p21 and p53 on CPX-induced senescence and apoptosis. (A)** Immunoblot analyses of HeLa or SiHa cells transfected with the indicated siRNAs and treated for 48 or 72 h with 10  $\mu$ M CPX or solvent control (EtOH) in medium containing 4.5 g/L glucose.  $\beta$ -Actin, representative loading control; Glc, glucose. **(B)** Cytotoxicity assays of HeLa mKate2 or SiHa mKate2 cells that were transfected with the indicated siRNAs and treated for 144 h with 10  $\mu$ M CPX in medium containing 1 g/L or 4.5 g/L glucose in the presence of 100 nM IncuCyte<sup>®</sup> Cytotox Green Reagent. Images were acquired every 4 h and dead cells were quantified as green counts per well and normalized to the cell confluence in percent. **(C)** Concomitant senescence assays and CFAs to (A). Cells were split after 48 or 72 h and cultured in drug free medium (1 g/L glucose) for 4 days before performing SA- $\beta$ -gal assays or for 12 days before fixing and staining colonies. Scale bars, 200  $\mu$ m.

Accordingly, in live-cell imaging experiments no cell death can be detected in cells treated with CPX under 4.5 g/L glucose, despite knockdown of E2F1, p21 or p53 (Figure 24B). In contrast, at 1 g/L glucose in the medium CPX induces cell death after 72-96 h, again independent of E2F1, p21 or p53 expression. Also senescence induction is not impaired by downregulation of any of the three proteins, despite their central roles in this pathway. In HeLa cells, no differences can be observed in senescence assays and CFAs, while in SiHa cells E2F1 or p21 silencing even leads to an increase in surviving senescent cells and colony outgrowth (Figure 24C). In conclusion, none of the investigated proteins seems to be crucial for the glucose-dependent senescence-to-apoptosis switch under CPX treatment, at least not as an isolated factor.

Furthermore, qRT-PCR analyses indicate that regulation of senescence-associated genes upon CPX treatment at the transcript level occurs mostly independent of glucose concentration (Figure 25). The SASP factors *IL1A* and *IL6* are upregulated, as are the pro-senescent factors *CDKN1A* (p21) and *SERPINE1* (PAI-1), while the anti-senescent factors *ID1* and *CCNB1* (Cyclin B1) are downregulated upon CPX treatment, with only subtle differences between the two glucose concentrations.

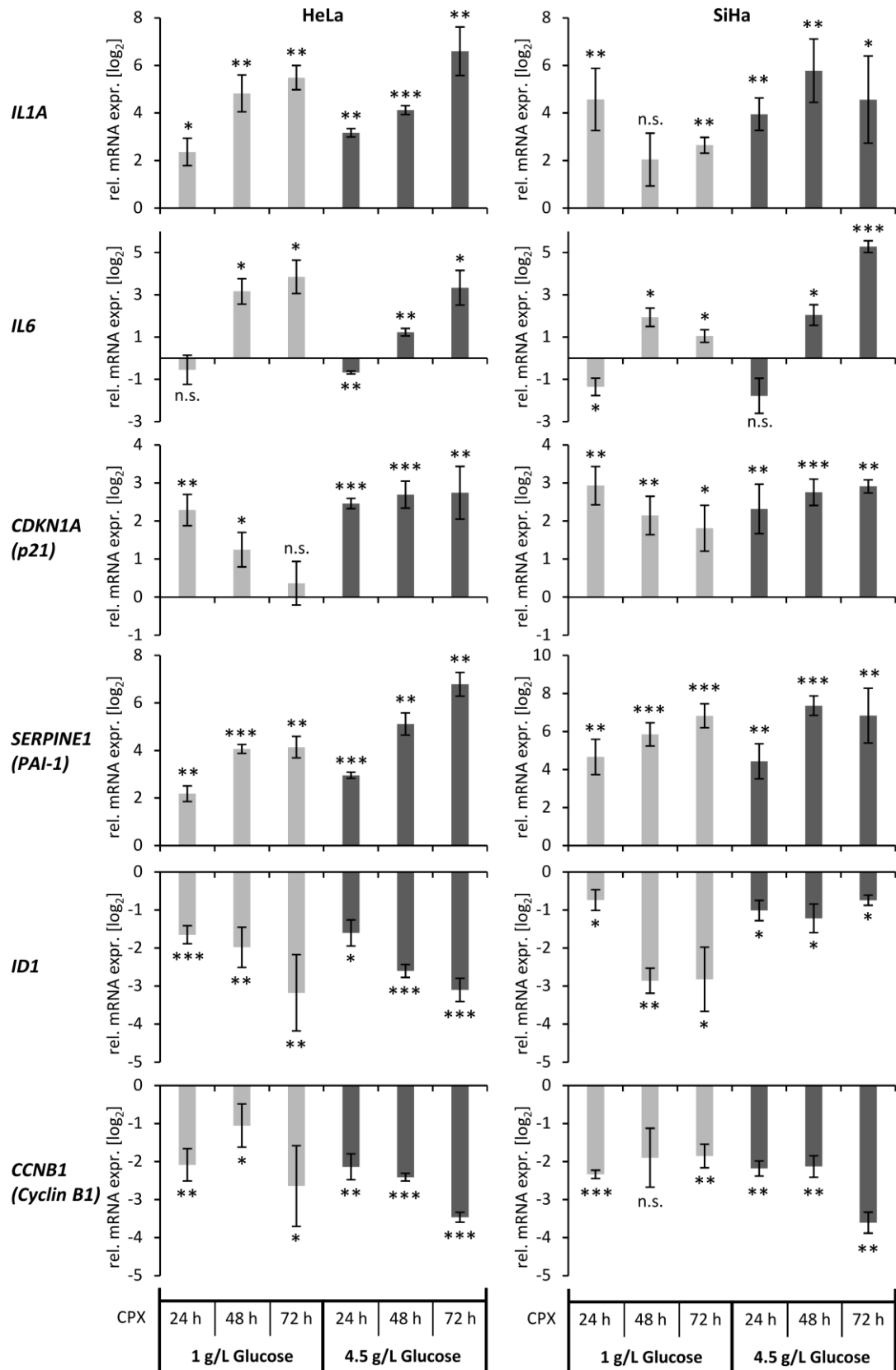


**Figure 25| CPX-mediated regulation of senescence-associated factors on mRNA level.** qRT-PCR analyses determining relative mRNA expression levels of senescence associated factors in HeLa (left panels) or SiHa (right panels) cells after 24, 48 or 72 h treatment with 10  $\mu$ M CPX at 1 g/L or 4.5 g/L glucose. Expression levels were normalized to control (EtOH) treated cells for each time point and are depicted as log<sub>2</sub> fold changes. Error bars represent standard deviations of 3-4 independent experiments. Asterisks indicate statistically significant differences compared to EtOH-treated cells. n.s., non-significant; \* =  $p \leq 0.05$ ; \*\* =  $p \leq 0.01$ , \*\*\* =  $p \leq 0.001$ .

### 2.3.3 Comparison of CPX with other OXPHOS inhibitors

In order to investigate if the glucose-dependent regulation of senescence and apoptosis induction is linked to the capacity of CPX to inhibit oxidative phosphorylation, the effects caused by CPX treatment were compared to those of established inhibitors of OXPHOS. Metformin, which is a widely used anti-diabetic, inhibits mitochondrial complex I and has potential to be repurposed as cancer therapeutic. Interestingly, like CPX also metformin efficiently suppresses E6 and E7 protein levels, which can be counteracted by increasing glucose supply (Figure 26A). This glucose dependence is corroborated by growth curve analyses: whereas metformin under increased glucose concentrations (4.5 g/L) causes hardly any growth inhibition, at lower glucose levels (1 g/L or 0.33 g/L) metformin strongly suppresses proliferation of HPV-positive tumor cells (Figure 26B).

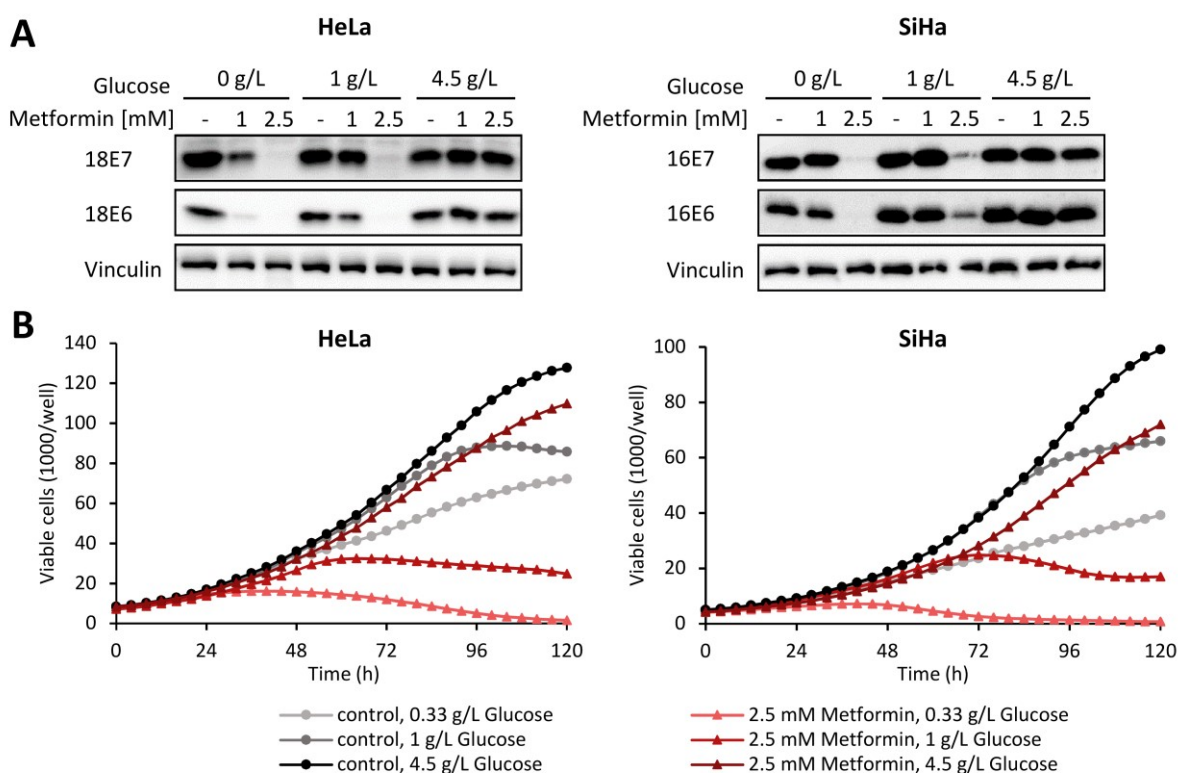


**Figure 26 | Metformin glucose-dependently represses E6/E7 and inhibits proliferation of cervical cancer cells.** (A) Immunoblot analyses of HPV18 or HPV16 E7 and E6 in HeLa or SiHa cells treated with the indicated doses of metformin for 24 h. Vinculin, representative loading control. Figure (A) is modified from Hoppe-Seyler, Herrmann et al., 2021. (B) Growth curves of HeLa mKate2 or SiHa mKate2 cells treated with 2.5 mM metformin in presence of the indicated glucose levels. Over the course of 120 h every 4 h viable cell count was assessed.

For investigation of apoptosis induction rotenone and antimycin A were included, two well-characterized OXPHOS inhibitors which are specific for complex I or III, respectively, but which may not be used clinically. Like CPX, the three other OXPHOS inhibitors induce apoptosis in HPV-positive tumor cells, as indicated by an increase in PARP cleavage and induction of cytotoxicity. Rotenone and metformin treatment in medium containing 1 g/L glucose leads to the induction of PARP cleavage which – analogous to CPX – can be counteracted by increased glucose supply

(4.5 g/L) (Figure 27A). While antimycin A also induced PARP cleavage in HeLa cells at 1 g/L glucose, this could not be observed in SiHa cells, possibly due to the fact that prolonged treatment with this drug downregulates total PARP levels due to unknown reasons.

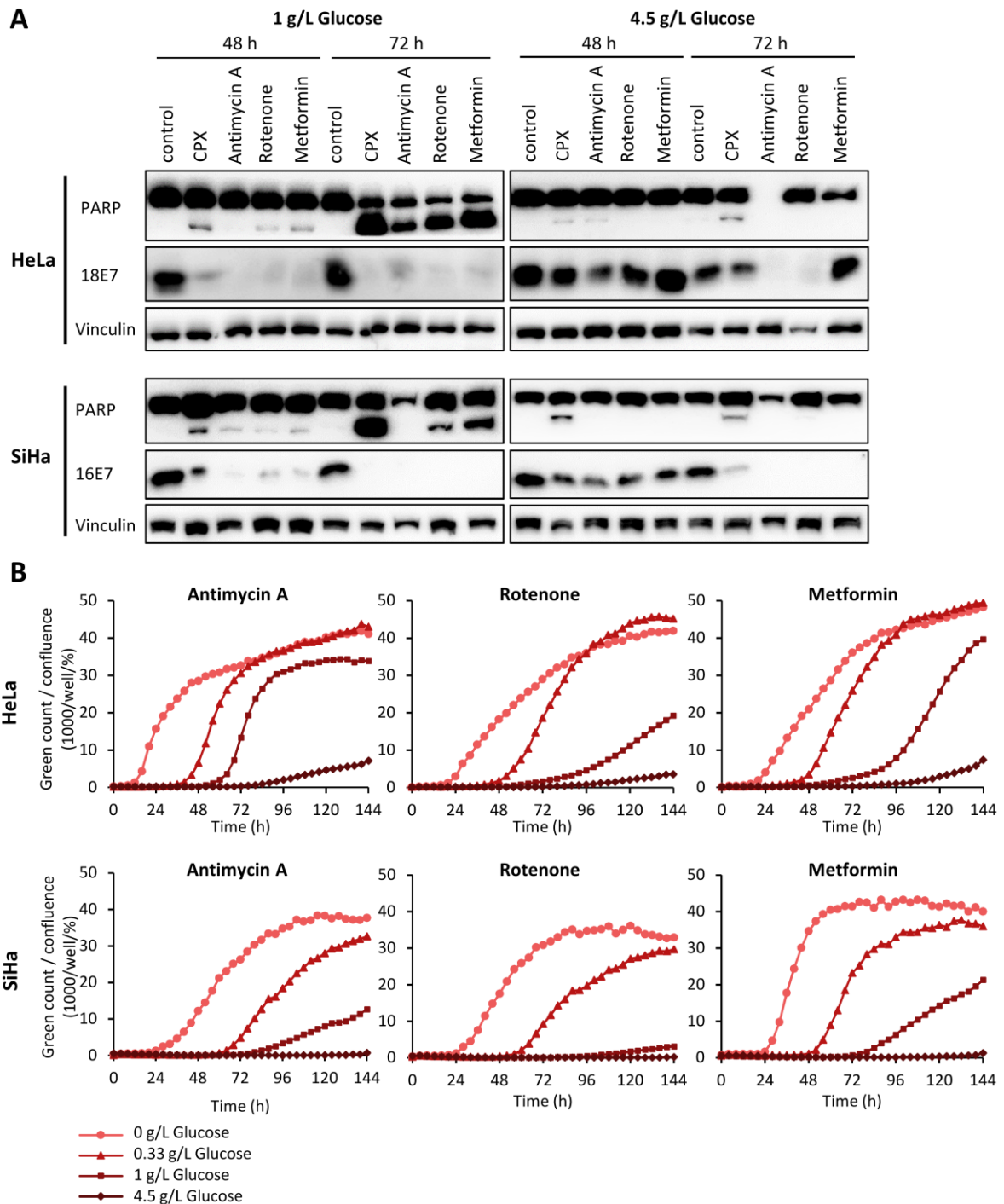


**Figure 27 | OXPHOS inhibitors glucose-dependently induce apoptosis in cervical cancer cells. (A)** Immunoblot analyses of (cleaved) PARP and HPV18 or HPV16 E7 levels in HeLa or SiHa cells after 48 or 72 h of treatment with the indicated OXPHOS inhibitors at 1 g/L or 4.5 g/L glucose in the medium. The following drug concentrations were used: 10  $\mu$ M CPX, 5 nM (HeLa)/10 nM (SiHa) antimycin A, 20 nM rotenone, 2.5 mM (HeLa)/7.5 mM (SiHa) metformin. Vinculin, representative loading control. **(B)** HeLa mKate2 or SiHa mKate2 cells were treated for 144 h with the indicated drugs under varying glucose levels in the presence of 100 nM IncuCyte<sup>®</sup> Cytotox Green Reagent. Via live cell imaging, green counts indicating dead cells were quantified every 4 h and normalized to cell confluence. The following drug concentrations were used: 10 nM antimycin A, 20 nM rotenone, 2.5 mM (HeLa)/5 mM (SiHa) metformin.

The glucose dependency of antimycin A, rotenone and metformin can also be observed by monitoring the induction of cytotoxicity under varying glucose concentrations. All three OXPHOS inhibitors induce cell death under 1 g/L glucose, which can be accelerated by further limiting glucose availability (0 g/L or 0.33 g/L) (Figure 27B). In contrast, under glucose-replete conditions (4.5 g/L) hardly any induction of cell death can be detected, analogous to CPX (Figure 18A). Moreover, as seen for CPX and metformin, also antimycin A and rotenone suppress expression of E7 protein, which again is delayed by increasing glucose availability (Figure 27A).

In respect to senescence induction, clear differences between CPX and the other tested OXPHOS inhibitors were observed. As seen before (Figure 19), CPX treatment leads to efficient induction of senescence independent of glucose concentrations, as indicated by many cells exhibiting morphological signs of senescence and staining positive for SA- $\beta$ -gal activity. In contrast, after treatment with antimycin A, rotenone or metformin only few cells stain SA- $\beta$ -gal positive at 1 g/L glucose and no SA- $\beta$ -gal positive cells can be detected under 4.5 g/L glucose (Figure 28A).

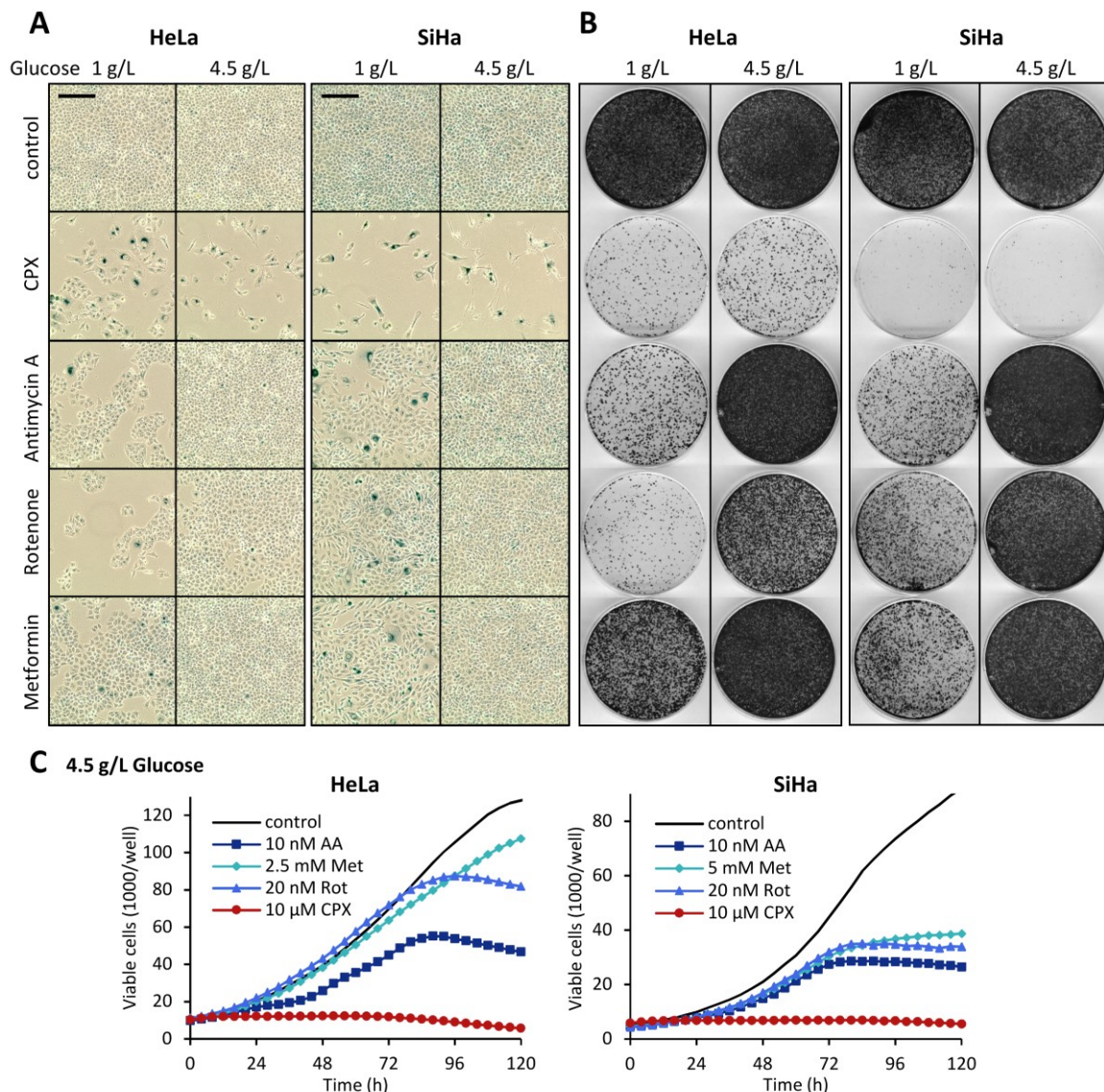


Figure 28 | (see legend on next page)

(see figure on previous page)

**Figure 28 | The capacity of CPX to induce senescence under increased glucose availability is not shared by other OXPHOS inhibitors. (A)** Senescence assays of HeLa or SiHa cells treated with the indicated OXPHOS inhibitors for 72 h at 1 g/L or 4.5 g/L glucose in the medium. Before SA- $\beta$ -gal assays were performed, cells were released in drug-free medium containing 1 g/L glucose for 4 days. The following drug concentrations were used: 10  $\mu$ M CPX, 2 nM (HeLa)/5 nM (SiHa) antimycin A (AA), 20 nM rotenone (Rot), 2.5 mM (HeLa)/7.5 mM (SiHa) metformin (Met). Scale bars: 200  $\mu$ m. **(B)** Concomitant CFAs to (A), cells were released for 11 days before fixing and staining colonies. **(C)** Growth curves of HeLa mKate2 or SiHa mKate2 cells treated with the indicated drugs in medium containing 4.5 g/L glucose, corresponding to Cytotox measurements in Figure 27. Over the course of 120 h every 4 h viable cell number was determined by counting red fluorescent cells.

CFAs corroborate this lack of senescence induction, as cells treated with the three compounds under glucose-replete conditions (4.5 g/L) are not or only mildly impaired in their colony forming capacity (Figure 28B). Also growth curves performed at 4.5 g/L glucose show that cells treated with antimycin A, rotenone or metformin grow nearly unrestricted for about 72 h, until glucose availability is decreased and proliferation is halted (Figure 28C). In contrast, CPX-treated cells are not able to form colonies or proliferate even under glucose-replete conditions.

Collectively, these results indicate that apoptosis induction by CPX likely is mediated via OXPHOS inhibition, whereas the induction of senescence is probably independent of the OXPHOS inhibiting capacity.

### **2.3.4 Comparison of CPX with other iron chelators**

To further investigate the mechanism behind the glucose dependence of senescence or apoptosis induction, CPX was compared to the two structurally unrelated iron chelators DFX and DFO. As seen for CPX and the other OXPHOS inhibitors, also DFX and DFO induce apoptosis at 1 g/L glucose as indicated by PARP cleavage (Figure 29A) and in cytotoxicity assays (Figure 29B), which can be counteracted by increasing glucose supply (4.5 g/L). This is plausible, as iron chelators generally also inhibit OXPHOS. Notably and in contrast to antimycin A, rotenone and metformin, treatment with DFX, DFO or CPX results in induction of senescence also in glucose-replete conditions, as characterized by positive SA- $\beta$ -gal staining and corroborated by a decreased colony forming capacity (Figure 29C).

Thus, both the induction of senescence and apoptosis by CPX are probably dependent on its capacity to chelate intracellular iron.

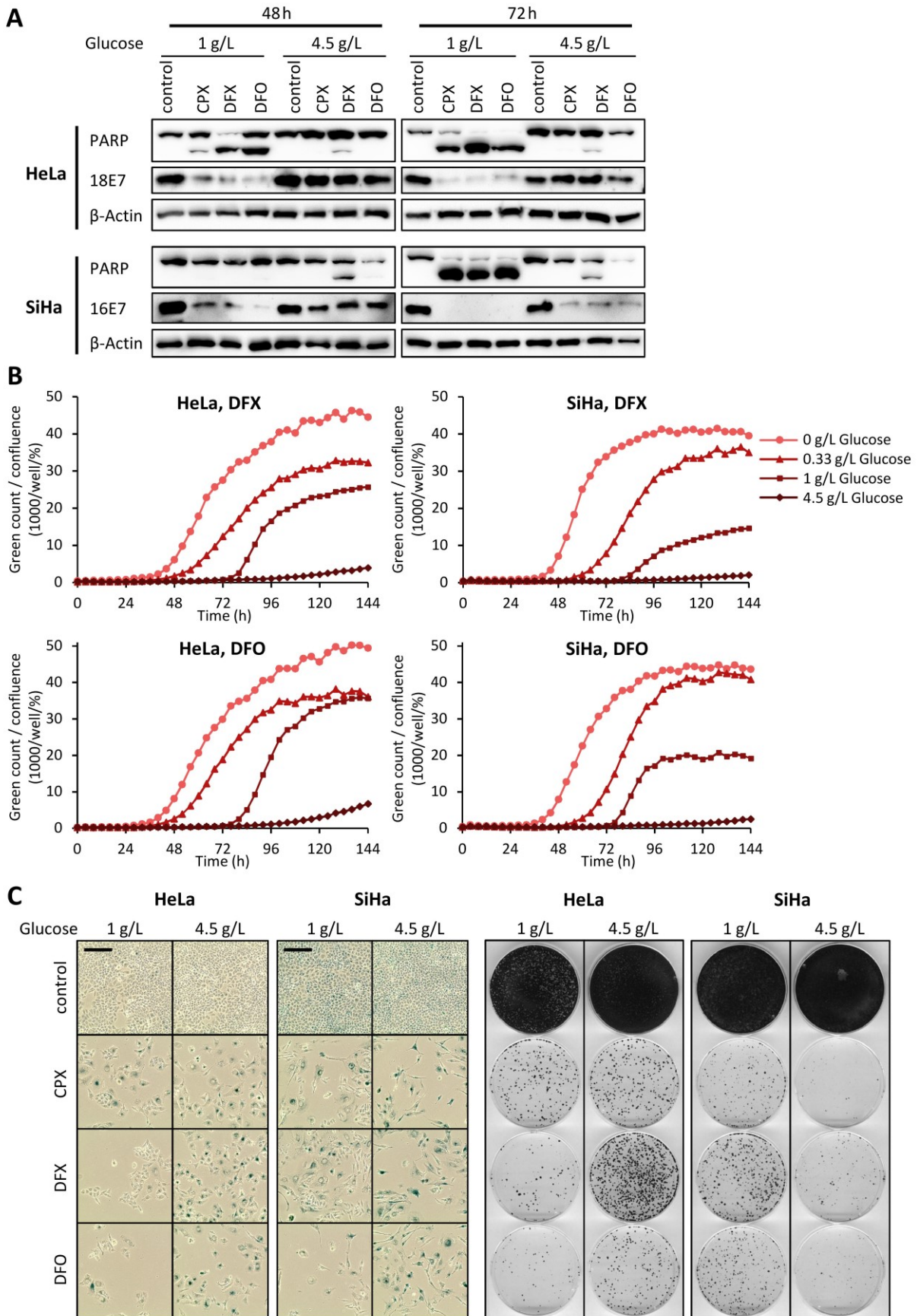


Figure 29 | (see legend on next page)

(see figure on previous page)

**Figure 29| Iron chelators induce apoptosis in a glucose-dependent manner and act pro-senescent under increased glucose availability.** (A) Immunoblot analyses of (cleaved) PARP and HPV18 or HPV16 E7 in HeLa or SiHa cells treated with iron chelators at 1 g/L or 4.5 g/L glucose in the medium for 48 or 72 h.  $\beta$ -Actin, loading control. (B) Cytotox assay of HeLa mKate2 or SiHa mKate2 cells treated with DFX or DFO over the course of 144 h under the indicated glucose concentrations. Green object counts indicating dead cells were assessed every 4 h and normalized to cell confluence in percent. (C) Senescence assays and CFAs of HeLa or SiHa cells treated with the indicated iron chelators for 72 h under 1 g/L or 4.5g/L glucose. Cells were released in drug-free medium for further 4 days before performing SA- $\beta$ -gal assays or for 13 days before fixing and staining colonies. Scale bars: 200  $\mu$ m. The following drug concentrations were used: 10  $\mu$ M CPX, 50  $\mu$ M DFX, 100  $\mu$ M DFO.

## 2.4 CPX regulates Notch signaling

One of the highest ranked differentially regulated proteins ( $\log_2FC = +2.0$ ) from the proteome screen was Notch1, which is of particular interest given the glucose dependence of CPX, since Notch has been shown to activate glycolysis and induce a Warburg phenotype.<sup>233</sup> Depending on the cellular context, Notch1 can be regarded as tumor suppressor or oncogene, however in epithelial tissues including squamous cell carcinoma (SCC) it is commonly believed to act tumor-suppressive<sup>150</sup>. This indicates that upregulation of Notch signaling could play a role for the anti-tumorigenic effects of CPX.

Consistent with the proteomics results, also in immunoblot analyses an upregulation of Notch1 intracellular domain (NICD), the active, cleaved form of Notch1, could be observed after 24 or 48 h CPX treatment (Figure 30A). Over time, NICD levels in untreated cells increase, probably due to the increase in cell confluence. Also on mRNA level *NOTCH1* was upregulated by CPX as demonstrated by qRT-PCR analyses (Figure 30B).

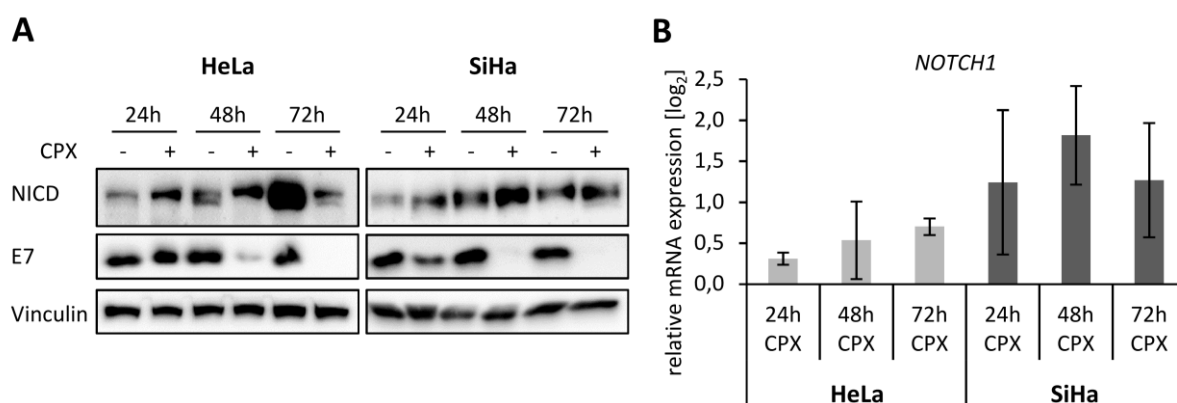


**Figure 30| CPX upregulates Notch1.** (A) Immunoblot analyses of Notch1 intracellular domain (NICD) and HPV18 or HPV16 E7 in HeLa or SiHa cells after treatment with 10  $\mu$ M CPX (+) or EtOH (-) as solvent control for 24, 48 or 72 h. Vinculin, loading control. (B) Expression levels of *NOTCH1* mRNA upon treatment with 10  $\mu$ M CPX for 24-72 h were determined via qRT-PCR. Mean  $\log_2FC$  values relative to EtOH-treated cells are depicted. Error bars represent standard deviations of 3 independent experiments.

Further analyses were performed in SiHa cells, as this cell line was used for the proteome measurements and also exhibits higher Notch1 expression levels than HeLa. To ensure functionality of the Notch signaling pathway, protein levels of Notch1 and NICD were assessed via immunoblot in cells treated with CPX and/or DAPT (*N*-[*N*-(3,5-difluorophenacetyl)-l-alanyl]-*S*-

phenylglycine t-butyl ester) (Figure 31A). DAPT is a  $\gamma$ -secretase inhibitor and prevents cleavage of Notch1 at S3 to release the NICD. As expected, it was observed that CPX upregulates protein levels of Notch1 and the NICD and that DAPT treatment prevents S3-cleavage of Notch1 and thus NICD is not induced anymore.

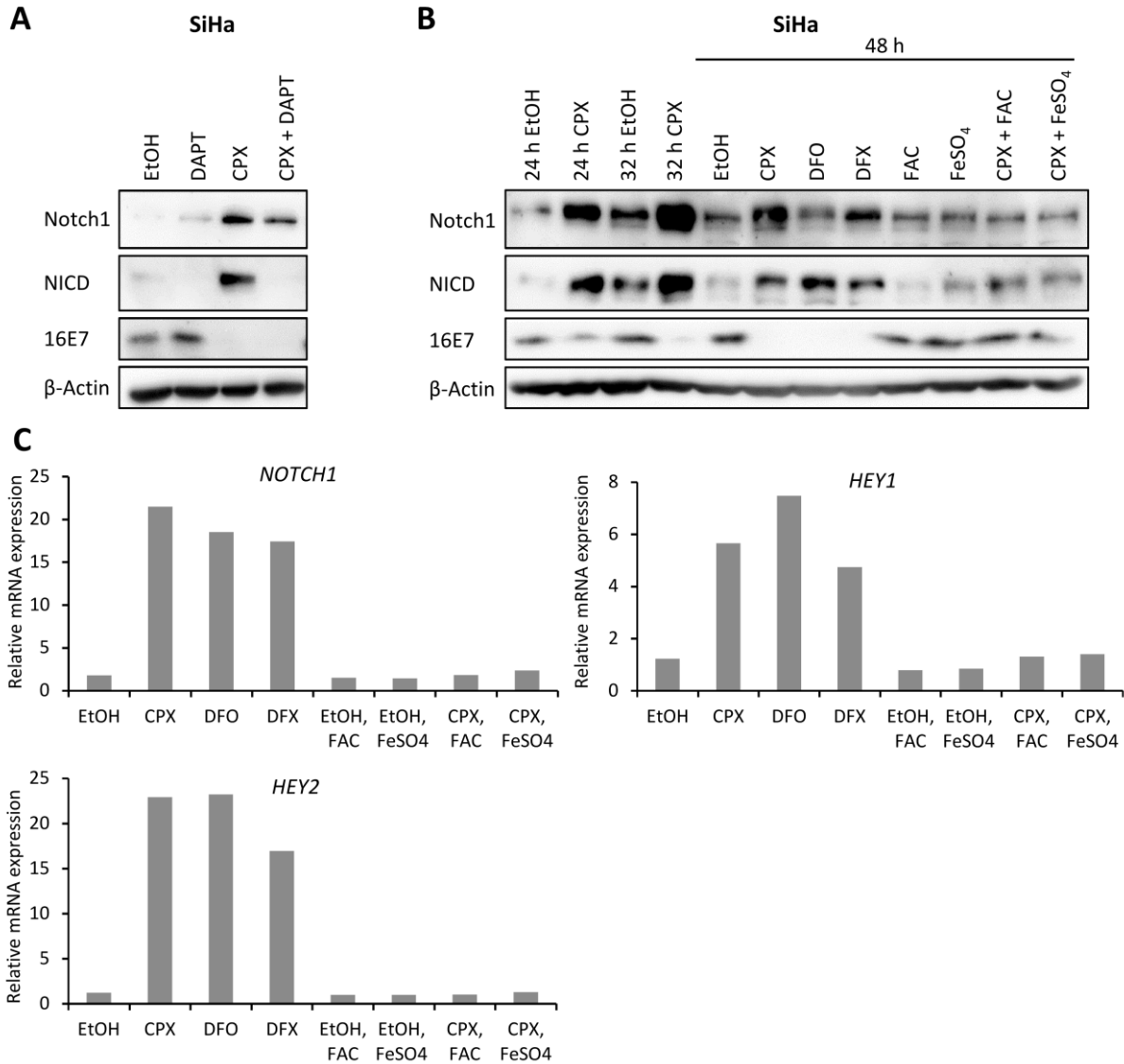


**Figure 31 | CPX activates Notch signaling in an iron-dependent manner. (A)** Immunoblot analyses of Notch1, NICD and HPV16 E7 in SiHa cells treated for 24 h with 10  $\mu$ M CPX and 5  $\mu$ M DAPT as indicated.  $\beta$ -Actin, representative loading control. **(B)** Protein levels of Notch1, NICD and HPV16 E7 were determined in SiHa cells upon treatment with 10  $\mu$ M CPX, 50  $\mu$ M DFO, 50  $\mu$ M DFX and/or iron supplementation with 6.67  $\mu$ M FAC or 6.67  $\mu$ M FeSO<sub>4</sub>.  $\beta$ -Actin, representative loading control. **(C)** Relative mRNA expression levels of *NOTCH1*, *HEY1* and *HEY2* corresponding to the 48 h time point in (B).

To investigate whether Notch1 upregulation by CPX is mediated via iron deprivation, cells were treated with different iron chelators (CPX, DFO and DFX) or an excess of iron in the form of iron sulfate (FeSO<sub>4</sub>) or ferric ammonium citrate (FAC) was added together with CPX. Immunoblot analyses show that iron chelators in general upregulate Notch1 and NICD and that the CPX-mediated upregulation can be rescued by supplementing iron (Figure 31B). Also on mRNA level, *NOTCH1* and the Notch1 target genes *HEY1* and *HEY2* are induced by treatment with different iron

chelators and this upregulation can again be counteracted by supplementation of iron (Figure 31C). These results indicate that CPX induces Notch1 signaling in SiHa cells in an iron-dependent manner.

However, when expanding the investigations to further HPV-positive cell lines it emerged that Notch regulation by CPX is more complex and strongly cell line-dependent. While on mRNA level *NOTCH1* and its target genes were at least weakly upregulated in six different tested cell lines, Notch1 and NICD protein levels were upregulated in three of the cell lines but downregulated in the other three cell lines. Interestingly, the 300 kDa uncleaved Notch1 precursor was upregulated in all cell lines where it was detectable. These results indicate a cell type-dependent heterogeneity of the Notch1 response towards CPX and are summarized in Table 2.

**Table 2 | Cell line-dependent effects of CPX on Notch1 signaling.** ↑, upregulated; ↓, downregulated; →, unchanged.

Cell line	HPV type	Notch1 protein	Uncleaved Notch1 precursor protein	NICD protein	<i>NOTCH1</i> mRNA	Target gene mRNA
SiHa	16	↑	undetectable	↑	↑	↑
MRI-H186	16	↑	↑	↑	↑	→
HeLa	18	first ↑ later ↓	undetectable	first ↑ later ↓	↑	↑
ME180	68	↓	↑	→	↑	→
CaSki	16	↓	↑	↓	↑	↑
SW756	18	↓	↑	↓	↑	↑

To assess whether the upregulation of Notch signaling is of functional relevance for the anti-proliferative effect of CPX, Notch1 was silenced by siRNA during CPX treatment or Notch signaling was inhibited with DAPT. In colony formation assays (Figure 32) no difference in colony formation capacity between cells with inhibited or active Notch1 signaling can be observed, indicating that

Notch1 does not play a pivotal role for the effects induced by CPX in HeLa and SiHa cells.

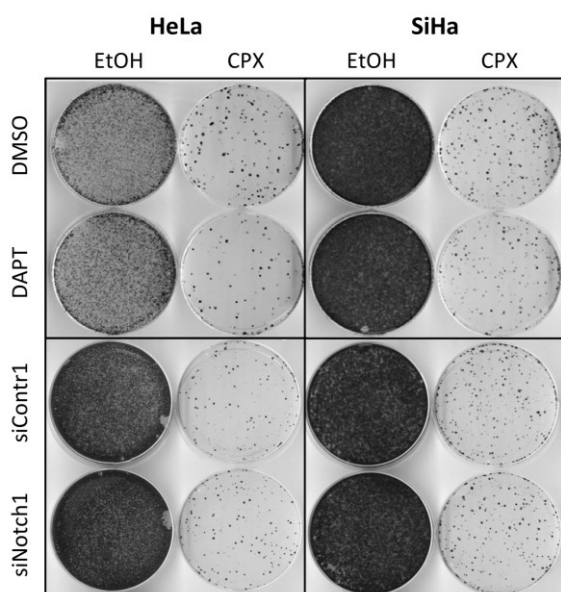


**Figure 32 | Notch inhibition does not counteract growth inhibition by CPX.** Colony formation assays of HeLa or SiHa cells treated for 72 h with 10  $\mu$ M CPX, either in combination with 5  $\mu$ M DAPT or DMSO as solvent control, or transfected with a control siRNA or siRNA against Notch1. Cells were split and grown in CPX-free medium for 13 days before fixation and staining.

## 2.5 Influence of HPV-status and tumor-status on CPX efficacy

As shown in this thesis and in other work from our group<sup>125</sup> CPX downregulates the viral *E6/E7* oncogenes, which is typically associated with the induction of senescence in HPV-positive tumor cells<sup>23</sup>. This raises the question if the downregulation of *E6/E7* renders HPV-positive cells particularly sensitive to CPX, compared to HPV-negative tumor cells. Furthermore, it should be addressed how specific CPX acts on tumor cells compared to non-transformed cells. This is an issue for many classical chemotherapeutics, because while these compounds preferentially target proliferating cells, which makes fast-dividing tumor cells more vulnerable to the therapy, also normal cells can be affected.

### 2.5.1 Effect of CPX in HPV-positive vs. HPV-negative cell lines

As a first step to address the aforementioned questions,  $IC_{50}$  values (half-maximal inhibitory concentrations) were determined for CPX in a panel of HPV-positive or negative cell lines established from cervical or head and neck cancer. Therefore, the cells were treated with varying doses of CPX and cell proliferation was recorded over 5 days via live-cell imaging (as exemplified for SiHa cells in Figure 33A). The area under the curve (AUC) of the generated proliferation curves was used to calculate  $IC_{50}$  values as shown in Figure 33B.

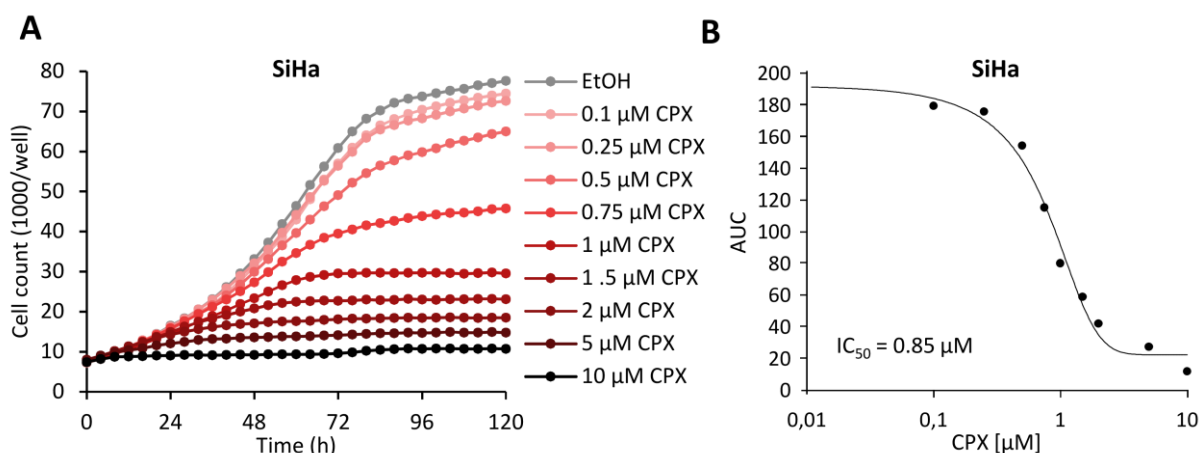


**Figure 33 | Determination of  $IC_{50}$  values for CPX via live-cell imaging.** (A) SiHa mCherry H2B cells were treated with the indicated doses of CPX and cell numbers were determined every 4 h over a period of 120 h via live-cell imaging. (B) Dose response curve using the area under the curve (AUC) from (A) as input. A standard curve was fit to the data in order to obtain the  $IC_{50}$  value for CPX.

In Table 3 the  $IC_{50}$  values for 6 cell lines are shown, representing average values of at least 3 independent experiments. Regardless of the HPV status or histological origin of the tumor cells, the calculated  $IC_{50}$  values lie around 1 µM, suggesting that the HPV status is not a major determinant for their sensitivity to CPX.

**Table 3 | IC<sub>50</sub> values for CPX in HPV-positive or negative cell lines.**

Cell line	HPV status	Origin	IC <sub>50</sub> [μM]	Standard dev. [μM]	n
C33a	-	cervix	0.94	0.04	3
CaSki	16	cervix	0.87	0.10	4
FaDu	-	hypopharynx	0.63	0.13	4
HeLa	18	cervix	1.78	0.15	5
SiHa	16	cervix	0.76	0.14	5
UDSCC2	16	hypopharynx	0.72	0.14	5

### 2.5.2 Effect of CPX in keratinocytes vs. keratinocytes expressing E6/E7

In order to more directly investigate the influence of the HPV-oncogenes on sensitivity to CPX treatment, immortalized human keratinocytes (normal oral keratinocytes, NOKs) were compared to NOKs expressing E6/E7<sup>234</sup>. Wild type NOK cells, NOK cells transduced with an HPV16 or HPV18 E6/E7-expressing lentiviral vector (NOK 16E6/E7, NOK 18E6/E7) or NOK cells transduced with the corresponding empty control vector (NOK pWPI) were treated with CPX for 24-72 h. On protein level it was observed that NOK cells expressing E6/E7 show higher levels of PARP cleavage after 48 or 72 h of CPX treatment compared to non-transduced or control vector-transduced NOKs, indicating an increased induction of apoptosis (Figure 34A).

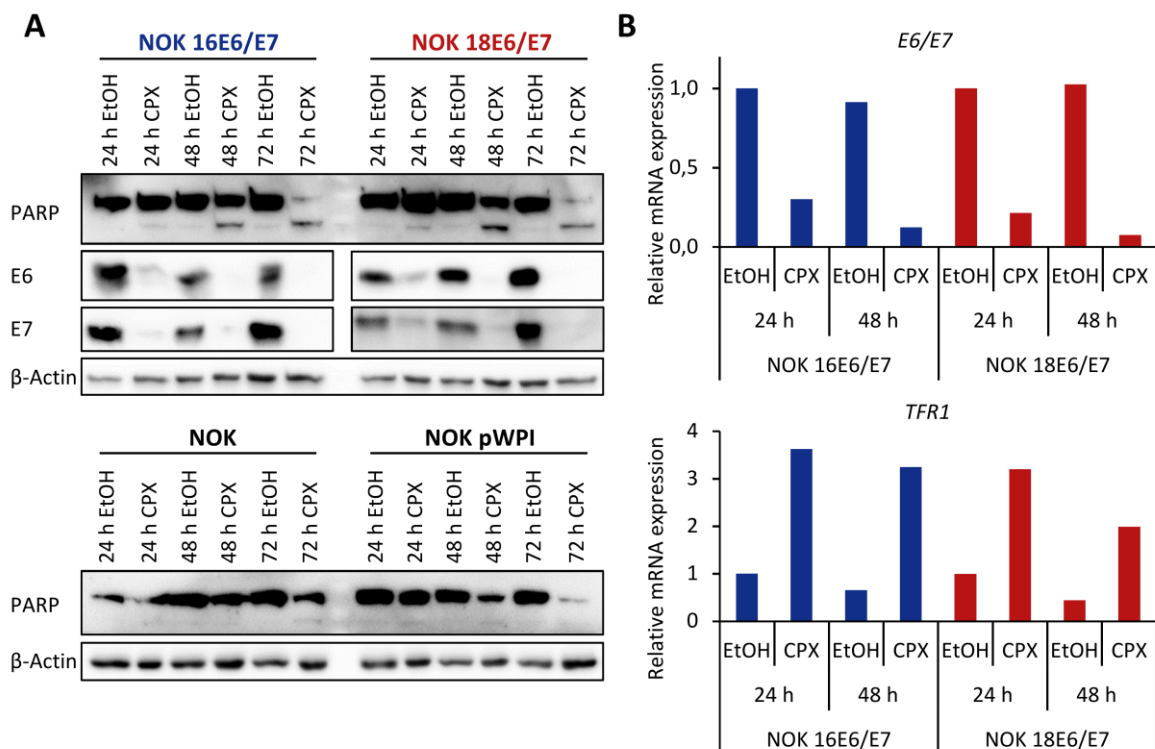


**Figure 34 | CPX-treatment of normal oral keratinocytes (non-)expressing E6/E7.** Normal oral keratinocytes (NOKs) and NOKs lentivirally transduced with an HPV16 or HPV18 E6/E7 expression plasmid or the control vector (pWPI) were treated with 10 μM CPX for 24, 48 or 72 h. **(A)** Protein levels of PARP (upper band) and cleaved PARP (lower band), 16E6, 16E7, 18E6 or 18E7 were analysed in immunoblot. β-Actin, loading control. **(B)** Relative mRNA expression levels of HPV16 or HPV18 E6/E7 and TFR1 after treatment with 10 μM CPX for 24 or 48 h in NOK 16E6/E7 and NOK 18E6/E7 cells.

CPX treatment also increases expression of *transferrin receptor 1* (*TFR1*) mRNA (Figure 34B), indicating depletion of intracellular iron. Interestingly – like in HPV-positive tumor cells – CPX is able to downregulate the lentivirally expressed E6/E7 on protein (Figure 34A) and mRNA level (Figure 34B).

Subsequently, the apoptosis induction by CPX was investigated in more detail in NOK cells expressing either HPV16 E6/E7 or the corresponding control vector. In TUNEL assays, a higher percentage of cells is apoptotic upon CPX treatment in the HPV16 E6/E7 expressing cells compared to the vector control (Figure 35A and B). This is corroborated by detection of caspase-3/7 activation via live-cell imaging. Also in this assay, the HPV16 E6/E7 expressing NOKs

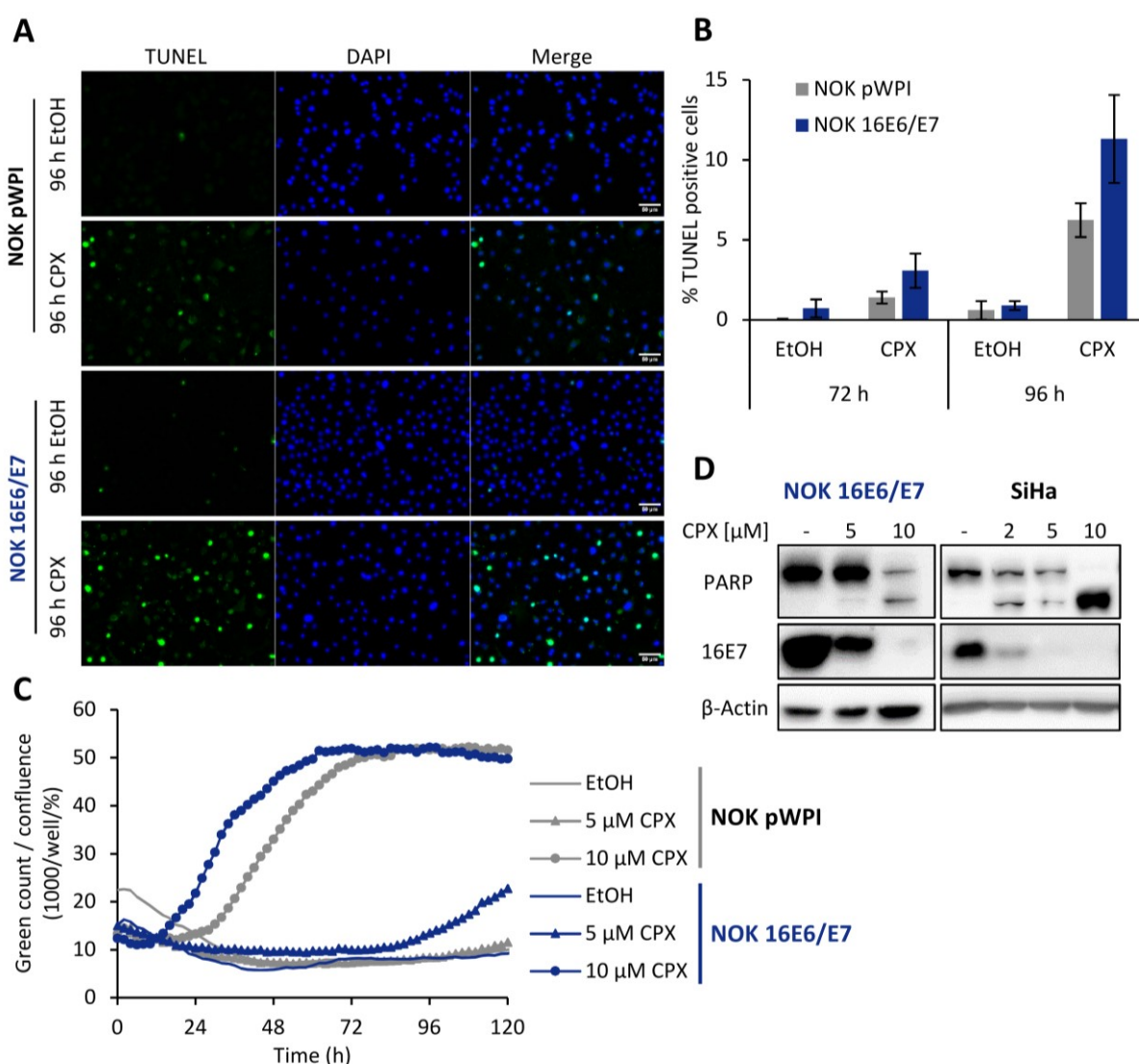


**Figure 35 | E6/E7 expression sensitizes NOK cells to apoptosis induction by CPX. (A)** Representative images of TUNEL assays in NOK pWPI and NOK 16E6/E7 cells with 10 μM CPX or EtOH as solvent control for 96 h. Scale bars: 50 μm. **(B)** Quantification of the percentage of TUNEL positive cells after 72 or 96 h treatment with 10 μM CPX. Average values from 3 independent experiments and the corresponding standard deviations are shown. **(C)** NOK pWPI and NOK 16E6/E7 cells were treated with 5 or 10 μM CPX or EtOH as solvent control in the presence of 5 μM IncuCyte® Caspase-3/7 reagent for apoptosis detection. Every 2 h over the course of 120 h the green object count, indicating apoptotic cells with activated caspase-3/7, was determined and normalized to the cell confluence in percent. **(D)** Immunoblot analyses of (cleaved) PARP and HPV16 E7 protein levels in NOK 16E6/E7 and SiHa cells treated with the indicated CPX concentrations for 72 h. β-Actin, loading control.

undergo apoptosis more rapidly than the control cells (Figure 35C). Taken together, these results suggest that E6/E7 expression sensitizes keratinocytes to CPX-induced apoptosis.

A further interesting observation is that the percentage of apoptotic cells in NOK cells (regardless of E6/E7 expression) is significantly lower than in HPV16-positive SiHa cells (please compare Figure 35B with Figure 18, 1 g/L glucose). After 96 h of CPX treatment, only 6% of NOK pWPI and 11% of NOK HPV16 E6/E7 cells are TUNEL positive, compared to nearly 40% of SiHa cells. Similarly, also immunoblot analysis of cleaved PARP indicates that SiHa cells are more sensitive to CPX than NOKs (Figure 35D). In SiHa cells, lower CPX concentrations (2 and 5  $\mu\text{M}$ ) are sufficient to induce PARP cleavage after 72 h of treatment, while in NOK HPV16 E6/E7 cells only treatment with a higher CPX concentration (10  $\mu\text{M}$ ) results in PARP cleavage.

Collectively, these findings indicate that E6/E7 expression could indeed increase sensitivity to CPX and show furthermore that HPV-positive tumor cells are more vulnerable towards CPX treatment than non-transformed keratinocytes expressing E6/E7.

### 2.5.3 Effect of CPX in primary cells

Subsequently, the effects of CPX were investigated in two primary keratinocyte isolates, one derived from ectocervix and one from foreskin. Also in these cells, TUNEL assays were performed after 72 or 96 h of CPX treatment. Compared to SiHa cells or NOKs, virtually no TUNEL positive cells (< 2%) can be detected in the primary isolates treated with CPX (Figure 36A and B).

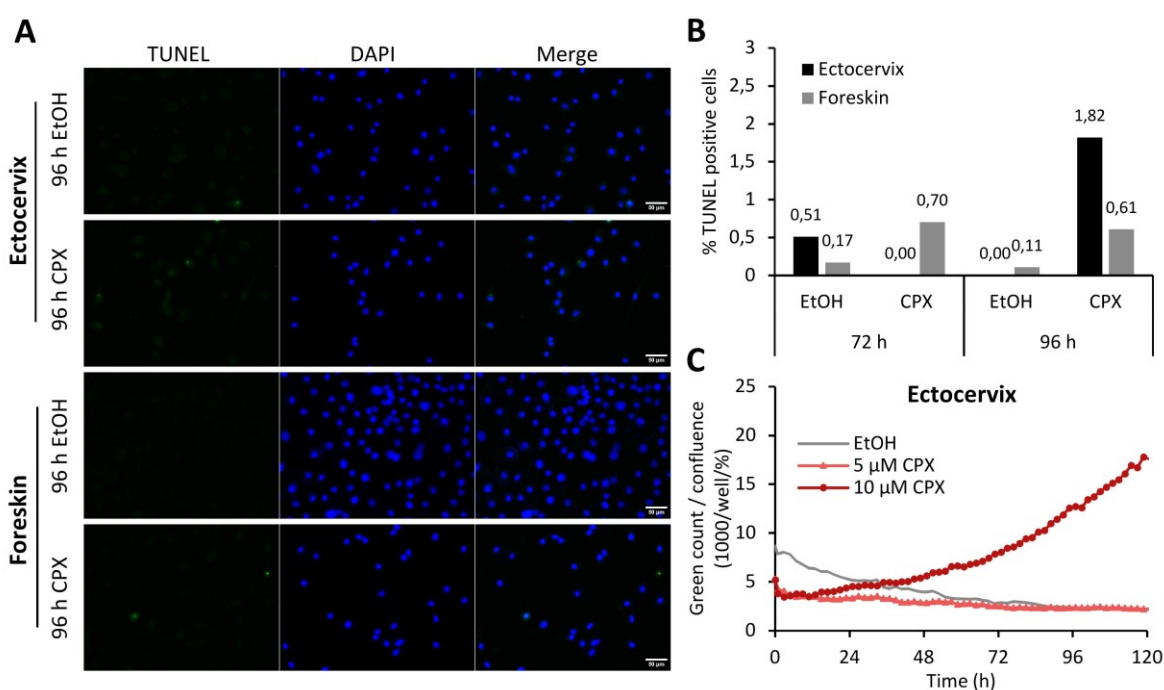


**Figure 36 | CPX only weakly induces apoptosis in primary keratinocytes.** (A, B) TUNEL assays were performed in two primary keratinocyte isolates from ectocervix or foreskin after treatment with EtOH or 10  $\mu\text{M}$  CPX for 72 or 96 h. (A) shows exemplary images, (B) quantification of the percentage of TUNEL positive cells from one experiment. Scale bars: 50  $\mu\text{m}$ . (C) Primary ectocervix keratinocytes were treated with 5 or 10  $\mu\text{M}$  CPX in the presence of 5  $\mu\text{M}$  IncuCyte<sup>®</sup> Caspase-3/7 reagent for apoptosis detection. The number of apoptotic cells was determined every 2 h over 120 h by counting green objects and normalized to the cell confluence in percent.

In addition, a caspase activation assay was conducted in the primary ectocervical cells. While 5  $\mu\text{M}$  CPX are not sufficient to induce apoptosis, 10  $\mu\text{M}$  CPX lead to an activation of caspase-3/7, indicating at least a small amount of apoptosis induction (Figure 36C). Due to these inconclusive results further research is needed to investigate the effect of CPX on non-malignant cells.

## 2.6 Combination therapies with CPX

Compared to cancer therapies using single agents, therapies combining two or more drugs are often advantageous, as they may allow to reduce the respective doses of the single drugs leading to reduced side effects. Thus it is of high interest to investigate if CPX can enhance the effect of other treatments for HPV-positive cancers. At present, the routine treatment for locally advanced cervical cancer is concurrent chemoradiotherapy, which combines radiation with a platinum-containing chemotherapeutic drug.<sup>52</sup> Hence, combination therapies of CPX with radiotherapy or with cisplatin (*cis*-diamminedichloroplatinum(II), CDDP) were investigated in HPV-positive tumor cells. As first experiments already had indicated that CPX has the potential to enhance efficacy of these therapies<sup>228</sup>, investigations were expanded in order to quantify the combinatorial anti-tumorigenic effects.

### 2.6.1 CPX synergizes with radiation

Clonogenic assays allow to determine the ability of single cells to undergo “unlimited” division. As hypoxic tumors are known to be more resistant towards radiotherapy, the combinatorial effect of CPX and radiotherapy was assessed under both normoxic (21%  $\text{O}_2$ ) and hypoxic (1%  $\text{O}_2$ ) conditions. In both HeLa and SiHa cells CPX enhances the effect of radiation and further reduces clonogenicity compared to only radiation (Figure 37), which indicates a synergistic effect. As expected, under hypoxia cells were more resistant towards radiation, resulting in a higher surviving fraction (SF) compared to normoxia. However, also under hypoxic conditions additional

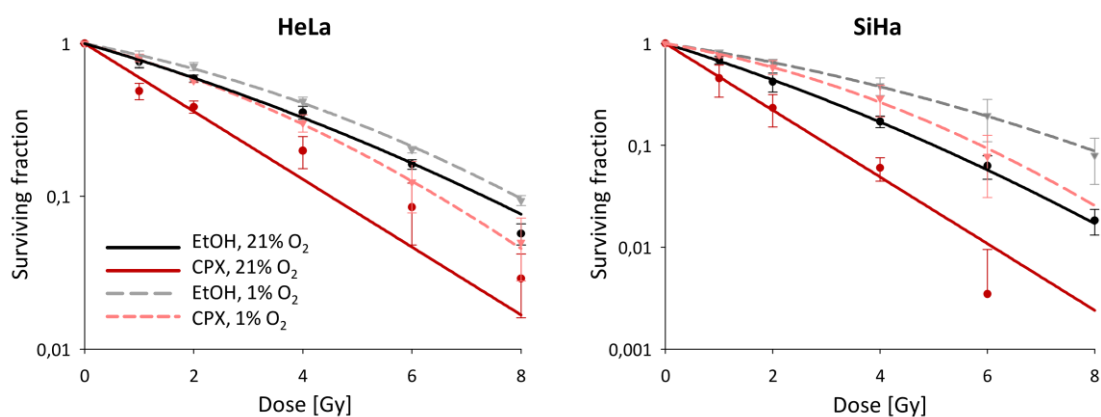


**Figure 37| CPX acts synergistically with radiation under normoxia and hypoxia.** HeLa or SiHa cells were irradiated with a dose of 0-8 Gy and concomitantly treated with 5  $\mu\text{M}$  (HeLa) or 2  $\mu\text{M}$  (SiHa) CPX under normoxic (21%  $\text{O}_2$ ) or hypoxic (1%  $\text{O}_2$ ) conditions for 72 h. After two weeks, colonies containing  $\geq 50$  cells were counted and the surviving fraction was calculated. Error bars represent standard deviations of 3 (HeLa) or 4 (SiHa) independent experiments.

treatment with CPX decreased the SF of irradiated cells. These results suggest that CPX synergistically enhances the effect of radiotherapy in HPV-positive tumor cells both under normoxia and hypoxia.

### 2.6.2 CPX cooperates with cisplatin

Next to radiotherapy, also the combination of CPX with cisplatin (CDDP) was examined. As seen in live-cell imaging experiments analyzing the number of viable cells over time, low doses of CPX or CDDP applied as single agents inhibit cell proliferation to some degree, however the combination of CPX plus CDDP is more effective and completely prevents proliferation, indicating a cooperation between the drugs (Figure 38A). In order to quantify the combinatorial effect of CPX with CDDP, the combination index (CI) was assessed according to the Chou-Talalay method<sup>235</sup>. Therefore, viable cell counts were assessed via live-cell imaging over the course of 5 days upon treatment with varying doses of CPX or CDDP or a combination (with constant ratio) of both drugs. Fraction affected (Fa) vs. CI plots show that CPX and CDDP act additive to slightly synergistic in HPV-positive tumor cells, with a better effect at higher doses, as indicated by a CI < 1 (Figure 38B).

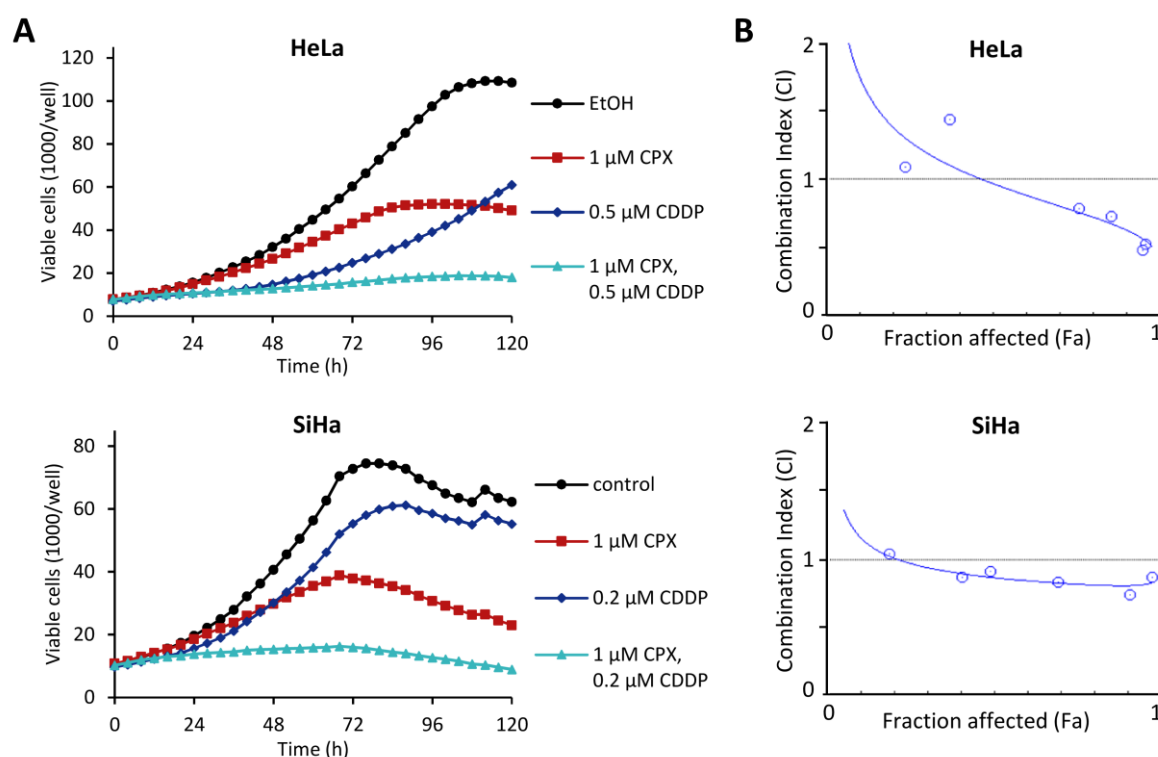


**Figure 38 | CPX cooperates with cisplatin.** HeLa mKate2 or SiHa mKate2 cells were treated with varying doses of CPX and CDDP in a constant drug ratio over the course of 120 h and every 4 h viable cell count was assessed via live-cell imaging. **(A)** Exemplary growth curves with the indicated doses of CPX and CDDP. **(B)** Fraction affected (Fa) vs. combination index (CI) plots based on viable cell count were created using the CompuSyn software. Data from one representative experiment is shown, respectively.

Interestingly, also the OXPHOS inhibitor metformin shows a cooperative effect with both radiation and cisplatin as indicated by clonogenic assays and 3D-cell culture experiments performed with HeLa cells, respectively (Figure 39A and B).

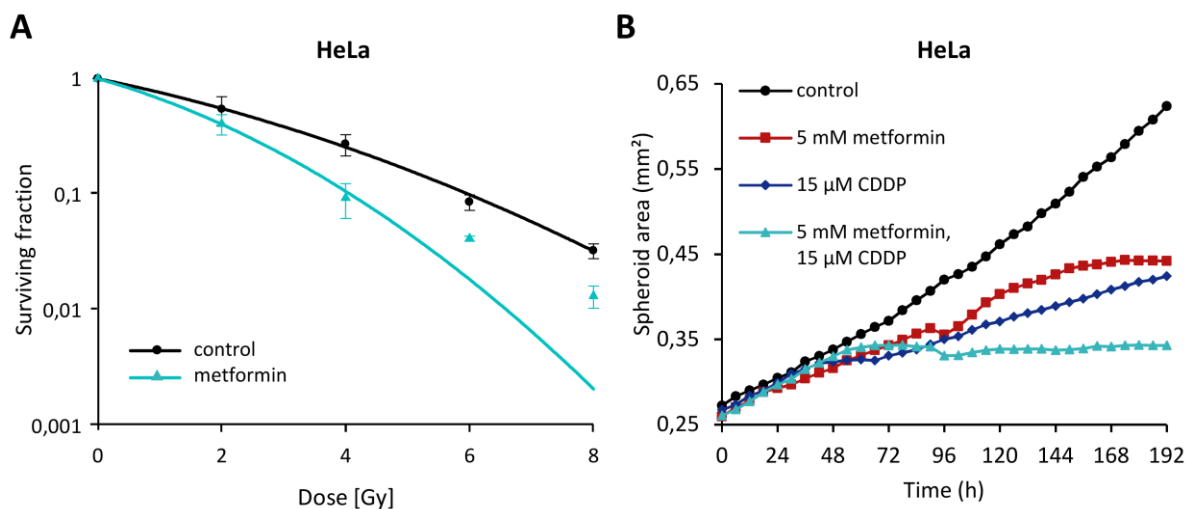


**Figure 39 | Metformin cooperates with radiation and cisplatin.** (A) HeLa cells were irradiated with a dose of 0-8 Gy and concomitantly treated with 2.5 mM metformin for 48 h. Colonies were counted two weeks later and SF calculated. Error bars represent standard deviation from 3 independent experiments. (B) The size of HeLa spheroids was determined upon treatment with metformin and/or CDDP over a period of 8 days.

### 2.6.3 CPX synergizes with glycolysis inhibitors

Next to radiation and cisplatin, also the combination of CPX with inhibitors of glycolysis was investigated. The rationale behind this approach is the assumption that combined treatment with an OXPHOS inhibitor like CPX and a glycolysis inhibitor should lead to energetic depletion, hindering cell proliferation and inducing cell death. This could allow a significant dose reduction of both drugs. One glycolysis inhibitor which is currently also investigated as a potential anticancer agent is the pyruvate analogue dichloroacetate (DCA). By inhibiting pyruvate dehydrogenase kinase (PDK1) this drug induces a shift of pyruvate metabolism from glycolysis towards OXPHOS, leading to a reversal of the Warburg effect.<sup>236</sup>

Notably, CPX and DCA exert profound synergistic effects in cervical cancer cell lines. In immunoblot analyses it can be observed that low doses of both drugs do not have significant effects on PARP cleavage and E7 protein levels, while their combination leads to an increase in cleaved PARP (only in HeLa cells) and downregulation of E7 (Figure 40A). Interestingly, the regulation of p53 differs between HeLa and SiHa cells. Single treatment with DCA upregulates p53, while single treatment with CPX weakly downregulates p53 in both cell lines. The combination treatment leads to p53 upregulation in HeLa, but downregulation in SiHa cells, potentially explaining the difference in PARP cleavage.

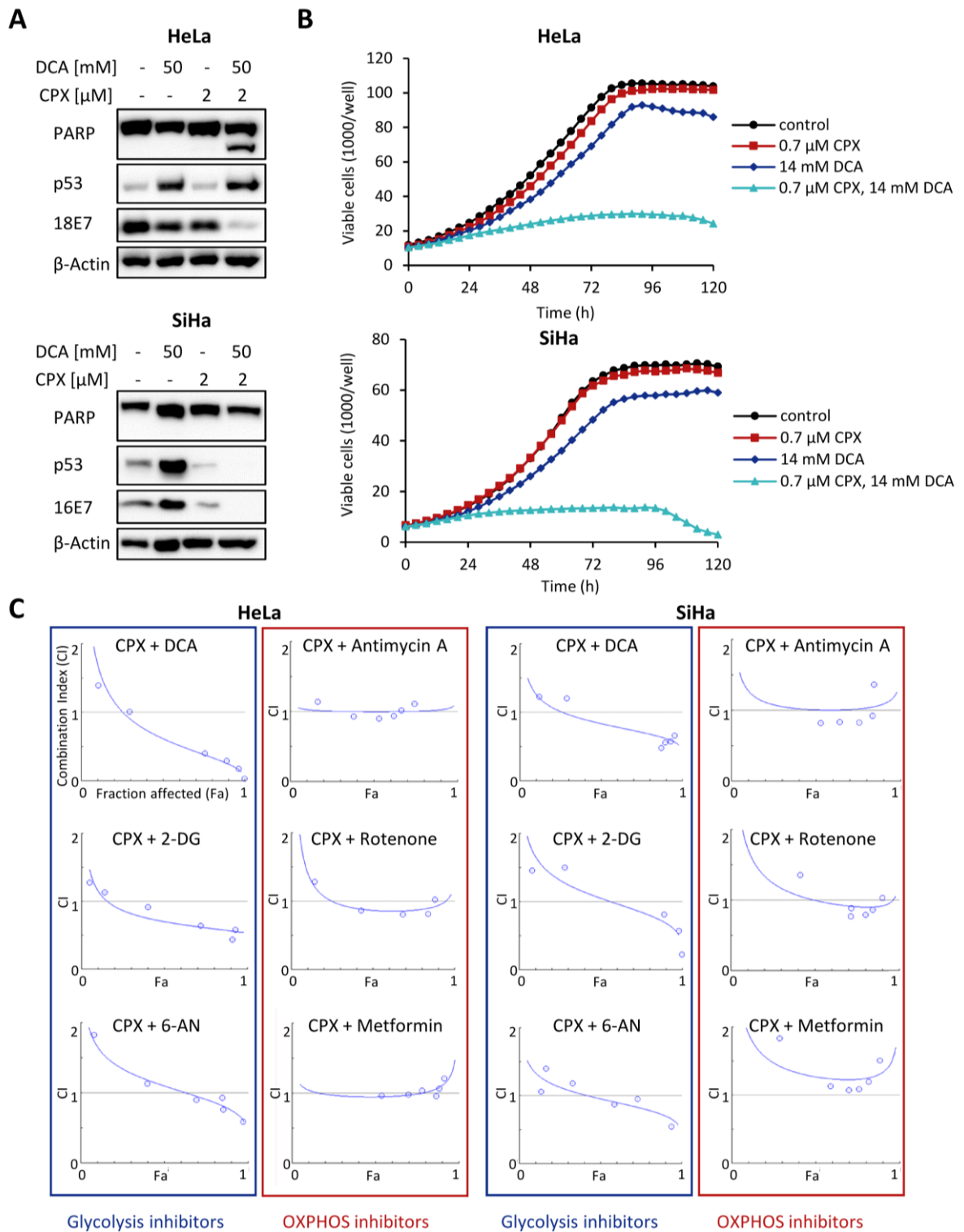


**Figure 40 | CPX synergizes with glycolysis inhibitors, but not OXPPOS inhibitors. (A)** Immunoblot analyses of (cleaved) PARP, p53 and HPV18 or HPV16 E7 levels in HeLa or SiHa cells after 48 h of treatment with the indicated doses of CPX and DCA.  $\beta$ -Actin, loading control. **(B)** Growth curves of HeLa mKate2 or SiHa mKate2 cells treated with the indicated doses of CPX and DCA. Red object count indicating viable cells was assessed every 4 h over a period of 120 h via live-cell imaging. **(C)** HeLa mKate2 or SiHa mKate2 cells were treated with varying doses of CPX and the indicated OXPPOS or glycolysis inhibitors in a constant ratio over the course of 120 h and every 4 h viable cell count was assessed. Fraction affected (Fa) vs. combination index (CI) plots were created using the CompuSyn software, based on viable cell count. Data from one representative experiment is shown, respectively.

Live-cell imaging analyses confirm the cooperative effect for CPX and DCA, here already very low doses of both drugs in combination are sufficient to strongly inhibit proliferation (Figure 40B). CI values for this combination were determined as described above for the combination of CPX with CDDP. Fa-CI plots indicate that the combination of CPX with DCA is indeed synergistic ( $CI < 1$ ) over a broad concentration range (Figure 40C, upper left panels). These analyses were then extended to further combinations of CPX with other glycolysis inhibitors (2-deoxy-D-glucose, 2-DG; 6-aminonicotinamide, 6-AN) or OXPHOS inhibitors (antimycin A; rotenone; metformin). Consistent with its OXPHOS inhibiting activity, CPX not only synergizes with DCA but also with the glycolysis inhibitors 2-DG and 6-AN ( $CI < 1$ ). In contrast, the combination of CPX with the OXPHOS inhibitors antimycin A, rotenone and metformin showed at most additive effects (CI around 1) (Figure 40C).

***CHAPTER 3***  
***DISCUSSION***



### 3. Discussion

Despite the existence of prophylactic vaccines, HPV-induced cancers of the cervix and head and neck region will remain a substantial clinical burden for decades to come. Thus, there is an urgent need for more specific and innovative treatment strategies.<sup>237</sup>

Metabolic drugs, targeting tumor specific metabolic alterations, are under intense research as potential anticancer agents. Ciclopirox, a topical antimycotic drug, has been identified as an iron chelator decades ago. As tumor cells rely on iron more heavily compared to normal cells, CPX has been investigated as an anticancer agent for several years and has proven antitumor efficacy in numerous preclinical and also first clinical studies.<sup>124</sup> More recently, CPX was shown to alter the cellular energy metabolism by inhibiting oxidative phosphorylation, which might add to its anti-tumorigenic potential.

Previous studies from our group have demonstrated that CPX downregulates viral *E6/E7* oncogene expression and strongly inhibits proliferation of HPV-positive cancer cells by induction of senescence and apoptosis.<sup>125, 227, 228</sup> These promising results warrant further exploration of the anti-tumorigenic effects of CPX in cervical cancer cells. Hence this thesis investigated potential mechanisms implicated in this anti-tumorigenic action and revealed, inter alia, a strong glucose dependence of the CPX-induced effects which could have profound clinical implications and allow the development of rational combination therapies with glycolysis inhibitors.

#### 3.1 Mechanistic insights into the anti-tumorigenic effects of CPX

As an iron chelator, CPX influences and regulates numerous cellular pathways and mechanisms. This was corroborated by our proteome analyses in SiHa cells, in which CPX significantly up- or downregulated 392 of the 5919 detected proteins. In other words, after 48 h of CPX treatment, 6.6% of all detected proteins were increased or decreased more than twofold. To gain more insights into how CPX regulates expression of these proteins, the CPX-induced changes on proteome composition were compared to those induced by hypoxia or the OXPHOS inhibitor metformin.

CPX and hypoxia both increased expression of the HIF-1 $\alpha$  transcription factor, roughly by a factor of two. This is supported by several publications showing that HIF-1 $\alpha$  is upregulated upon iron chelation.<sup>117, 238</sup> Under normoxic conditions HIF-1 $\alpha$  is constantly targeted for degradation by the von Hippel-Lindau tumor suppressor (pVHL), which binds to HIF upon hydroxylation by prolyl hydroxylase 2 (PHD2).<sup>239, 240</sup> PHDs are dependent on oxygen and iron, thus under normoxic, iron-replete conditions HIF-1 $\alpha$  is hydroxylated and degraded, while hypoxia or iron depletion lead to its stabilization. HIF-1 is the master transcriptional regulator of the cellular hypoxia response and as such regulates numerous proteins and processes. As the proteome screen revealed an overlapping regulation of many proteins under hypoxia and iron depletion, it can be hypothesized

that a subset of the observed alterations is mediated via HIF-1 $\alpha$ . For example the growth and metastasis suppressor NDRG1 is upregulated both by hypoxia and CPX. It has been shown previously that iron chelators like DFO can increase NDRG1 expression via HIF-1 $\alpha$ -dependent and independent pathways<sup>241, 242</sup>, which may inhibit TGF- $\beta$  induced EMT, decrease cell viability, reduce migration and induce apoptosis<sup>243, 244</sup>. In contrast, hypoxia also activates factors and pathways which enhance migration, invasion and EMT, e.g. Snail, Twist, Wnt, TGF- $\beta$  or hedgehog signaling.<sup>245</sup> Some of these pathways, like TGF- $\beta$  signaling are regulated in a similar manner by CPX, however other pathways like Wnt signaling are regulated contrarily by CPX. Due to this differential findings, it would be of interest to investigate the effects of CPX on migration, invasion and EMT. In preliminary scratch assays, however, no clear influence of CPX on the migration of cervical tumor cells could be observed, yet it would be desirable to evaluate these processes with other methods such as transwell assays or the analysis of EMT markers.

In contrast to CPX, the antidiabetic drug metformin, which is an inhibitor of OXPHOS complex I slightly downregulated HIF-1 $\alpha$  in the proteome screen, which is supported by literature demonstrating that metformin and other OXPHOS inhibitors can target HIF-1 and alleviate hypoxia.<sup>204, 246, 247</sup> It is interesting to note that in this context the induction of HIF-1 $\alpha$  due to the iron chelating properties of CPX is dominant over a potential HIF-1 $\alpha$  downregulation due to its OXPHOS inhibiting properties. In contrast, several cancer-related proteins were regulated in a similar manner by CPX and metformin, indicating that regulation of those factors could be mediated by inhibition of OXPHOS. Interestingly, despite being an OXPHOS inhibitor metformin did in contrast to CPX not or only weakly regulate expression of the proteins comprising the mitochondrial ETC complexes.

A further protein which was upregulated in the screen by both CPX and hypoxia is Notch1. Hypoxia and iron chelators were previously shown to upregulate Notch, probably also via HIF-1.<sup>248</sup> Conversely, Notch also can upregulate HIF-1 $\alpha$  via STAT3, suggesting an interdependence of both pathways.<sup>249</sup> On a side note, data from our lab demonstrated that CPX strongly downregulates STAT3 by decreasing its protein stability<sup>250</sup>, thus this feedback loop should not be functional under CPX treatment. Notch signaling is required for the hypoxic stimulation of EMT and for maintaining cells in a dedifferentiated state under hypoxia.<sup>251, 252</sup> Furthermore, Notch can induce oncogenic Myc and PI3K-Akt signaling, increase glucose transporter expression and enhance chemotherapy resistance, which has led to the classification of Notch as an oncogene in several cancers such as AML and ALL.<sup>142</sup> However, more recent research showed that the effects of Notch are strongly cell- and context-dependent and established Notch as a tumor suppressor in other cancers including SCC, small-cell lung cancer, some types of glioma and hepatocellular carcinoma.<sup>150</sup> In these types of cancer, strategies to activate Notch signaling constitute an

interesting therapeutic option and according drugs are under development.<sup>150</sup> However, such treatments only possess potential for tumors in which the Notch cascade is still functional and not for cancers with e.g. Notch loss-of-function mutations.<sup>150</sup> The role of Notch in HPV-positive cancers is still somewhat controversial. The majority of conducted studies shows that Notch1 signaling suppresses the growth of cervical cancer cells<sup>253-255</sup>, however, also the opposite effect has been observed<sup>256, 257</sup>. Furthermore, there are studies reporting that Notch1 inhibits E6/E7 expression via AP-1 suppression<sup>258</sup> and vice versa E6 can downregulate Notch1<sup>259, 260</sup>, arguing for a tumor-suppressive role of Notch1 in HPV-positive cancers.

Interestingly, Notch overexpression leads to a glycolytic switch, inducing a Warburg phenotype due to transcriptional upregulation of metabolic regulator genes and vice versa a disturbed cellular metabolism modulates Notch signaling.

Due to the potential anti-tumorigenic function of Notch in cervical cancers, it is of interest to investigate the effect of CPX on Notch signaling. Consistent with studies showing upregulation of Notch in early stages of cervical cancer but downregulation in later stages<sup>261</sup>, only low levels of Notch could be detected in all tested cervical cancer cell lines. Nonetheless, Notch signaling seemed to be functional in cervical cancer cells as  $\gamma$ -secretase inhibition by DAPT prevented Notch cleavage and CPX not only activated Notch1, but also expression of its target genes *HEY1* and *HEY2*. The upregulation of Notch signaling by CPX can probably be attributed to its iron chelating properties as it could be counteracted by supplementation of iron and also treatment with the iron chelators DFX and DFO enhanced Notch1 signaling, consistent with the hypothesis that this regulation is mediated via HIF-1 $\alpha$ . However, the effects of CPX on Notch signaling were found to be rather inconsistent across a panel of six cervical SCC cell lines. On mRNA level, *NOTCH1* and its target genes were upregulated at least slightly in all tested cell lines, however on protein level Notch1 was upregulated only in half of the cell lines, but downregulated in the other half. It is not clear what determines this cell line specificity, however it is not surprising when considering the highly converse roles of Notch signaling in different types of cancers and also between different studies on the same cancer type. In this context a recent study by Weir and colleagues<sup>130</sup> is of interest, who investigated the effect of fosciclopirox, a CPX prodrug, in bladder cancer. While in their system CPX also increased Notch1 protein levels, it suppressed activation of Notch signaling by inhibition of the  $\gamma$ -secretase complex. However, this study did not examine if the Notch inhibitory effect of CPX is relevant for its anti-tumorigenic actions. In the present work, inhibition of Notch signaling via siRNA or with the small molecule DAPT could not rescue growth inhibition after CPX treatment, suggesting that the upregulation of Notch1 by CPX is not of particular functional relevance for its anti-tumorigenic effects.

In general, it probably will be fairly difficult to trace back certain anti-tumorigenic effects of CPX to the regulation of only one protein or pathway. Our proteome screen demonstrated that CPX influences the expression of hundreds of proteins, among them transcription factors like HIF-1 $\alpha$ , STAT3 or JUN, thus regulating a plethora of cellular processes. Most of these effects are probably due to the iron-chelating properties of CPX and will be observed as well with other iron chelators. Despite these limitations it is still worthwhile to closer investigate pathways regulated by CPX, as this may for example allow to identify sub-populations of tumors or certain types of cancers, which could be particularly sensitive to CPX treatment. Furthermore, a better knowledge of the CPX-regulated factors might facilitate discovery and development of rational combination treatments. In this context, it would for example be interesting to closer investigate, which effects are mediated via HIF-1 $\alpha$ . This could experimentally be addressed by inhibiting HIF-1 $\alpha$  during CPX treatment or by comparing the effects of CPX with cobalt chloride, which is commonly used as hypoxia mimetic as it inactivates PHDs by replacing Fe<sup>2+</sup> with Co<sup>2+</sup> and should thus mimic the effect of iron chelation on HIF-1 $\alpha$ . Depending on these results, it could be beneficial to combine CPX with a HIF-1 $\alpha$  inhibitor<sup>262</sup> in order to mitigate pro-tumorigenic effects such as invasion and metastasis which are mediated via HIF-1 $\alpha$ .

### 3.2 Glucose dependence of CPX

Tumor cells typically rewire certain metabolic processes, which allows them to thrive in a nutrient-poor environment. Thus, a deregulated cellular metabolism is considered one of the hallmarks of cancer.<sup>263</sup> The most prominent metabolic alteration featured by tumor cells is their increased glycolysis rate even under oxygen-replete conditions, which is commonly known as Warburg effect. Interestingly, oncogenic HPVs can increase the rate of aerobic glycolysis and thus contribute to the Warburg effect. This is mediated by the viral *E6/E7* oncogenes, which promote glycolytic flux by enhancing expression of HKII via c-Myc<sup>264</sup> and increasing activity of pyruvate kinase M2<sup>265</sup>. Despite this glycolysis promoting function of *E6/E7*, HPV-positive HeLa and SiHa cells were demonstrated to exhibit an oxidative phenotype and are sensitive to lactate signaling<sup>266-268</sup>, thus they should be sensitive to OXPHOS inhibition as well.

While Warburg initially hypothesized that defect mitochondria are causal for the increase in glycolysis observed in many tumor cells, this has been disproven in the meantime. Instead, it has turned out that many cancer cells rely on OXPHOS to a similar rate than normal cells and can also enter a hybrid state, where both the oxidative and glycolytic state coexist.<sup>269</sup>

During OXPHOS electrons are transferred from electron donors provided via the TCA and glycolysis to oxygen as electron acceptor. These electrons are transported along the mitochondrial respiratory complexes in a series of redox reactions, allowing to convert the released energy to an electrochemical proton gradient. The OXPHOS complexes contain numerous iron-sulfur

complexes, in which iron acts as electron acceptor and donor by switching between its ferric ( $\text{Fe}^{3+}$ ) and ferrous ( $\text{Fe}^{2+}$ ) states.<sup>231</sup> Cytochromes are another type of electron carrier in the ETC, which use iron coordinated in the form of hemes as redox centers.<sup>194</sup> Iron depletion was shown to induce downregulation of mitochondrial transcript and protein levels and thus reduce oxidative capacity.<sup>270</sup> This is in line with the results from our proteome screen upon CPX treatment. GSEA analyses revealed that CPX downregulates proteins involved in OXPHOS, among them many proteins comprising the mitochondrial ETC complexes, which could also be confirmed in immunoblot analyses. A particular strong downregulation was observed for subunits of complex I, which is in accordance with a study by Rensvold et al. reporting that the iron chelator DFO mainly downregulates complexes I and II, which each contain multiple iron-sulfur clusters. This downregulation is achieved via a decrease in transcription of genes encoding mitochondrial proteins.<sup>271</sup>

Thus, it is little surprising that a number of studies has provided evidence that iron depletion leads to a downregulation of energy production via OXPHOS. Already in 1999 a study by Oexle et al. showed that the iron chelator DFO does not only inhibit the TCA cycle, but also decreases oxygen consumption in a leukemic cell line.<sup>272</sup> This was confirmed by experiments by Yoon and colleagues, which investigated the effect of DFO treatment in “Chang hepatocytes”, a cell line which was meanwhile demonstrated to be HeLa cells. The authors could show that DFO reduces cellular ATP levels by half and inhibits the activity of mitochondrial complex II, but not complex I.<sup>273</sup> Inhibition of mitochondrial respiration probably is a common effect of iron chelators and a recent study from 2020 provides evidence that also CPX inhibits OXPHOS, decreases expression of several subunits from complex I and III and induces ROS production in colorectal cancer cells.<sup>127</sup> Furthermore, the authors report that CPX promotes glycolysis, glucose uptake and lactate production.

Consistently, the proteome screen performed in the present work also revealed an upregulation of glycolytic enzymes and of factors involved in the PPP, which was verified by immunoblot analyses. This indicates that cells attempt to compensate for the decreased energy production via OXPHOS with an increased activity of glycolysis and PPP. The ability to switch between glycolytic and oxidative energy production is characteristic for tumor cells, which exhibit a high metabolic plasticity allowing them to adapt to different microenvironments and nutrient sources to ensure sufficient energy supply.<sup>274</sup>

One would expect that due to the increased rate of glycolysis, CPX-treated cells consume a higher amount of glucose. Thus, glucose levels in the medium of CPX-treated and untreated cells were determined. An issue that needs to be considered in this context is that CPX-treated cells, in contrast to untreated cells, do not proliferate anymore. To account for this, the consumed glucose was normalized to the number of cells to determine the glucose consumption relative to cell count.

By doing so, the initial assumption could be confirmed, as CPX-treated cells indeed consumed more glucose per cell.

Upregulation of glycolysis by CPX could not only be an attempt of treated cells to compensate for decreased OXPHOS activity but could also independently be regulated via HIF-1 $\alpha$ . Under hypoxic conditions, HIF-1 $\alpha$  promotes a switch from oxidative to glycolytic metabolism by increasing expression of glucose transporters and glycolytic enzymes.<sup>275</sup> Additionally, HIF-1 $\alpha$  activates PDK1 and lactate dehydrogenase A (LDHA), thus pyruvate is not further metabolized via the TCA cycle but converted to lactate.<sup>275</sup>

The upregulation of glycolysis upon CPX treatment allows cells to meet their energetic demand independent of OXPHOS. Thus, increased levels of glucose, enabling enhanced flux through the glycolytic pathway protect cells against CPX-induced cell death. Consequently, it was hypothesized that glycolysis suppression should revert this protective effect. While HKII knockdown indeed restored sensitivity to CPX-induced apoptosis under increased glucose levels, downregulation of PFKP and/or GPI could not replicate this effect. Hexokinase catalyzes the phosphorylation of glucose to glucose-6-phosphate, which can either be further processed in the glycolytic pathway by PFK-1 or alternatively be shuttled towards the PPP. To test if inhibition of PPP is relevant for the observed apoptosis induction upon HKII knockdown, G6PD which catalyzes the first and rate-limiting step of PPP<sup>276</sup> was silenced while cells were treated with CPX in glucose-abundant conditions. However, this did not re-sensitize cells towards apoptosis induction, suggesting that the PPP is not relevant for the glucose-dependent protection against CPX-induced apoptosis.

Another possible explanation for the observed differences is that PFKP and GPI knockdown is not as effective in inhibiting glycolysis as HKII knockdown and thus less efficient in depleting cells of energy. Three enzymes, namely hexokinase, phosphofructokinase and pyruvate kinase, catalyze irreversible steps during glycolysis and are known to be regulatory enzymes. It would be of interest to also investigate the effect of pyruvate kinase knockdown to determine if the observed sensitization by HKII is due to glycolysis inhibition or constitutes a HKII specific effect. Furthermore, to directly analyze the effects of knockdown of either glycolytic enzyme on the glycolysis rate, measuring extracellular acidification rate (ECAR) should be insightful.

Notably, besides its involvement in glycolysis, HKII, when associated with mitochondria, also functions to protect cells from apoptotic stimuli<sup>277</sup>, which could also explain the increased apoptosis upon HKII knockdown. If the pro-apoptotic effect upon HKII silencing was due to the mitochondrial function of HKII, it should be mimicked by dissociating HKII from mitochondria. In preliminary experiments, however, the drugs clotrimazole or methyl jasmonate, which detach HKII from the voltage-dependent anion channel in the mitochondrial membrane, could not restore

sensitivity to CPX-induced apoptosis under glucose-replete conditions. Thus, more research is needed to further resolve the effects of HKII and glycolysis inhibition on the regulation of CPX-induced apoptosis.

### **3.3 Induction of senescence and apoptosis by CPX**

As shown in this thesis and also in previous work from our group, CPX treatment of cervical cancer cells can result in both induction of senescence, an irreversible growth arrest, or induction of apoptosis, a form of programmed cell death.<sup>125</sup> It was observed that this outcome mainly depends on treatment duration: while shorter CPX treatment of 48-72 h programs cells to induce senescence, prolonged treatment of 72-96 h or longer results in the induction of apoptosis. The capacity to induce both senescence and apoptosis is not unique to CPX but can be observed for many established chemotherapeutics as well. However, the factors determining if a chemotherapeutic drug rather induces senescence or apoptosis are still mainly elusive. Possible determinants are the amount and type of DNA damage induced, but also molecular pathways like the p53-p21 axis and PI3K-AKT-mTOR signaling can have implications on the therapeutic outcome.<sup>153</sup> While mild or short-term stress rather induces senescence, more severe DNA-damage preferentially triggers apoptosis induction, suggesting treatment time and dose as important factors. Also the particular cell type may influence the response to a treatment – while most cells in principle are capable of both responses, some cells like fibroblasts or epithelial cells preferentially undergo senescence, whereas others like lymphocytes rather undergo apoptosis upon DNA damage.<sup>153</sup>

Data obtained in this thesis suggests the energetic status of cells as a novel determinant of cell fate decision after treatment with the iron chelator CPX. As long as glucose is abundant, CPX preferentially induces senescence in cervical cancer cells and consequently increased glucose levels efficiently protect cells from CPX-induced apoptosis. In contrast, when glucose availability is limited apoptosis induction is facilitated. This is in agreement with the fact that senescent cells are highly energy-consuming and rely more heavily on glycolysis.<sup>278</sup> Senescent cells remain metabolically active and typically exhibit an increased glucose utilization and higher ATP production. This renders senescent cells particularly vulnerable to inhibition of glycolysis by genetic or pharmacological means.<sup>279</sup> The combination of CPX with glycolysis inhibitors could in this respect be doubly effective: on the one hand the simultaneous inhibition of OXPHOS and glycolysis deprives cells of energy, on the other hand CPX induces senescence, which should make the cells vulnerable to glycolytic inhibition.

Elucidation of the molecular factors determining the glucose-dependent switch between CPX-induced senescence and apoptosis would be of great interest. Promising candidates in this respect might be the tumor suppressor p53 and its transcriptional target p21, which are at the core of the

senescence signaling network. Both p53 and p21 are initially induced upon CPX treatment and are downregulated after prolonged treatment, which can be counteracted by increased glucose concentrations. Thus it could be hypothesized that sustained activation of the p53-p21 pathway under high glucose levels keeps cells in a senescent state, while downregulation under glucose deprivation leads to induction of apoptosis. This would be consistent with studies showing that chemotherapies induce senescence in p53 wild type cells, whereas p53 mutation or deletion shifts the response from senescence to apoptosis induction.<sup>280, 281</sup>

An interesting study in this context by Yao et al. investigated the effects of the drug pseudolaric acid B, which also induces both senescence and apoptosis. In this case, the treatment outcome was linked to glucose consumption and p53 status. While treatment of p53 wild-type cells preferentially resulted in senescence accompanied by an increase in glucose consumption, the absence of p53 enhanced apoptosis induction while decreasing glucose utilization.<sup>282</sup> In the case of CPX, however, p53 status is probably not a decisive factor, as both senescence and apoptosis can be induced in “p53 null” HeLa cells and p53 mutant cells as well.<sup>125</sup> This is also supported by experiments conducted in this thesis, where p53 knockdown neither did prevent senescence induction, nor could revert the protective effect of increased glucose concentrations against CPX-induced apoptosis. Similarly, also p21 knockdown was not effective in tipping the balance from senescence to apoptosis under increased glucose conditions. This is in contrast e.g. to cells treated with topoisomerase inhibitors, where p21 disruption shifts the cellular response from senescence to apoptosis.<sup>283</sup>

Another factor, which was regulated in the same manner as p21 and p53 is the transcription factor E2F1, which acts downstream of pRb and promotes cell cycle progression. E2F1 has been identified as an important regulator of the DNA damage response, which after activation by ATM or ATR induces expression of DNA damage repair genes.<sup>284</sup> Interestingly, some studies show that E2F1 overexpression induces senescence<sup>285, 286</sup> while others report that E2F1 overexpression programs cells to undergo apoptosis via p53-dependent and independent pathways.<sup>287, 288</sup> Furthermore, E2F1 is also implicated in metabolic reprogramming of cancer cells by enhancing glycolysis and repressing oxidative phosphorylation.<sup>289</sup> Due to this multifaceted role of E2F1, it was tested if E2F1 plays a role in the senescence vs. apoptosis decision upon CPX treatment. However, like p21 and p21 also E2F1 knockdown did not influence senescence or apoptosis induction.<sup>289</sup>

As silencing of E2F1, p21 or p53 partly affected the protein levels of the other factors, respectively, it might be that several redundant pathways exist, which would have to be targeted in combination to observe effects on the induction of senescence and apoptosis. Moreover, it will be worthwhile to explore other pathways implicated in metabolism as possible determinants for the glucose-dependent induction of senescence or apoptosis. In this context, AMPK and HIF1 $\alpha$  could

be interesting candidates. These master regulators of OXPHOS and glycolysis are at the core of a metabolic regulatory network, controlling the uptake and utilization of glucose.<sup>290</sup> As mentioned before, CPX and other iron chelators strongly upregulate HIF-1 $\alpha$ , which promotes glycolysis and reduces mitochondrial metabolism. HIF-1 $\alpha$  furthermore impacts many senescence promoting pathways and can prevent senescence induction.<sup>291, 292</sup> AMPK, known as a central energy sensor, was on the one hand shown to counteract senescence induction<sup>293-295</sup>, on the other hand sustained activation of AMPK is a hallmark of senescence<sup>296-298</sup>.

Overall, further elucidating the underlying pathways of the glucose-dependent response to CPX treatment could provide valuable insights into the general regulation of senescence and apoptosis.

As both senescence and apoptosis irreversibly block the growth of cancer cells, one might question if and why it matters if a chemotherapeutic drug induces senescence or apoptosis. Both senescence and apoptosis probably evolved as mechanisms to prevent tumorigenesis by hindering damaged cells from proliferating, and as such in principle can both be regarded as a desirable outcome of anticancer therapy. However, this perception is under debate, as it became clearer over the last years that induction of senescence can also exert various adverse effects. On the one hand, senescence turned out to be not as irreversible as originally thought, but instead may represent an opportunity for tumor cells to escape therapy. After enduring in a dormant state for years some senescent cells may potentially re-enter the cell cycle resulting in tumor recurrence.<sup>299</sup> On the other hand, senescent cells secrete certain pro-inflammatory factors including chemokines, cytokines and matrix metalloproteases, collectively known as senescence-associated secretory phenotype or SASP.<sup>155</sup> The SASP can vary depending on the pro-senescent stimulus and cell type and is only expressed when senescence is triggered by DNA damage but not when senescence is caused by overexpression of p16 or p21.<sup>155</sup> As shown in this work, CPX treatment induces expression of SASP factors, such as IL6 and IL1 $\alpha$  in HPV-positive tumor cells, consistent with the observed induction of the DNA damage markers phospho-p53 (S15) and phospho-RPA32 (S33) in CPX-treated cells.

The secreted SASP factors allow senescent cells to communicate with surrounding cells and can have both beneficial and deleterious effects. Notably, the SASP of senescent tumor or stromal cells can exert growth-promoting effects on neighboring cells<sup>300, 301</sup> and enhance invasion<sup>302</sup> and metastasis of surrounding tumor cells<sup>303</sup>. Moreover, senescent cells typically exert an increased resistance towards apoptosis-inducing stimuli, such as chemotherapy, an effect which can further be enhanced via the SASP in an autocrine and paracrine manner.<sup>304, 305</sup>

A growing body of literature demonstrates that the protein kinase mTOR is implicated in SASP expression and is responsible for some of its pro-tumorigenic effects.<sup>306</sup> In general, mTOR inhibition counteracts induction of senescence, which has also been shown to be the case in HPV-

positive cancer cells under pro-senescent treatment.<sup>307</sup> Interestingly, CPX like other iron chelators is an mTOR inhibitor and thus induces senescence in an mTOR-independent manner.<sup>125</sup> This poses the question if the SASP expressed by CPX-treated cells differs from the SASP induced by other treatments and may be less tumorigenic.

However, senescence and the SASP also confer certain advantages to the organism. SASP factors recruit immune cells and elicit an immune response against the senescent cells and thus contribute to tumor clearance.<sup>308</sup> This positive effect is further enhanced by the fact that senescent cells can reinforce senescence-associated cell cycle arrest in an autocrine and paracrine manner, thus establishing a self-amplifying secretory network, which facilitates targeting of further, initially non-senescent tumor cells.<sup>309</sup>

The double-edged role of senescence for cancer induction can be understood by the evolutionary theory of antagonistic pleiotropy, which describes that a process can be on the one hand beneficial early in life, but on the other hand become detrimental later in life.<sup>310, 311</sup> In sight of this theory, cellular senescence might protect young organisms against premature onset of carcinogenesis, but contribute to aging or exert tumorigenic effects in old organisms when senescent cells accumulate. This increasingly becomes a problem when lifespans are prolonged. In an attempt to alleviate the deleterious effects of senescent cells, major research is undertaken to develop senolytic drugs, capable of the selective removal of senescent cells from the tumor microenvironment.<sup>312</sup> These drugs could also aid in alleviating certain adverse effects of chemotherapy, as recent research showed that cells induced to senesce by chemotherapeutic agents contribute to common chemotherapy side effects such as cardiac dysfunction, bone marrow suppression, chemotherapy-induced fatigue and cancer recurrence.<sup>313</sup> Eliminating these therapy-induced senescent cells in mice could ameliorate some of the adverse reactions.

With the aim to gain mechanistic insights into the induction of senescence and apoptosis by CPX, the OXPHOS inhibitors metformin, antimycin A and rotenone were investigated for their potential to induce senescence or apoptosis under different glucose concentrations. Analogous to CPX these drugs induce apoptosis in a glucose-dependent manner in that limiting glucose availability facilitates apoptosis induction while increasing glucose supply protects cells against the pro-apoptotic effect. These results indicate that the pro-apoptotic activity of CPX is exerted via its capacity to block OXPHOS.

In contrast, the pro-senescent activity of CPX is probably independent of OXPHOS inhibition. Treatment with metformin, antimycin A or rotenone resulted in comparable, low efficacies of senescence induction at 1 g/L glucose, but all these three established OXPHOS inhibitors were in contrast to CPX not effective in inducing senescence under increased glucose levels. Interestingly, in live-cell imaging experiments it could be shown that metformin treatment only results in a

reversible growth inhibition as cells could resume proliferation after releasing them from treatment. This argues against the induction of senescence, which is classically defined as irreversible growth arrest. Moreover, we found that metformin impairs senescence induction through E6/E7 inhibition or etoposide treatment in HPV-positive cancer cells.<sup>230</sup> In contrast to metformin, CPX induces an irreversible growth arrest, consistent with the definition of senescence.

Contrarily to the OXPHOS inhibitors metformin, antimycin A and rotenone, other iron chelators, such as DFX and DFO share both the pro-apoptotic and pro-senescent activities of CPX. Alike CPX they efficiently induce senescence also under glucose-replete conditions, indicating that CPX-induced senescence depends on its iron chelating capacity.

Several studies have shown that OXPHOS inhibitors and other mitochondrial perturbations can induce a specific type of senescence coined mitochondrial dysfunction-associated senescence (MiDAS), potentially via ROS induction or activation of AMPK.<sup>298</sup> Vice versa, senescent cells are characterized by mitochondrial changes, including enhanced ROS generation and increased mitochondrial biogenesis, pointing to an intricate bidirectional relationship between mitochondria and cellular senescence.<sup>314</sup> Accordingly, Yoon and colleagues report that the iron chelator DFO induces senescence by causing mitochondrial dysfunction and induces an altered, elongated mitochondrial morphology.<sup>273</sup>

As CPX in contrast to other OXPHOS inhibitors also induces senescence under increased glucose levels, mitochondrial dysfunction is probably not the main trigger for senescence upon CPX treatment. Previously, CPX was shown to induce DNA damage<sup>125, 315</sup> and results from the present thesis confirm that CPX upregulates DNA damage markers also under increased glucose supply. This indicates that CPX mediates senescence induction via a DNA damage-dependent pathway, which also fits to the observed downregulation of p62. The ubiquitin-binding protein p62 is central for autophagy and is inhibited upon DNA damage via ATM and ATR.<sup>173</sup> This leads to stabilization of the transcription factor GATA4, which is normally targeted for autophagic degradation by p62. GATA4 then activates *IL1 $\alpha$* , which finally leads to SASP induction as confirmed by an increase of *IL1A* and *IL6* mRNA levels upon CPX treatment.

However, it is not yet fully elucidated how CPX induces DNA damage. One option reported by Shen et al. is the CPX-mediated degradation of Cdc25A, which is associated with DNA damage.<sup>315</sup> Alternatively, the inhibition of RR by CPX could also result in DNA damage, as this may lead to an insufficient supply with dNTPs during DNA replication. Consistently, knockdown of the RR subunit M2 was previously shown to induce a DNA damage response, resulting in senescence.<sup>316</sup> To gain more insights into the CPX-induced senescence, it would be of high interest to further investigate the underlying mechanisms and elucidate the roles of mitochondrial dysfunction and DNA damage pathways. As MiDAS is characterized by a distinct SASP compared to other types of

senescence inducers<sup>298</sup>, lacking pro-inflammatory factors depending on IL1R, investigating the SASP composition of CPX-induced senescent cells under varying glucose concentrations could give important insights on this. Interestingly, the mTOR inhibitor rapamycin reduces the IL1R-dependent arm of the SASP by inhibiting translation of IL1 $\alpha$ <sup>298</sup>, thus CPX as an mTOR inhibitor could probably reproduce this effect. It would also be informative to include metformin-treated cells in these analyses, as metformin can inhibit the SASP by interfering with IKK/NF- $\kappa$ B activation.<sup>317</sup>

It is well established that the E6 and E7 oncoproteins can modulate the senescence and apoptosis response of HPV-positive tumor cells. More specifically, cells undergo apoptosis when E6 alone is suppressed in the presence of E7, due to reactivation of p53 signaling. In contrast, inhibition of E7 alone or combined repression of both E6 and E7 leads to rapid induction of senescence, which is probably related to reactivation of the p53 and pRb pathways and dependent on mTOR signaling.<sup>12</sup>

Interestingly, not only CPX but all OXPHOS inhibitors investigated in this thesis did repress E6/E7 expression, which could be counteracted by increased glucose supply. Similarly, also the hypoxia-mediated downregulation of the HPV-oncogenes can be rescued through increased glucose availability<sup>307</sup>, indicating that expression of E6/E7 is coupled to the host cell's energetic status. Release experiments support this notion, as cells released from CPX treatment and cultured in fresh medium re-express E6/E7, even though they are stably arrested in a senescent state. Accordingly, also short-term treatment with the glycolysis inhibitor 2-DG was previously shown to reversibly suppress transcription of *E6/E7* and inhibit cell growth.<sup>318</sup> The mechanisms behind this metabolic regulation of E6/E7 are not well characterized yet. While hypoxic E6/E7 downregulation is mediated via the PI3K/mTORC2/AKT signaling pathway<sup>319</sup>, E6/E7 repression upon metformin treatment is independent of AKT, but can be reversed by PI3K inhibition<sup>230</sup> and CPX-mediated E6/E7 inhibition does neither rely on AKT or PI3K (J. Braun, unpublished data). Elucidation of these mechanisms might provide valuable insights into the cellular regulation of E6/E7 expression and even might create opportunities to therapeutically manipulate the respective pathways.

As E6/E7 inhibition induces senescence and CPX represses E6/E7, an obvious assumption would be that CPX induces senescence via E6/E7 downregulation. However there are several hints that argue against this explanation. Firstly, while increased glucose levels counteract E6/E7 downregulation, they do not impact senescence induction upon CPX treatment. Secondly, the other OXPHOS inhibitors investigated in this thesis also repress E6/E7, however they do not lead to a robust senescence response. Finally, CPX also induces senescence in HPV-negative cell lines

and in p53-negative cells<sup>125, 133</sup> thus excluding E6-mediated p53 reconstitution as senescence trigger.

### 3.4 Tumor specificity of CPX

While E6/E7 do not seem to play a crucial role in CPX-induced senescence, it is still of interest whether E6/E7 expression influences sensitivity of cells to CPX-induced proliferation inhibition or apoptosis induction. A similar selective sensitivity towards CPX treatment has been shown by Yang et al.<sup>128</sup> in neuroblastoma cells, which are 200-fold more sensitive to CPX compared to normal fibroblasts. The authors of this study demonstrate that CPX inhibits KDM histone demethylases, on which Myc-driven neuroblastoma depend in order to inhibit tumor-suppressive pathways and activate oncogenic signaling. Furthermore, CPX via KDM4B suppression inhibits the Myc signaling pathway, which may explain the increased sensitivity (roughly by factor 4) of Myc-dependent neuroblastoma cells compared to non MYCN-amplified neuroblastoma.

To test, if E6/E7 expression plays a role for the sensitivity of cancers towards CPX, the IC<sub>50</sub> values of HPV-positive or negative cervical cancer and HNSCC cells were determined in the present thesis. Cervical SCCs are virtually all HPV-positive, with the C33a cell line being a rare example of an HPV-negative cervical cancer cell line. The IC<sub>50</sub> value determined for CPX in C33a cells was similar to that of the HPV16- or HPV18-positive SiHa, CaSki and HeLa cell lines. In contrast to cervical SCCs, HNSCCs can be subdivided into HPV-positive and HPV-negative cases. Thus the HPV-negative HNSCC cell line FaDu was compared to the HPV16-positive HNSCC cell line UDSCC2. Also these two cell lines, showed no difference in sensitivity to CPX and exhibited a very similar IC<sub>50</sub> values of less than 1 μM. Thus, investigations in these exemplary cell lines do not allow to deduce an influence of the HPV-status on CPX-sensitivity.

Apart from the difference in HPV-status, these cell lines harbor numerous other differences between each other, including deregulations of p53, which could overshadow a possible influence of the oncogenes on treatment response towards CPX. Thus, in order to more directly investigate the influence of E6/E7 expression on CPX-sensitivity, immortalized human keratinocytes (NOKs) were compared to NOKs stably expressing the HPV16 or HPV18 *E6* and *E7* oncogenes<sup>234</sup>. While CPX treatment in NOKs expressing E6/E7 induced PARP cleavage, indicative for apoptosis induction, no cleaved PARP could be detected in the wild type or vector control NOKs. Also TUNEL assays and live-cell imaging experiments of CPX-treated NOK cells corroborated the increased pro-apoptotic effect of CPX in NOKs expressing HPV16 E6/E7, indicating that expression of the viral *E6/E7* oncogenes indeed renders keratinocytes more sensitive towards CPX-induced apoptosis. To further reinforce these findings, it would be interesting to investigate the consequences of restoring E6/E7 expression in HPV-positive cells under CPX treatment.

Another interesting observation made in the NOK cells is that CPX efficiently downregulates the lentivirally expressed E6/E7 on mRNA and protein level. This is intriguing as it implies that E6/E7 downregulation by CPX is independent of the viral promoter or *cis*-regulatory elements in the upstream regulatory region (URR) of the HPV genome, which usually regulate E6/E7 transcription.<sup>320</sup> Previous work has shown that CPX reduces E6/E7 protein stability<sup>228</sup>, which could explain the decrease on protein level. However, no influence on mRNA stability could be found in these studies<sup>228</sup>, thus reduction of *E6/E7* transcript levels could be a consequence of a reduced transcription rate.

Toxicities due to the targeting of non-malignant cells could constitute a potential limitation in the use of iron chelators for cancer therapy. Like many other chemotherapeutic drugs, iron chelators such as CPX preferentially damage fast-proliferating tumor cells, which have particularly high requirements for iron.<sup>321</sup> However, also non-malignant but particularly iron-dependent or fast-proliferating tissues like the bone marrow or gastrointestinal tract can be affected by these therapies, explaining common side effects and toxicities associated with chemotherapies. Thus, the tumor cell specificity of CPX is an important issue to consider as it determines a possible therapeutic window. One hint on this may be deduced from the comparison of HPV16 E6/E7 expressing NOK cells with HPV16-positive SiHa cells. These cell lines have similar proliferation rates and also a potential influence of E6/E7 can be excluded by this model. In TUNEL assays, four times more apoptotic cells could be detected in SiHa cells than in HPV16 E6/E7 expressing NOKs. Furthermore, in SiHa cells lower levels of CPX were sufficient to induce PARP cleavage in comparison to NOK cells. Thus, these results indicate that HPV-positive cervical cancer cells are more sensitive to iron chelation with CPX than (E6/E7-expressing) non-transformed keratinocytes.

Furthermore, the effect of CPX on primary cells, namely two keratinocyte isolates derived from ectocervix or foreskin, was investigated. In TUNEL assays hardly any apoptotic cells could be observed after four days of CPX treatment. In contrast, live-cell imaging analyses revealed that in cells subjected to 10  $\mu$ M CPX caspase-3/7 was activated, indicating the induction of apoptosis. The dynamics of caspase activation however did strikingly differ from what is observed after CPX treatment in cancer cells. While in HPV-positive tumor cells, CPX normally leads to a steep increase of caspase activation after 72-96 h, in the primary cells caspases were activated earlier and more continuously. Thus, to elucidate the effects of CPX on primary cells, further investigations are required.

Additionally, one has to keep in mind that primary cells and NOKs cannot be compared directly to tumor cell lines, as they for example are cultured in different media containing different concentrations of iron. However, as the keratinocyte growth medium contains less iron due to the

absence of FCS, this rather supports the notion that non-transformed cells are less sensitive towards CPX than HPV-positive cancer cells.

### 3.5 CPX in combination therapies

Cancer therapies based on the combination of multiple compounds can be advantageous compared to the use of single agents. The coordinated action of the combined agents may allow to reduce the doses of the single drugs, thus mitigating potential side effects and decreasing the risk of emerging drug resistances. An ideal drug combination exerts a synergistic or more-than-additive anti-tumorigenic effect, however, also an additive combination may be valuable in light of the before-mentioned benefits. Additionally, the combined drugs should have minimal overlap in their toxicity spectra and show no cross-resistance.<sup>322</sup> Finally, the optimal doses and treatment schedules have to be determined in order to provide patients with an ideal combination treatment.

Due to the described advantages of combination therapies, this thesis investigated the combination of CPX with other treatment regimens. Standard treatment options for patients with cervical carcinoma include surgery for early stages, radiation for early to advanced stages and cisplatin or other chemotherapeutic agents for advanced stages, or combinations of these regimens.<sup>52</sup> Therefore, it first was investigated if CPX can enhance the effects of radiotherapy in HPV-positive tumor cells. Indeed, in clonogenic assays a profound synergistic effect of CPX and irradiation was observed. This was the case not only under normoxic but also under hypoxic conditions, which is of special interest as cervical tumors often contain hypoxic regions and it is well-known that hypoxia reduces the efficacy of radiotherapy<sup>323</sup>. Mechanistically, the observed cooperative effect could be explained by inhibition of the RR by CPX: due to the excessive DNA damage conferred by radiation, cells are particularly dependent on the DNA building blocks produced by RR, which also is consistent with a study showing the upregulation of RR after radiation of cervical cancer cells<sup>324</sup>. Accordingly, other RR inhibitors like the iron chelator 3-AP or hydroxyurea are potent radiosensitizers.<sup>325, 326</sup>

Next to CPX also the combination of metformin and irradiation synergistically inhibited the growth of HPV-positive tumor cells, thus possibly also the OXPHOS inhibitory effect of CPX plays a role in the cooperation with radiation. Indeed there is a growing body of literature demonstrating a radiosensitizing effect of metformin, which can partly be ascribed to inhibition of mitochondrial complex I.<sup>327</sup> The OXPHOS inhibition by CPX and metformin could also alleviate tumor hypoxia by decreasing oxygen consumption and thus contribute to sensitizing hypoxic cells to radiotherapy.

While the combination of CPX and radiation so far has not been investigated in other studies, several publications examined combinations of CPX with chemotherapeutic agents with promising results, as summarized in Table 4. Interestingly, the authors proposed diverse mechanisms to which they attributed these cooperative effects, ranging from inhibition of Wnt or mTOR signaling to decreasing levels of ferritin or RR inhibition.

**Table 4 | Overview of preclinical studies investigating CPX in combination therapies.**

Cancer	Agent(s)	Effect	Suggested mechanism	Reference
ALL	Rapamycin	Enhancement	Downregulation of ferritin by CPX	328
ALL	Dexamethasone	Synergistic	Inhibition of $\beta$ -catenin/c-Myc signaling	131
AML	Parthenolide	Enhancement	mTOR inhibition by CPX	135
AML	Cytarabine	Synergistic	RR inhibition	95
AML	Daunorubicin	Additive	-	95
CML	Imatinib	Synergistic	Inhibition of eIF5A hypusination by CPX	132
Glioblastoma	Bortezomib	Synergistic	ROS-mediated JNK/p38 MAPK and NF- $\kappa$ B signaling	133
Myeloma (murine)	Doxorubicin Rituximab Bortezomib	No cooperation	-	94
Myeloma (murine)	Lenalidomide Thalidomide	Cooperative	Wnt inhibition	94
Pancreatic cancer	Gemcitabine	Enhancement	ROS production	126

As shown in live-cell imaging experiments conducted in the present thesis, CPX also enhanced the growth inhibitory effect of cisplatin on HPV-positive tumor cells. Quantification of the combinatorial effect confirmed a moderate synergism of the both drugs in HeLa and SiHa cells. Tumor cells exhibit a high metabolic flexibility, thus a strong reliance on OXPHOS or glycolysis does not equal to dependence on this energetic pathway, but instead cells may switch to compensatory bioenergetic pathways.<sup>329</sup> To prevent this evasion mechanism, glycolysis and OXPHOS can be inhibited simultaneously, which should lead to cell death by energy depletion. This is an example for metabolic synthetic lethality or anti-austerity, a concept describing that the simultaneous targeting of several metabolic pathways trigger metabolic stress and results in a lethal phenotype.<sup>330</sup> Furthermore, combining glycolysis and OXPHOS inhibitors could allow a dose reduction of the single compounds and thus decrease toxic side effects, which currently limit the use of glycolysis inhibitors as single agents.<sup>331</sup> Several studies have investigated such potential combination therapies, examples include the combination of glucose deprivation and complex I inhibition<sup>332</sup>, combining 2-DG with several OXPHOS inhibitors<sup>333-335</sup> or a treatment with DCA and arsenic trioxide<sup>336</sup>.

Following this concept, this thesis investigated potential combination therapies of CPX with glycolysis inhibitors. Indeed, CPX acted synergistically with all glycolysis inhibitors tested. The strongest synergism could be achieved by combining CPX with DCA. Already low doses of each compound could in combination induce apoptosis, repress viral oncogene expression and strongly inhibit proliferation of cervical cancer cells. DCA is a small molecule, which is clinically used for the treatment of lactic acidosis and inherited mitochondrial diseases<sup>337, 338</sup> and has proven anticancer activity *in vitro* and *in vivo*<sup>339-342</sup>. It acts by reverting the Warburg effect via inhibition of pyruvate dehydrogenase kinase and consequent increase of pyruvate dehydrogenase activity, resulting in a switch of pyruvate metabolism from glycolysis towards OXPHOS.<sup>236</sup> In clinical trials, however, it could not meet expectations, mainly due to dose-limiting toxicities<sup>340</sup>, thus co-administering it with OXPHOS inhibitors such as CPX could be an interesting option. These promising results suggest the combination of iron chelation with glycolysis inhibition as a novel therapeutic approach for cancer therapy. CPX in this respect offers a potential advantage compared to classical OXPHOS inhibitors as it acts via multiple additional mechanisms, leading to a multifaceted cellular response which complicates the development of resistances.

### 3.6 Clinical aspects

A major finding of the present work is that glucose availability critically shapes the therapeutic response of cervical cancer cells to CPX. While under lower glucose concentrations cells primarily die via apoptosis, under increased glucose concentrations cells survive and are arrested in a state of senescence. Due to the aforementioned deleterious effects exerted by senescent cells, these different treatment responses might be of clinical importance. Generally, glucose is known to be heterogeneously distributed in tumors, similar to oxygen its levels decrease with increasing distance from blood vessels. Therefore, glucose distribution strongly depends on factors like tumor size and vascularization. Typically, glucose concentrations in the tumor interstitium are considerably lower than in normal tissues<sup>343</sup>, which should enhance CPX efficacy. However, due to the metabolic heterogeneity of cancer cells, there will probably be zones with low and high glucose concentrations in tumors. Furthermore, drugs or disorders such as diabetes can lead to a hyperglycemic state<sup>344</sup> and in the tumor microenvironment diverse types of cells compete for different nutrients<sup>345</sup>. Further in-depth studies on the influence of other nutrients and metabolites on the senescence and apoptosis induction by CPX would be of interest in this context. An important limitation of the standard cell culture model used in this thesis is that glucose concentrations decrease over time, while physiologic glucose concentrations are held rather constant. Thus, certain aspects can only be addressed in *in vivo* models.

Glucose levels mainly influences treatment outcomes in two ways. On the one hand, under lower glucose levels cells proliferate slower, rendering them less vulnerable to chemotherapies, which

typically primarily target proliferating cells. On the other hand, increased glucose levels were shown to contribute to chemoresistance and influence drug sensitivity.<sup>346-350</sup> These divergent effects can also be seen in the response of HeLa cells to CPX – a minimum of colony outgrowth is observed under glucose concentrations corresponding to normal serum levels in humans, while both under lower and higher glucose supply more colonies form. Consistently, a maximum of PARP cleavage is induced at glucose levels, which are typical for human serum.

Dose-limiting toxicities might constitute a major obstacle for the therapeutic application of metabolic inhibitors. While cancer cells undoubtedly require higher amounts of nutrients, there are also normal tissues with high metabolic turnover, which might be affected by these therapies. This problem could be resolved by using more localized treatment regimens instead of systemic therapies. In this context, it is beneficial that CPX can not only be administered orally but also be used as a topical agent. This could particularly be interesting for the treatment of HPV-linked (pre-)neoplastic lesions, which are typically located easily accessible in skin or mucosa. CPX could possibly even be applied to HPV-infected patients as a chemopreventive agent.<sup>351</sup> According to literature therapeutically relevant concentrations should be achievable by topical administration of CPX. Upon treatment of dead human skin with 1% CPX cream, millimolar concentrations were reported<sup>352</sup> and also a study performed *in vivo* demonstrates that topical treatment with a 1% CPX cream results in concentrations of 8 to 340  $\mu\text{M}$  in the upper epidermis<sup>353</sup>. Moreover, vaginal suppositories or other drug delivery systems could enable a continuous release of CPX, compensating the short half-life *in vivo*. To evaluate the efficacy of CPX as a topical agent for the treatment of HPV-positive neoplasia, in cooperation with the group of Magnus von Knebel-Döberitz (DKZF, Heidelberg) CPX is currently being tested in a 3D organotypic co-culture model<sup>354</sup>.

Although possible side effects are expected to be more pronounced compared to topical treatment, CPX might also be administered as an oral agent. A first phase I trial in leukemia patients showed that oral treatment with 40 mg/m<sup>2</sup> CPX once daily was well tolerated, while 80 mg/m<sup>2</sup> four times daily led to gastrointestinal toxicities.<sup>129</sup> Apart from dose-limiting side effects, the short plasma half-life and low bioavailability constitute problems in utilizing CPX as an oral anticancer agent. Novel delivery approaches e.g. via nanoparticles or liposomes could circumvent these obstacles.<sup>355</sup> As an alternative method to administer CPX, a team from the University of Kansas developed a prodrug called fosciclopirox, which is rapidly metabolized to CPX and can be formulated in aqueous solutions and thus administered parenterally.<sup>356</sup> After the drug proved to be safe in a first phase I clinical study (NCT03348514), currently a phase I expansion study (NCT04608045) and a phase 2 clinical trial (NCT04525131) in urothelial cancer patients are ongoing, raising hope towards a clinical application of CPX for cancer therapy in the near future.

### 3.7 Conclusions

In summary, results from this study give valuable insights into the anti-tumorigenic effects of the iron chelator CPX in HPV-positive tumor cells and add to the growing body of literature suggesting the repurposing of CPX as an anticancer agent. Analysis of proteome data of CPX-treated cervical cancer cells allowed the identification of pathways which might be implicated in the phenotypic responses of HPV-positive cells towards iron chelation. As a main finding, the induction of senescence and apoptosis was linked to the bifunctionality of CPX as iron chelator and OXPHOS inhibitor (see scheme in Figure 41). While, as previously demonstrated, iron deprivation by CPX is crucial for the induction of DNA damage upon treatment and consequently leads to an irreversible growth arrest, the further cell fate is highly glucose-dependent. As long as glucose is abundant, cells will survive and stably remain growth arrested in a senescent state, which is linked to the secretion of pro-tumorigenic and pro-inflammatory SASP factors. However, when glucose becomes scarce, cells will undergo apoptosis due to energy depletion, which can be attributed to the OXPHOS inhibiting capacity of CPX. Accordingly, other OXPHOS inhibitors such as the antidiabetic drug metformin share the glucose-dependent induction of apoptosis. Due to the potential deleterious paracrine effects of senescent cells, this differential treatment outcomes might have a profound impact on clinical response towards iron chelators. Finally, since glycolysis inhibitors can mimic the effect of glucose deprivation, it was shown that the combination of CPX with glycolysis inhibitors synergistically inhibits proliferation of HPV-positive tumor cells and could thus represent a promising strategy in the treatment of cervical cancers or pre-neoplastic lesions.

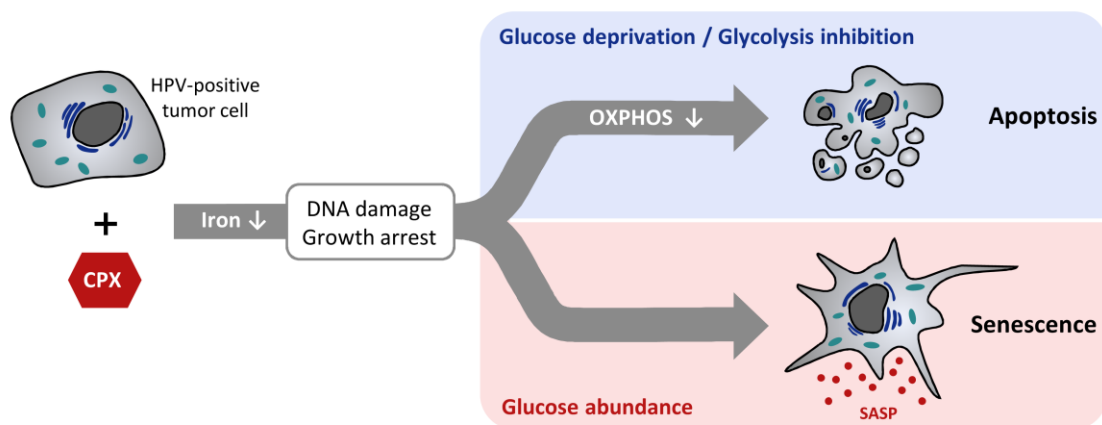


**Figure 41 | Glucose-dependent senescence vs. apoptosis induction by CPX.** Chelation of iron by CPX leads to DNA damage and growth arrest in HPV-positive tumor cells. CPX inhibits OXPHOS, thus when in parallel blocking glycolysis with chemical inhibitors or by limiting the availability of glucose, cells are deprived of energy and undergo apoptosis. If glucose is abundant, either by culturing cells in medium containing increased levels of glucose or releasing them after shorter CPX treatment, senescence, an irreversible growth arrest, is induced. Senescent cells remain metabolically active and secrete inflammatory factors, the SASP, through which they can communicate with neighboring cells.



***CHAPTER 4***  
***MATERIALS AND METHODS***



## 4. Materials and Methods

### 4.1 Reagents and materials

Molecular biology grade reagents were applied where possible. All standard material and reagents for buffers and media were supplied by AppliChem (Darmstadt, Germany), BD Biosciences (Heidelberg, Germany), Bio-Rad (Munich, Germany), Biozym Scientific (Hessisch Oldendorf, Germany), Carl Roth (Karlsruhe, Germany), Corning (Corning, NY, USA), Enzo Life Sciences (Lörrach, Germany), Eppendorf (Hamburg, Germany), GE Healthcare (Chalfont St Giles, UK), Gerbu (Heidelberg, Germany), Greiner Bio-One (Kremsmünster, Austria), Merck (Darmstadt, Germany), New England Biolabs (NEB, Frankfurt, Germany), Nerbe Plus (Winsen, Germany), Promega (Madison, WI, USA), Sigma-Aldrich (St. Louis, MO, USA), Thermo Fisher Scientific (Waltham, MA, USA), Roche Diagnostics (Basel, Switzerland), Saliter (Obergünzburg, Germany), Santa Cruz Biotechnology (Dallas, TX, USA), Sartorius (Göttingen, Germany) and Vector Laboratories (Burlingame, CA, USA). Manufacturers of non-standard reagents are specified in the text.

All buffers and solutions were prepared with distilled H<sub>2</sub>O if not stated otherwise.

### 4.2 Cell-based methods and assays

#### 4.2.1 Cultivation of cells

The cell lines used in this thesis are listed in Table 5 including their origin, HPV status and the medium they were cultured in. Normal oral keratinocyte (NOK) cell lines expressing HPV16 or HPV18 E6/E7 were generated by Dr. Ruwen Yang, AG Rösl, DKFZ, Heidelberg.<sup>234</sup> HeLa mCherry H2B and SiHa mCherry H2B were generated by Dr. Joschka Willemsen, AG Binder, DKFZ, Heidelberg. Generation of the other mCherry and mKate2 expressing cell lines is described below. All other cell lines are standard cell lines. Additionally, experiments were performed with two isolates of primary keratinocytes, from human ectocervix and from human foreskin, which were cultured in Keratinocyte-SFM medium.

If not otherwise stated, Dulbecco's minimal essential medium (DMEM, Gibco, Thermo Fisher Scientific) containing 1 g/L (5 mM) glucose and 2 mM L-glutamine was used. DMEM and RPMI-1640 (Gibco, Thermo Fisher Scientific) were supplemented with 10% fetal calf serum (FCS, Gibco, Thermo Fisher Scientific), 100 U/ml penicillin and 100 µg/ml streptomycin (Sigma-Aldrich). Stock cultures of mCherry and mKate2 transduced cells were additionally kept under selection with 0.5 or 1 µg/ml puromycin (Sigma-Aldrich), which was omitted during experiments. NOK cells were cultured in Keratinocyte-SFM (Gibco, Thermo Fisher Scientific), supplemented with Human Recombinant Epidermal Growth Factor (EGF 1-53) & Bovine Pituitary Extract (BPE) (Gibco, Thermo Fisher Scientific). As standard, all cells were cultured in a humidified incubator at 37°C, 21% O<sub>2</sub> and 5% CO<sub>2</sub>. For experiments under hypoxic conditions, cells were grown at 37°C,

1% O<sub>2</sub> and 5% CO<sub>2</sub> in an InvivoO<sub>2</sub> 400 physiological oxygen workstation (Ruskin Technology Ltd, Bridgend, UK). Stock cultures were passaged twice a week when 80-90% confluence was reached, using 0.25 % Trypsin-EDTA solution (Gibco, Thermo Fisher Scientific). In order to determine cell numbers, prior to experiments cells were counted in duplicates or triplicates by trypan blue technique using the Countess™ Automated Cell Counter (Invitrogen, Carlsbad, CA).

**Table 5 | Cell lines used in this thesis.**

Cell line	Origin and type	HPV-status	Medium
C33a mCherry H2B	Cervical SCC	-	DMEM + 1 µg/ml puromycin
CaSki	Cervical SCC	HPV16	DMEM
CaSki mCherry H2B	Cervical SCC	HPV16	DMEM + 0.5 µg/ml puromycin
FaDu mCherry H2B	HNSCC	-	DMEM + 0.5 µg/ml puromycin
HeLa	Cervical adenocarcinoma	HPV18	DMEM
HeLa mCherry H2B	Cervical adenocarcinoma	HPV18	DMEM + 1 µg/ml puromycin
HeLa mKate2	Cervical adenocarcinoma	HPV18	DMEM + 1 µg/ml puromycin
ME180	Cervical SCC	HPV68	DMEM
MRI-H186	Cervical SCC	HPV16	RPMI-1640
NOK	Normal oral keratinocytes	-	Keratinocyte-SFM
NOK 16E6E7	Normal oral keratinocytes	"HPV16 E6/E7"	Keratinocyte-SFM
NOK 18 E6E7	Normal oral keratinocytes	"HPV18 E6/E7"	Keratinocyte-SFM
NOK pWPI	Normal oral keratinocytes	-	Keratinocyte-SFM
SiHa	Cervical SCC	HPV16	DMEM
SiHa mCherry H2B	Cervical SCC	HPV16	DMEM + 1 µg/ml puromycin
SiHa mKate2	Cervical SCC	HPV16	DMEM + 1 µg/ml puromycin
SW756	Cervical SCC	HPV18	DMEM
UDSCC2 mCherry H2B	HNSCC	HPV16	DMEM + 0.5 µg/ml puromycin

#### 4.2.2 Cryopreservation of cells

For long-term storage cells were cryopreserved in liquid nitrogen. Therefore, cells were trypsinized, pelleted at 800 x *g* for 3 min and resuspended in cryo-medium (respective medium + 30% FCS + 10% DMSO). Aliquots were transferred to cryotubes and frozen at -80°C in an isopropanol-filled freezing container (Nalgene, Thermo Fisher Scientific) to ensure gradual, slow freezing. After several days, cryotubes were transferred to liquid nitrogen.

For thawing, cryopreserved cells were warmed in a water bath at 37°C, resuspended in fresh medium and seeded in a cell culture flask. The day after, when cells had settled, medium was exchanged to remove residual DMSO.

#### 4.2.3 Generation of mCherry and mKate2 expressing cell lines

For live-cell imaging analyses, cells with red fluorescent nuclei were used to enable assessment of the cell count. IC<sub>50</sub> measurements for CPX were performed in cell lines stably expressing a

fluorescently labeled version of histone H2B. These cells were generated from the standard cell lines by lentiviral transduction with a pMOWS hH2B mCherry vector. All other live-cell imaging experiments were performed with cells expressing the nuclear restricted, red fluorescent protein mKate2. These cell lines were generated by lentiviral transduction with the IncuCyte® NuCLight Lentivirus Reagent (Sartorius, Göttingen, Germany) and offer the advantage that only living cells are labeled red, while dying cells lose their fluorescence. Lentiviral transduction was performed with standard cell lines, using lentivirus at a multiplicity of infection (MOI) of 3, diluted in DMEM supplemented with 8 µg/ml polybrene. Antibiotic selection with puromycin was applied from day two after transduction to remove non-transduced cells.

#### **4.2.4 3-Dimensional cell culture**

3-Dimensional tumor spheroids better resemble the tumor microenvironment as they mimic for example oxygen and nutrient gradients. Spheroids were grown in 96-well non-adhesive round bottom tissue culture dishes with polymer-coated surface to prevent cells from adhering to the bottom. Additionally, cells were provided with a semi-solid basis, by growing them in medium supplemented with 30% of methylcellulose stock solution. This solution was prepared by adding 2.4% of sterile methylcellulose powder to preheated (60°C) DMEM without supplements. After stirring for 20 min an emulsion formed and an equal amount of DMEM at room temperature without supplements was added. Then FCS, penicillin, streptomycin and L-glutamine were added at standard concentrations and the solution was stirred overnight at 4°C. The resulting clear and viscous solution was centrifuged at 4500 g for 2 h to remove potentially undissolved methylcellulose powder. The supernatant was aliquoted using a syringe and stored at -20°C.

To generate spheroids, 5000 cells per well were seeded in 96-well low attachment U-bottom plates (Corning Costar, USA) in 200 µl DMEM with 30% methylcellulose stock solution. After two days, stable spheroids had formed and were treated by removing 100 µl of the medium and adding 100 µl medium with drugs at twice the final concentration. Every 3 to 4 days, half of the medium was replaced with fresh medium containing the respective drugs.

#### **4.2.5 Transfection of synthetic siRNAs**

To silence gene expression via RNA interference (RNAi) cells were transfected with siRNAs. Cells were seeded at a number sufficient to reach 30-40% confluence after one day. For one 6-cm dish 6 µl DharmaFECT I Transfection reagent (Dharmacon, Horizon Discovery, Cambridge, UK) were mixed with 194 µl of Opti-MEM medium (Gibco, Thermo Fisher Scientific) and incubated for 5 min at RT. In parallel, 2-6 µl siRNA (Silencer Select siRNA, Ambion, Thermo Fisher Scientific) were filled to 200 µl with Opti-MEM to yield a final siRNA concentration of 10-30 nM. The DharmaFECT mix was added to the siRNA dilution and the mixture was incubated for 20 min at RT. Meanwhile,

medium in the cell culture dishes was exchanged to 1.6 ml DMEM containing 10% FCS, but lacking penicillin, streptomycin and glutamine. After incubation, 400  $\mu$ l transfection mix per 6-cm dish was added dropwise to the cells. 24 h after transfection, medium was exchanged to standard medium with drugs as applicable.

Cells in 96-well plate format were reverse transfected. Per well, 0.15  $\mu$ l (HeLa) or 0.1  $\mu$ l (SiHa) DharmaFECT I were filled to 10  $\mu$ l with Opti-MEM, mixed and incubated for 5 min. Meanwhile, 0.3  $\mu$ l siRNA were mixed with 9.7  $\mu$ l Opti-MEM and added to the DharmaFECT mix. 20  $\mu$ l of the final transfection mix were added to each well and incubated for 30 min at RT. Afterwards, 6000 cells per well (in DMEM + 10% FCS) were seeded on top of the siRNA to yield a volume of 100  $\mu$ l. 24 h later, medium was exchanged to standard medium with or without treatments.

Sequences for all siRNAs used are listed in Table 6. As control a non-targeting siRNA (siContr1) was used, which is designed to contain at least 4 mismatches to all known human genes.

**Table 6 | siRNAs used in this thesis.**

Target transcript	Name	Sequence
-	siContr1	CAGUCGCGUUUGCGACUGG
<i>CDKN1A</i>	siP21	CAAGGAGUCAGACAUUUUA
<i>E2F1</i>	siE2F1_2	GUCACGCUAUGAGACCUCA
<i>G6PDH</i>	siG6PDH_2	CAGAUACAAGAACGUGAAG
<i>GPI</i>	siGPI	CUGGGUAUCUGGUACAUCA
<i>HK2</i>	siHK2	CCTGGGTGAGATTGTCCGT
	siHK2_2	CACGATGAAATTGAACCTG
<i>NOTCH1</i>	siNotch1-1	GGAGCAUGUGUAACAUCAA
<i>PFKP</i>	siPFKP	CGGGCAACCUGAACACCUA
<i>TP53</i>	siP53	GACUCCAGUGGUAUCUAC

#### 4.2.6 Treatment of cells with chemotherapeutics

The chemotherapeutics and chemical compounds used for treatment of cells are listed in Table 7 with their respective supplier and solvent. Typically, cells were treated one to two days after seeding with a simultaneous change of cell culture medium and the respective solvents were used as controls as indicated. The maximum of solvent concentration was 0.1%, which was tested to not be toxic to the cells.

**Table 7 | Chemical compounds used in this thesis.**

Compound	Abbreviation	Supplier	Solvent
2-Deoxy-D-glucose	2-DG	Sigma-Aldrich	DMEM
6-Aminonicotinamide	6-AN	Cayman Chemical, Ann Arbor, MI	DMSO
Antimycin A	AA	Sigma-Aldrich	EtOH
Ciclopirox olamine	CPX	Santa Cruz Biotechnology, Dallas, TX	EtOH
Cisplatin	CDDP	Sigma-Aldrich	0.9% NaCl

Deferasirox	DFX	LKT Laboratories, St. Paul, MN	DMSO
Deferoxamine mesylate	DFO	Sigma-Aldrich	H <sub>2</sub> O
Ferric ammonium citrate	FAC	Sigma-Aldrich	H <sub>2</sub> O
Ferrous sulfate	FeSO <sub>4</sub>	Sigma-Aldrich	H <sub>2</sub> O
Metformin	Met	Enzo Life Sciences, Lörrach, Germany	DMEM
N-[N-(3,5-Difluorphenacetyl)-L-alanyl]-S-phenylglycin-tert-butylester	DAPT	Hölzel Diagnostika, Köln, Germany	DMSO
Rotenone	Rot	MP Biomedicals, Santa Ana, CA	DMSO
Sodium dichloroacetate	DCA	Santa Cruz Biotechnology	DMEM

#### 4.2.7 Irradiation of cells

Cells were irradiated with the indicated doses of  $\gamma$ -rays using a Gammacell® 40 Exactor Low Dose Rate Research Irradiator (Best Theratronics, Ottawa, Canada) with a Caesium-137 source at a constant rate of 0.933 Gy/min. Cells under hypoxic conditions were transported and irradiated in airtight boxes (LocknLock, Seoul, South Korea). Controls were sham-irradiated.

#### 4.2.8 Live-cell imaging

All live-cell imaging experiments were performed in an IncuCyte® S3 system (Essen Bio Science, Sartorius) using the IncuCyte® 2019B software. For HeLa, SiHa and C33a cells 3000 cells/well were seeded, for CaSki, FaDu and UDSCC2 4500 cells/well were seeded in 96-well plates. Treatments were applied two days after seeding and subsequently life-cell imaging was started. As a standard, four images per well were taken every 2 or 4 h at 10x magnification and average values from three wells are shown.

##### 4.2.8.1 IC<sub>50</sub> calculation

To calculate IC<sub>50</sub> values for CPX, mCherry H2B expressing cells were treated in triplicates with increasing doses of CPX in 200  $\mu$ l medium. Over the course of 5 days the cell number (equaling red object count per well) was determined every 4 h. Subsequently, cell count was plotted versus time and the area under the curve (AUC) was determined with SigmaPlot. To create a dose-response curve, AUC was then plotted against the logarithm of CPX concentration and IC<sub>50</sub> values were determined with SigmaPlot by nonlinear regression, using the standard curve (Four

Parameter Logistic Curve) function ( $f = \min + \frac{\max - \min}{1 + \left(\frac{x}{IC_{50}}\right)^{-Hillslope}}$ ).

##### 4.2.8.2 Cytotox assay

To assess cell death, the Incucyte® Cytotox Green Reagent (Essen Bio Science, Sartorius) was used. This reagent includes a dye that can permeate the plasma membrane of dying cells, which then fluoresce green. Cells were seeded in 96-well plates and two days later 100  $\mu$ l medium

containing the respective chemotherapeutics and Cytotox Green agent at a final concentration of 250 nM were added. Green fluorescent objects equaling dead cells were counted every 4 h over the course of 5 days and normalized to the cell confluence to account for differences in cell proliferation upon treatment.

### *4.2.8.3 Caspase-3/7 activation assay*

Induction of apoptosis can more specifically be measured by assessing activation of caspases-3 and -7. To this end, the IncuCyte® Caspase-3/7 Green Reagent for Apoptosis (Essen Bio Science, Sartorius) was used, which contains a DNA-intercalating dye coupled to a DEVD caspase recognition motif. The substrate is intrinsically non-DNA binding and non-fluorescent. Upon apoptosis induction caspases-3 and -7 are activated and cleave the reagent, so that the dye is released and can bind to DNA, resulting in a fluorescent signal. To conduct this assay, cells were treated two days after seeding by exchanging the medium to 100 µl fresh medium containing the respective drugs and Caspase-3/7 Reagent at a final concentration of 5 µM. Apoptosis was quantified over 5 days by determining the count of green fluorescent cells and normalizing it to cell confluence.

### *4.2.9 TUNEL assay*

A further method to detect apoptosis is the terminal deoxynucleotidyl transferase-mediated dUTP nick end labeling (TUNEL) assay. One hallmark of apoptosis is the fragmentation of cellular DNA caused by the activation of endonucleases. These DNA double strand breaks can be detected with the TUNEL assay that utilizes terminal deoxynucleotidyl transferase, an enzyme which attaches fluorescently labeled nucleotides to the exposed 3'-hydroxyl termini.

Cells were seeded and treated as usual in 6-cm dishes containing glass coverslips. After 3 or 4 days of treatment, coverslips were removed and washed in PBS. The cells were fixed for 30 min in 4% paraformaldehyde in PBS and washed twice with PBS. If necessary, coverslips with fixated cells were stored in 70% EtOH at -20°C before staining. Coverslips were then again washed in PBS and cells were permeabilized for 2 min at 4°C in 0.1% Triton X-100, 0.1% sodium citrate in PBS. The coverslips were washed twice in PBS and placed in a wet chamber before apoptotic cells were stained using the In Situ Cell Death Detection Kit, Fluorescein (Roche, Basel, Switzerland). Coverslips were incubated for 60-90 min with 25 µl TUNEL solution (1:10, enzyme solution:label solution) in a humidified chamber at 37°C. Coverslips were then washed two times for 10 min with PBS and stained with 1 µg/ml DAPI (4',6-diamidino-2-phenylindole) for 5 min in the dark. Afterwards the coverslips were dipped 5 times in PBS, washed with PBS for 2x 10 min, dipped once in water and once in ethanol. After air-drying, the coverslips were mounted on microscope slides with Vectashield Antifade Mounting Medium (Vector Laboratories Inc., USA). Five to ten

images per coverslip were taken with a Cell Observer microscope (LED module colibri.2, 20x/0.4 LD PlnN Ph2 DICII objective) from Zeiss (Jena, Germany) and percentage of TUNEL positive cells was determined using an ImageJ macro (Damir Krunic, Light Microscopy Core Facility, DKFZ) in relation to total cell count determined by DAPI staining.

#### **4.2.10 Senescence assay**

Senescent cells were identified by detecting activity of senescence-associated  $\beta$ -galactosidase (SA- $\beta$ -gal). This assay is based on the observation that in senescent cells  $\beta$ -galactosidase activity is detectable at pH 6.0, which is in contrast to its normal activity at pH 4.0 within lysosomes.<sup>357, 358</sup> SA- $\beta$ -gal activity was detected with the artificial chromogenic substrate X-gal (5-bromo-4-chloro-3-indolyl  $\beta$  D-galactopyranoside), which results in blue staining of senescent cells. Cells were split after treatment at a ratio of 1:2 (treated cells) or 1:5 (untreated controls) and cultivated for 4 days in DMEM (1 g/L glucose) without drugs. During this time, medium was exchanged every 2-3 days. Cells were then washed once with PBS, fixed with 1 ml senescence assay fixation buffer (2% PFA, 0.2% glutaraldehyde in PBS) for 3 min and washed again with PBS. Cells were incubated overnight in 1.5 ml of senescence assay buffer (40 mM citric acid, 150 mM NaCl, 2 mM MgCl<sub>2</sub>, adjusted to pH 6.0 with Na<sub>2</sub>HPO<sub>4</sub>; 5 mM K<sub>3</sub>[Fe(CN)<sub>6</sub>], 5 mM K<sub>4</sub>[Fe(CN)<sub>6</sub>] and 1 mg/ml X-gal in DMF were added freshly) at 37°C in a wet chamber. Afterwards cells were washed once with PBS and images were acquired using the EVOSxl Core Cell Imaging System (Invitrogen, Thermo Fisher Scientific) with 20x magnification.

#### **4.2.11 Colony formation assay**

Colony formation assays (CFAs) were used to assess the effect of treatments on the clonogenic potential of cells. Cells were seeded and two days later treated or irradiated, with concurrent medium change. After the indicated treatment period, cells were split in a ratio of 1:100 in fresh, drug-free medium (1 g/L glucose). Cells were allowed to grow into colonies for 11-13 days, during which medium was replaced every 3-4 days. Subsequently, cells were washed with PBS and then fixed and stained with 350  $\mu$ l crystal violet staining solution (12 mM crystal violet, 29 mM NaCl, 3% formaldehyde, 22% EtOH) per 6-cm dish for 5 min. After washing the dishes with water, they were dried overnight at 37°C. Images of the stained dishes were taken with an Epson Perfection 4990 Photo Scanner (Epson, Suwa, Japan).

#### **4.2.12 Clonogenic assay**

The clonogenic assay represents a variation of the colony formation assay, which is preferentially used in radiation research and enables quantification of the surviving fraction of cells. Therefore, a small number of cells (100 cells for controls, increasing numbers for treated samples according

to the expected survival fraction) was seeded in 6-cm dishes in triplicates and grown under normoxic conditions for 16 h. In parallel, medium was pre-incubated under hypoxic conditions. On the next day when cells had attached, medium was replaced with 3 ml fresh normoxic or hypoxic medium and hypoxic samples were transferred to 1% O<sub>2</sub>. After 2 h, cells were treated as indicated and immediately afterwards irradiated with doses of 1-8 Gy. Hypoxic samples were irradiated under hypoxic conditions by transporting them in airtight boxes. After 2 or 3 days, medium was replaced with 6 ml fresh medium without drugs and cells were grown under normoxic conditions for 10-13 days before staining and fixing as described above for CFAs. Afterwards, colonies consisting of >50 cells were counted with an ImageJ Macro (written by Damir Krunic, Light Microscopy Core Facility) and surviving fractions (SF) were calculated as follows:

$$SF (\%) = \frac{\# \text{ of colonies formed}}{\# \text{ of cells seeded} \times PE} \times 100$$

with plating efficiency (PE):

$$PE = \frac{\# \text{ of colonies formed in control}}{\# \text{ of cells seeded in control}}$$

SF was then logarithmically plotted against radiation dose and data fitted to the linear quadratic equation  $f = e^{-\alpha D - \beta D^2}$  with D indicating the radiation dose in Gy.

### **4.2.13 Glucose measurements**

Glucose measurements were performed in cooperation with Barbara Leuchs (DKFZ, Heidelberg). 6000 cells/well were seeded in 96-well plates and two days later cells were treated with CPX or EtOH as solvent control in 100 µl fresh medium containing 1 or 4.5 g/L glucose. After 0, 12, 24 and 48 h supernatant from 4 wells per condition was removed and pooled, centrifuged for 5 min at 1000 g and then subjected to glucose measurements. In parallel, cell counts were determined every 4 h with the IncuCyte® S3. Glucose concentrations were measured with a Cedex Bio Analyzer (Roche, Basel, Switzerland).

## **4.3 Protein-based methods**

### **4.3.1 Harvest of cells and protein extraction**

For protein extraction, cells were harvested by scraping them in ice-cold PBS. Subsequently, the cell suspension was centrifuged for 15 s at 13,000 g at room temperature and the supernatant was discarded. Protein pellets were either frozen at -20°C until further processing or immediately lysed by resuspension in 20-80 µl CSK-1 lysis buffer (300 mM NaCl, 300 mM sucrose, 10 mM Pipes, 1 mM MgCl<sub>2</sub>, 1 mM EDTA, 0.5% Triton X-100; 1x PhosSTOP phosphatase inhibitor cocktail (Roche Diagnostics), 2.5 mM Pefabloc serine protease inhibitor (Merck) and 1% P8340 phosphatase inhibitor cocktail (Sigma-Aldrich) were freshly supplemented). After incubation on

ice for 30 min, samples were centrifuged for 5 min at 13,000 g at 4°C. The supernatant was transferred to a fresh reaction tube and protein concentration was determined via Bradford assay. Therefore, 1 µl of lysate was added to 1 ml Bradford assay solution (BioRad, USA) in disposable plastic cuvettes, incubated for 5 min at room temperature and absorption at 595 nm was measured using a BioPhotometer D30 (Eppendorf). Protein concentrations were determined by comparing absorption to a standard curve generated with bovine serum albumin (BSA). Subsequently, lysates were diluted to the desired concentration with 4x protein loading buffer (250 mM Tris-HCl (pH 6.8), 40% glycerol, 20% 2-mercaptoethanol, 8% SDS, 0.008% bromophenol blue) and boiled for 5 min at 95°C to denature secondary structures. Protein lysates were stored at -80°C.

#### 4.3.2 SDS-PAGE and western blot

Via SDS-PAGE (sodium dodecyl sulfate polyacrylamide gel electrophoresis) proteins can be separated by molecular weight or more exactly by their electrophoretic mobility. SDS-PAGE gels were prepared as in Table 8 using glass plates sealed with 1% agarose. Gels were installed in an XCell SureLock™ Mini-Cell Electrophoresis System (Life Technologies). Equal amounts of protein (15-30 µg per lane) were loaded next to 2 µl peqGOLD pre-stained Protein-marker IV (PeqLab) for size determination. The chamber was filled with tris-glycine SDS running buffer (2.5 mM Tris, 19.2 mM glycine, 0.1 % SDS) and gels were run at a constant voltage of 100-120 V for ca. 2 h.

**Table 8 | Components for SDS-PAGE gels.**

Stacking gel (5%)	For 2 gels	Resolving gel (12.5%)	For 2 gels
H <sub>2</sub> O	3.5 ml	H <sub>2</sub> O	4.5 ml
30% Acrylamide/bisacrylamide	830 µl	30% Acrylamide/bisacrylamide	4.2 ml
0.47 M Tris-HCl (pH 6.7)	620 µl	3 M Tris-HCl (pH 8.9)	1.2 ml
10% SDS	50 µl	10% SDS	100 µl
10% APS	100 µl	10% APS	10 µl
TEMED	5 µl	TEMED	50 µl

Afterwards, protein was transferred to an Immobilon-P PVDF membrane (Merck Millipore) via semi-dry electroblotting. The membrane was shortly activated in methanol and then incubated in Towbin transfer buffer (19.2 mM glycine, 2.5 mM Tris, 20% methanol, pH 8.3) together with Whatman paper. A stack was formed with four Whatman filter papers at the bottom followed by the PVDF membrane, then the protein gel and topped with four more Whatman filter papers. Electroblotting was performed in a Trans-Blot® SD Semi-Dry Electrophoretic Transfer Cell (BioRad) at a constant voltage of 20 V for 1 h. Afterwards the stack was disassembled and the membrane blocked for at least 1 h in blocking solution (0.2% Tween-20, 5% skim milk powder, 1% BSA in PBS) to prevent unspecific binding.

### 4.3.3 Immunodetection of Proteins

For immunodetection of proteins, the western blot membrane was incubated with the primary antibody diluted in blocking solution overnight at 4°C. Primary antibodies are listed in Table 9. The membrane then was washed 3 times for at least 10 min with PBST (0.2% Tween-20 in PBS) and incubated with the secondary antibody diluted in blocking solution for 1 h at room temperature. Secondary antibodies are listed in Table 10. After 3 more washes with PBST, target proteins were detected via enhanced chemiluminescence (ECL). ECL luminol and peroxide solutions (ECL Prime Western Blotting Detection Reagent, Cytiva or WesternBright Sirius HRP Substrate, Advansta) were mixed in a ratio of 1:1 and added to the membrane. The horseradish peroxidase (HRP) coupled to the secondary antibodies catalyzes the oxidation of luminol to 3-aminophthalate, a reaction emitting light which was detected with the Fusion SL Gel Detection System (Vilber Lourmat, Eberhardzell, Germany).

**Table 9 | Primary antibodies.**

Name	Species	Supplier	#	Dilution
cleaved caspase-9 (Asp330) (D2D4)	rabbit	Cell Signaling	7237	1:1000
cleaved PARP (Asp214) (19F4)	mouse	Cell Signaling	9546	1:1000
COX4 (20E8C12)	mouse	Invitrogen	A21348	1:2000
COX6B1 (C-3)	mouse	Santa Cruz Biotechnology	393233	1:500
E2F1 (KH95)	mouse	Santa Cruz Biotechnology	251	1:500
Ferritin heavy chain (B-12)	mouse	Santa Cruz Biotechnology	376594	1:1000
Fn14	rabbit	Cell Signaling	4403	1:1000
G6PD (G-12)	mouse	Santa Cruz Biotechnology	373886	1:500
GPI (H-10)	mouse	Santa Cruz Biotechnology	365066	1:500
HKI (G-1)	mouse	Santa Cruz Biotechnology	46695	1:500
HKII (C-14)	goat	Santa Cruz Biotechnology	6521	1:200
HPV16 E6 (clone 849)	mouse	Arbor Vita Corporation		1:3000
HPV16 E7 (NM2)	mouse	kind gift of Dr. Martin Müller, DKFZ, Heidelberg		1:1000
HPV18 E6 (clone 399)	mouse	Arbor Vita Corporation		1:2000
HPV18 E7	chicken	Zentgraf, DKFZ, Heidelberg		1:1000
ID1 (B-8)	mouse	Santa Cruz Biotechnology	133104	1:1000
NDRG1 (D8G9)	rabbit	Cell Signaling	9485	1:2000
NDUFS1 (E-8)	mouse	Santa Cruz Biotechnology	271510	1:500
NDUFS2 (B-3)	mouse	Santa Cruz Biotechnology	390596	1:500
NICD (Val1744) (D3B8)	rabbit	Cell Signaling	4147	1:1000
Notch1 (C-10)	mouse	Santa Cruz Biotechnology	373891	1:250
p21 (C-19)	rabbit	Santa Cruz Biotechnology	397	1:250
p53 (DO-1)	mouse	Santa Cruz Biotechnology	126	1:1000
p62	mouse	BD Pharmingen	610832	1:1000
PFKP (F-7)	mouse	Santa Cruz Biotechnology	514824	1:500
phospho-p53 (Ser15)	rabbit	Cell Signaling	9284	1:1000

phospho-RPA32 (Ser33)	rabbit	Bethyl Laboratories	A300-246A	1:1000
RhoB (C-5)	mouse	Santa Cruz Biotechnology	8048	1:250
STAT3 (C-20)	rabbit	Santa Cruz Biotechnology	482	1:1000
Vinculin (7F9)	mouse	Santa Cruz Biotechnology	73614	1:4000
$\beta$ -Actin (C-4)	mouse	Santa Cruz Biotechnology	47778	1:50,000

**Table 10 | Secondary antibodies.**

Name	Species	Supplier	#	Dilution
$\alpha$ -chicken IgG-HRP	goat	Santa Cruz Biotechnology	2428	1:5000
$\alpha$ -goat IgG-HRP	donkey	Santa Cruz Biotechnology	2020	1:5000
$\alpha$ -mouse IgG-HRP	goat	Santa Cruz Biotechnology	2005	1:5000
$\alpha$ -rabbit IgG-HRP	goat	Santa Cruz Biotechnology	2004	1:5000

#### 4.3.4 Proteome analysis via TMT-MS

For proteome analyses, SiHa cells were treated with 10  $\mu$ M CPX or EtOH for 48 h, harvested by scraping in ice-cold PBS, pelleted by centrifugation and stored at -80°C until further processing (experiment performed by Julia Braun).

Proteome analyses were performed by Bianca Kuhn in the group of Dr. Jeroen Krijgsveld, DKFZ, Heidelberg. The 10plex tandem mass tag (TMT) system from Thermo Fisher Scientific was used to label proteins, which allows the relative quantification of protein abundances of up to 10 samples. A liquid chromatography mass spectrometric (LC-MS/MS) approach was applied and data was analyzed with Proteome Discoverer 2.1.0.81 (Thermo Fisher Scientific). The detailed protocol for protein sample preparation and mass spectrometry-based proteome analysis can be found in Bossler et al. 2019.<sup>319</sup> The mass spectrometry proteomics data have been deposited to the ProteomeXchange Consortium via the PRIDE<sup>359</sup> partner repository with the dataset identifier PXD011095.

Gene set enrichment analysis (GSEA) was performed using GSEA v. 4.0.3 and MSigDB v. 7.0. Average log<sub>2</sub>FC values of all detected proteins from three replicates were used as input for a pre-ranked enrichment analysis with the following settings: number of permutations, 1000; enrichment statistic, weighted; gene set size, min: 15, max: 500; This resulted in 12,338 gene sets being used in the analysis of which 1409 were significantly ( $p < 0.05$ ) positively enriched and 1355 were significantly negatively enriched.

A heat map was created by comparing the following proteome data: (1) 48 h 10  $\mu$ M CPX at 21% O<sub>2</sub> vs. 48 h EtOH at 21% O<sub>2</sub>; (2) 48 h 10  $\mu$ M CPX at 1% O<sub>2</sub> vs. 48 h EtOH at 1% O<sub>2</sub>; (3) 48 h 1% O<sub>2</sub> vs. 48 h 21% O<sub>2</sub> and (4) 24 h 7.5 mM metformin vs. 24 h untreated. All experiments were performed in triplicates in SiHa cells and run in one 10plex TMT MS analysis per replicate. Proteins of interest were manually selected and clustering was performed with the Morpheus software (Broad

Institute, Cambridge, MA, USA) with the following settings: hierarchical clustering; one minus Pearson correlation; average linkage.

### **4.4 RNA-based methods**

#### **4.4.1 RNA isolation**

Total RNA was isolated from cells using the PureLink™ RNA Mini Kit (Invitrogen, Thermo Fisher Scientific). Cells were either harvested by scraping in PBS as described in 4.3.1 followed by resuspension of the pellet in 600 µl lysis buffer containing 1% 2-mercaptoethanol, or cells were directly lysed in the cell culture dish after washing with PBS. The kit was used according to manufacturer's instructions, including the optional on-column DNA digestion for 15 min using the PureLink DNase Set (Invitrogen, Thermo Fisher Scientific). RNA was eluted from the columns with 20-80 µl RNase-free water and RNA concentration and quality were evaluated with the NanoDrop ND-1000 spectrophotometer (Peqlab). Purified RNA was stored at -80°C.

#### **4.4.2 Reverse transcription**

The extracted and purified total RNA was transcribed into cDNA using the ProtoScript® II First Strand cDNA Synthesis Kit (NEB). 500 ng total RNA were used as input and filled up to 3 µl with RNase free water. 1 µl primer mix containing random and oligo dT primers at a ratio of 1:1 was added. To allow RNA denaturation and primer annealing, the mixture was incubated for 5 min at 70°C in a thermal cycler. Afterwards 5 µl 2x M-MuLV Reaction mix (contains dNTPs and an optimized buffer) and 1 µl M-MuLV Enzyme mix (contains reverse transcriptase and murine RNase inhibitor) were added. This 10 µl reaction mix was then incubated for 5 min at 25°C, followed by 60 min at 42°C to facilitate cDNA transcription. A final incubation step at 80°C for 5 min was performed to deactivate the reverse transcriptase. The cDNA products were diluted with 40 µl RNase free water and stored at -20°C.

#### **4.4.3 Quantitative real-time PCR**

Expression of mRNAs was determined by quantitative real-time PCR (qRT-PCR). Therefore, 2 µl of the cDNA generated via reverse transcription was mixed with 7.2 µl RNase free water, 10 µl SYBR® Green PCR master mix (Applied Biosystems) and 0.4 µl forward and reverse primer, respectively. All primers were used at a final concentration of 100 nM with the exception of 18S rRNA primers, which were used at a final concentration of 50 nM. The primer sequences used are listed in Table 11. All reactions were run in duplicates and an H<sub>2</sub>O control without cDNA was included to control for contaminations. qRT-PCRs were performed in MicroAmp™ Optical 96-Well Reaction Plates (Life Technologies) or PCR 96-Well TW-MT-Plates (Biozym) and run on the 7300 Real Time PCR System (Applied Biosystems, Invitrogen) according to the PCR program in

Table 12. HPV16 and HPV18 *E6/E7* primers recognize all three transcript classes of HPV16 and HPV18 *E6/E7*, respectively.

**Table 11| Primers for qRT-PCR.**

Target gene	Forward primer (5'-3')	Reverse primer (5'-3')
<i>18S rRNA</i>	CATGGCCGTTCTTAGTTGGT	ATGCCAGAGTCTCGTTCGTT
<i>CCNB1</i>	GCCTCTACCTTTGCACTTCCT	TGTTGTAGAGTTGGTGTCCATT
<i>CDKN1A</i>	GACCATGTGGACCTGTCACT	GCGGATTAGGGCTTCTCTT
<i>HPV16 E6/E7</i>	CAATGTTTCAGGACCCACAGG	CTCACGTCGCAGTAACTGTTG
<i>HPV18 E6/E7</i>	ATGCATGGACCTAAGGCAAC	AGGTCGTCTGCTGAGCTTTC
<i>ID1</i>	AATCCGAAGTTGGAACCCCC	GAACGCATGCCGCTCG
<i>IL1A</i>	AACCAACGGGAAGTTCTGA	AGGCTTGATGATTTCTTCTCT
<i>IL6</i>	CCACCGGGAACGAAAGAGAA	CGAAGGCGCTTGTGGAGAA
<i>SERPINE1</i>	GACCGCAACGTGGTTTTCTC	GCCATGCCCTTGTATCAAT
<i>TFR1</i>	TGCTGGAGACTTTGGATCGG	TATACAACAGTGGGCTGGCA

**Table 12| qRT-PCR program.**

Stage	1: Primer annealing	2: DNA denaturation	3: Elongation		4: Dissociation			
Repetitions	1	1	40		1			
Temperature (°C)	50	95	95	60	95	60	95	60
Time	2 min	10 min	15 s	60 s	15 s	60 s	15 s	15 s

Relative expression of target genes was calculated according to the comparative Ct ( $2^{\Delta\Delta Ct}$ ) method<sup>360</sup> and normalized to 18S rRNA as internal reference. Statistical analyses were performed after logarithmic transformation of the fold change data.

#### 4.5 Combination Index (CI) analyses

To quantify the combinatorial effects of two drugs, combination indices (CI) were calculated according to the Chou-Talalay method, which is based on the median-effect equation.<sup>235</sup> Cells were treated in triplicates with varying doses of single drugs or drug combinations with a constant drug ratio. Proliferation curves were recorded over the course of 5 days as described in 4.2.8. Subsequently, the area under the curve (AUC) values of the growth curves were determined using SigmaPlot version 14.0 (Systat Software Inc., San Jose, CA) and used as input for CI calculation with the CompuSyn software (ComboSyn, Inc., Paramus, NJ, USA). CI > 1, CI = 1 and CI < 1 indicate antagonistic, additive and synergistic effects, respectively.

#### 4.6 Statistical analyses

Statistical tests were performed using SigmaPlot. Fold change values were analyzed after logarithmic transformation. For comparison of relative mRNA levels after CPX treatment, an

one-sample *t*-test was performed with a test mean of zero. Shapiro-Wilk normality analysis was performed with an alpha-value of 0.05. For comparison of TUNEL-positive cell percentages, a two-sided Student's *t*-test was used.

Statistical significance was assumed for *p*-values  $\leq 0.05$  (\*),  $\leq 0.01$  (\*\*),  $\leq 0.001$  (\*\*\*)).

# ***APPENDIX***



## Appendix

### Supplemental data

**Table S1| Gene symbols and log2FC values upon CPX treatment for the gene set “GO oxidative phosphorylation”.**

Symbol	log2FC	Symbol	log2FC	Symbol	log2FC	Symbol	log2FC
ATP5MC3	1,27	PGK2	0,18	SHMT2	-0,13	NDUFA12	-0,63
ACTN3	0,67	COX4I1	0,15	UQCRC1	-0,17	NDUFA8	-0,67
SDHAF2	0,65	ATP5F1D	0,14	MSH2	-0,20	NDUFA7	-0,73
COQ9	0,63	UQCC2	0,14	NDUFB10	-0,20	COX7C	-0,86
PPIF	0,52	COX5A	0,11	NDUFB9	-0,22	CDK1	-0,88
DNAJC30	0,49	PDE12	0,09	COX5B	-0,26	NDUFA5	-0,89
SURF1	0,48	NIPSNAP2	0,09	NDUFC2	-0,33	PARK7	-0,96
COX7A2L	0,39	NDUFB6	0,06	UQCRB	-0,33	NDUFS3	-1,01
MT-ND4	0,39	CYCS	0,05	NDUFB8	-0,35	NDUFA13	-1,03
ABCD1	0,37	NDUFAF1	0,05	COX6C	-0,36	COX7A2	-1,04
ATP5F1A	0,33	RHOA	0,01	UQCRC2	-0,38	COX6B1	-1,16
UQCR10	0,32	NDUFB11	-0,01	UQCRFS1	-0,44	NDUFV1	-1,23
ATP5F1C	0,32	MT-ATP8	-0,01	NDUFA9	-0,47	NDUFS8	-1,27
ATP5F1E	0,31	NDUFB5	-0,04	CCNB1	-0,48	NDUFA4	-1,28
SDHA	0,31	MT-ND3	-0,04	NDUFB7	-0,50	NDUFA6	-1,30
ATP5F1B	0,27	VCP	-0,05	BID	-0,50	NDUFS1	-1,34
DLD	0,27	NDUFAB1	-0,06	NDUFB4	-0,51	NDUFS5	-1,37
MECP2	0,25	CYC1	-0,06	NDUFS2	-0,53	NDUFS7	-1,41
STOML2	0,25	NDUFS6	-0,10	NDUFB3	-0,55	NDUFV2	-1,49
COX15	0,24	UQCRH	-0,10	NDUFA11	-0,55	NDUFA2	-1,49
FXN	0,24	UQCRQ	-0,12	NDUFA10	-0,57	NDUFS4	-1,53
COA6	0,23	PGK1	-0,13	MT-CO2	-0,59		

**Table S2| Gene symbols and log2FC values upon CPX treatment for the gene set “GO glycolytic process”.**

Symbol	log2FC	Symbol	log2FC	Symbol	log2FC	Symbol	log2FC
HK2	1,52	NUP155	0,51	PGK2	0,18	ALDOA	-0,39
PFKFB3	1,16	NUP35	0,49	NUP50	0,17	TPI1	-0,4
HIF1A	1,05	NUP160	0,45	ZBTB7A	0,17	LDHA	-0,5
ENO2	0,76	RANBP2	0,41	NUPL2	0,12	EIF6	-0,51
ADPGK	0,75	OGDH	0,41	NUP188	0,07	GAPDH	-0,52
HK1	0,75	SEH1L	0,4	POM121C	0,01	PFKFB2	-0,58
NUP37	0,7	NUP43	0,4	SEC13	0	GALK1	-0,6
ACTN3	0,67	NUP98	0,36	NUP93	-0,06	PGM1	-0,65
NUP210	0,64	NUP214	0,32	NCOR1	-0,06	PFKM	-0,65
TPR	0,58	NDC1	0,3	PFKP	-0,06	PGAM1	-0,68
NUP153	0,57	NUP88	0,29	ALDOC	-0,06	PKM	-0,71
ARNT	0,57	AAAS	0,26	PFKL	-0,08	OGT	-0,77
NUP54	0,57	NUP205	0,25	PGK1	-0,13	ENO1	-0,79

NUP62	0,57	INSR	0,23	DHTKD1	-0,28	ECD	-0,82
NUP133	0,54	RAE1	0,2	TIGAR	-0,3	GPI	-0,83
NUP107	0,54	NUP85	0,2	PRKAG1	-0,31	STAT3	-1,47
NUP58	0,53	ENTPD5	0,18	PRKAA1	-0,36		

### List of figures

Figure 1  Genome organization of HPV16.	3
Figure 2  HPV life cycle.	4
Figure 3  Cancer cases attributable to HPV in 2018.	5
Figure 4  Overview of cellular interaction partners of HPV E6 and E7.	6
Figure 5  Cellular iron metabolism.	10
Figure 6  The regulatory IRE-IRP system.	11
Figure 7  Iron coordination by chelators.	12
Figure 8  Anti-tumorigenic effects of ciclopirox.	15
Figure 9  Notch signaling pathway.	16
Figure 10  Molecular pathways involved in senescence induction and how they are altered by HPV E6/E7.	18
Figure 11  The mitochondrial electron transport chain.	22
Figure 12  Anti-tumorigenic effects of metformin.	23
Figure 13  Proteome analyses of differentially expressed proteins under CPX treatment.	30
Figure 14  Validation of proteomics hits.	31
Figure 15  CPX upregulates factors involved in OXPHOS and downregulates factors involved in glycolysis.	32
Figure 16  CPX-treated cells exhibit an increased glucose consumption.	33
Figure 17  Increased glucose availability counteracts E6/E7 downregulation by CPX.	34
Figure 18  Increased glucose availability protects cells against CPX-induced apoptosis.	35
Figure 19  Inhibition of cell proliferation by CPX is glucose-dependent.	37
Figure 20  Influence of glycolysis inhibition on the protective effects exerted by increased glucose levels.	38
Figure 21  CPX induces an irreversible, metformin a reversible growth arrest.	40
Figure 22  Release from CPX treatment.	41
Figure 23  Regulation of senescence and apoptosis-related factors by CPX under different glucose conditions.	42
Figure 24  Influence of E2F1, p21 and p53 on CPX-induced senescence and apoptosis.	43
Figure 25  CPX-mediated regulation of senescence-associated factors on mRNA level.	45
Figure 26  Metformin glucose-dependently represses E6/E7 and inhibits proliferation of cervical cancer cells.	46

Figure 27  OXPHOS inhibitors glucose-dependently induce apoptosis in cervical cancer cells.	47
Figure 28  The capacity of CPX to induce senescence under increased glucose availability is not shared by other OXPHOS inhibitors.	48
Figure 29  Iron chelators induce apoptosis in a glucose-dependent manner and act pro-senescent under increased glucose availability.	50
Figure 30  CPX upregulates Notch1.	51
Figure 31  CPX activates Notch signaling in an iron-dependent manner.	52
Figure 32  Notch inhibition does not counteract growth inhibition by CPX.	53
Figure 33  Determination of IC <sub>50</sub> values for CPX via live-cell imaging.	54
Figure 34  CPX-treatment of normal oral keratinocytes (non-)expressing E6/E7.	55
Figure 35  E6/E7 expression sensitizes NOK cells to apoptosis induction by CPX.	56
Figure 36  CPX only weakly induces apoptosis in primary keratinocytes.	57
Figure 37  CPX acts synergistically with radiation under normoxia and hypoxia.	58
Figure 38  CPX cooperates with cisplatin.	59
Figure 39  Metformin cooperates with radiation and cisplatin.	60
Figure 40  CPX synergizes with glycolysis inhibitors, but not OXPHOS inhibitors.	61
Figure 41  Glucose-dependent senescence vs. apoptosis induction by CPX.	83

### List of tables

Table 1  Overview of iron chelators with anti-tumorigenic potential.	13
Table 2  Cell line-dependent effects of CPX on Notch1 signaling.	53
Table 3  IC <sub>50</sub> values for CPX in HPV-positive or negative cell lines.	55
Table 4  Overview of preclinical studies investigating CPX in combination therapies.	80
Table 5  Cell lines used in this thesis.	88
Table 6  siRNAs used in this thesis.	90
Table 7  Chemical compounds used in this thesis.	90
Table 8  Components for SDS-PAGE gels.	95
Table 9  Primary antibodies.	96
Table 10  Secondary antibodies.	97
Table 11  Primers for qRT-PCR.	99
Table 12  qRT-PCR program.	99
Table S1  Gene symbols and log <sub>2</sub> FC values upon CPX treatment for the gene set “GO oxidative phosphorylation”.	103
Table S2  Gene symbols and log <sub>2</sub> FC values upon CPX treatment for the gene set “GO glycolytic process”.	103

**Abbreviations**

1,3-BP	1,3-bisphosphoglycerate
2-DG	2-deoxy-D-glucose
3-AP	triapine
6-AN	6-aminonicotinamide
AA	antimycin A
ADAM	a disintegrin and metalloproteinase
ADP	adenosine diphosphate
AIDS	acquired immune deficiency syndrome
ALL	acute lymphoblastic leukemia
AML	acute myeloid leukemia
AMP	adenosine monophosphate
AMPK	5'AMP-activated protein kinase
APS	ammonium persulfate
ATM	ataxia telangiectasia mutated
ATP	adenosine triphosphate
ATR	ataxia telangiectasia and Rad3 related
AUC	area under the curve
bp	base pair
BSA	bovine serum albumin
CDDP	<i>cis</i> -diamminedichloridoplatinum(II), cisplatin
CDKN1A	cyclin-dependent kinase inhibitor 1 A
cDNA	complementary DNA
CFA	colony formation assay
CHK1/2	checkpoint kinase 1/2
CI	combination index
CIN	cervical intraepithelial neoplasia
CML	chronic myeloid leukemia
CO <sub>2</sub>	carbon dioxide
COX4	cytochrome c oxidase subunit 4
COX6B1	cytochrome c oxidase subunit 6B1
Cp	ceruloplasmin
CPX	ciclopirox (olamine)
CSL	CBF1, Suppressor of Hairless, Lag1
CT	chemotherapy
Ct	cycle threshold
DAPI	4',6-diamidino-2-phenylindole
DAPT	<i>N</i> -[ <i>N</i> -(3,5-difluorophenacetyl)- <i>l</i> -alanyl]- <i>S</i> -phenylglycine <i>t</i> -butyl ester
DCA	dichloroacetate
DDR	DNA damage response
DFO	deferoxamine
DFX	deferasirox
DISC	death-inducing signaling pathway
DMEM	Dulbecco's minimal essential medium
DMSO	dimethyl sulfoxide
DMT1	divalent metal transporter 1
DNA	deoxyribonucleic acid
dNTP	deoxynucleoside triphosphate
DOHH	deoxyhypusine hydroxylase
DR4/5	death receptor 4/5
DREAM	dimerization partner, Rb-like, E2F and multi-vulval class B
e.g.	<i>exempli gratia</i>
E2F	elongation factor 2
E6AP	E6-associated protein
ECAR	extracellular acidification rate
ECL	enhanced chemoluminescence

---

EDTA	ethylenediaminetetraacetic acid
eIF5A	eukaryotic translation initiation factor 5A
EMT	epithelial-mesenchymal transition
ER	endoplasmatic reticulum
et al.	<i>et alii</i>
ETC	electron transport chain
EtOH	ethanol
FAD	flavin adenine dinucleotide
FADD	Fas-associated protein with death domain
FCS	fetal calf serum
Fe <sup>2+</sup>	ferrous iron
Fe <sup>3+</sup>	ferric iron
FMN	flavin mononucleotide
Fn14	fibroblast growth factor-inducible 14
FPN1	ferroportin
G418	geneticin
G6PD	glucose-6-phosphate dehydrogenase
GA-3P	glyceraldehyde-3-phosphate
Glc	glucose
GPI	glucose-6-phosphate isomerase
GSEA	gene set enrichment analysis
GTP	guanosine triphosphate
Gy	Gray
H <sub>2</sub> O	water
HAMP	hepcidin antimicrobial peptide
HIF	hypoxia-inducible factor
HKI/II	hexokinase I/II
HNSCC	head and neck squamous cell carcinoma
HPV	human papillomavirus
HRP	horseradish peroxidase
HSPG	heparin sulfate proteoglycan
IC <sub>50</sub>	half maximal inhibitory concentration
IL	interleukin
IRE	iron responsive element
IRF1	interferon regulatory factor 1
IRP	iron regulatory protein
JAK	janus kinase
kb	kilo base
kDa	kilo dalton
LC	liquid chromatography
LCR	long control region
LDHA	lactate dehydrogenase A
LIP	labile iron pool
LKB1	liver kinase B1
log <sub>2</sub>	binary logarithm
log <sub>2</sub> FC	log <sub>2</sub> fold change
MAM	mastermind
Met	metformin
MiDAS	mitochondrial dysfunction-associated senescence
MMP	matrix metalloproteinase
MOI	multiplicity of infection
MOMP	mitochondrial outer membrane permeability
mRNA	messenger RNA
MS	mass spectrometry
mTOR	mechanistic/mammalian target of rapamycin
mTORC1/2	mTOR complex 1/2
NAD/NADH	nicotinamide adenine dinucleotide

NDRG1	N-myc downstream regulated gene 1
NDUFS1/2	NADH:Ubiquinone oxidoreductase core subunits S1/S2
NEXT	notch extracellular truncation
NF- $\kappa$ B	nuclear factor kappa-light-chain-enhancer of activated B cells
NICD	notch intracellular domain
NO	nitric oxide
NOK	normal oral keratinocyte
O <sub>2</sub>	oxygen
OXPPOS	oxidative phosphorylation
PARP	poly (adenosine diphosphate-ribose) polymerase
PBS	phosphate-buffered saline
PCR	polymerase chain reaction
PDH	pyruvate dehydrogenase
PDK1	pyruvate dehydrogenase kinase 1
PEP	phosphoenolpyruvate
PFA	paraformaldehyde
PFK-1	phosphofructokinase 1
PFKP	phosphofructokinase 1, platelet isoform
PHD2	prolyl hydroxylase 2
PPP	pentose phosphate pathway
pRb	retinoblastoma protein
PVDF	polyvinylidene difluoride
pVHL	von Hippel-Lindau tumor suppressor
qPCR	quantitative real-time polymerase chain reaction
qRT-PCR	quantitative real-time reverse transcription-polymerase chain reaction
RhoB	Ras homolog family member B
RNA	ribonucleic acid
RNAi	RNA interference
RNAse	ribonuclease
rNDP	ribonucleoside diphosphates
rNTP	ribonucleoside triphosphates
ROS	reactive oxygen species
Rot	rotenone
RR	ribonucleotide reductase
RT	radiotherapy
SASP	senescence-associated secretory phenotype
SA- $\beta$ -gal	senescence-associated- $\beta$ -galactosidase
SCC	squamous cell carcinoma
SDS	sodium dodecyl sulfate
SDS-PAGE	sodium dodecyl sulfate polyacrylamide gel electrophoresis
SF	surviving fraction
siRNA	small interfering RNA
Smac/DIABLO	second mitochondria derived activator of caspases/direct IAP binding protein with low PI
STAT3	signal transducer and activator of transcription 3
STEAP	six-transmembrane epithelial antigen of prostate
STING	stimulator of interferon genes
T-ALL	T-cell acute lymphoblastic leukemia
TCA	tricarboxylic acid
TEMED	tetramethylethylenediamine
TERT	telomerase reverse transcriptase
TfR	transferrin receptor
TMT	tandem mass tag
TNF	tumor necrosis factor
TNFR1/2	tumor necrosis factor receptor 1/2
TRAIL	TNF-related apoptosis-inducing ligand
Tris	tris(hydroxymethyl)aminomethane

TS	transferrin saturation
TUNEL	terminal deoxynucleotidyltransferase-mediated dUTP-biotin nick end labeling
TWEAK	tumor necrosis factor like weak inducer of apoptosis
UTR	untranslated region
VLP	virus like particle
X-gal	5-bromo-4-chloro-3-indolyl- $\beta$ -D-galactopyranoside
$\alpha$ -TOS	$\alpha$ -tocopherol

The one-letter code for nucleotides was applied according to declarations by the International Union of Pure and Applied Chemistry (IUPAC).

## Units and prefixes

### Units

Symbol	Unit
%	percent
$^{\circ}\text{C}$	degree Celsius
d	day
Da	Dalton
<i>g</i>	gravitational acceleration
g	gram
Gy	Gray
h	hour
L	liter
M	molar
m	meter
min	minute
mol	mole
s	second
U	enzyme activity unit
V	volt

### Prefixes

Symbol	Prefix	Factor
p	pico	$10^{-12}$
n	nano	$10^{-9}$
$\mu$	micro	$10^{-6}$
m	milli	$10^{-3}$
c	centi	$10^{-2}$
k	kilo	$10^3$

**References**

1. Sung, H., et al., *Global Cancer Statistics 2020: GLOBOCAN Estimates of Incidence and Mortality Worldwide for 36 Cancers in 185 Countries*. CA Cancer J Clin, 2021. 71(3): p. 209-249.
2. Peto, J., *Cancer epidemiology in the last century and the next decade*. Nature, 2001. 411(6835): p. 390-5.
3. Schottenfeld, D., et al., *Current perspective on the global and United States cancer burden attributable to lifestyle and environmental risk factors*. Annu Rev Public Health, 2013. 34: p. 97-117.
4. de Martel, C., et al., *Global burden of cancer attributable to infections in 2018: a worldwide incidence analysis*. Lancet Glob Health, 2020. 8(2): p. e180-e190.
5. Cancer, I.A.f.R.o. *International Agency for Research on Cancer, Biological agents. Volume 100B: a review of human carcinogens*. 2012 [27.07.2021]; Available from: <https://monographs.iarc.fr/wp-content/uploads/2018/06/mono100B.pdf>.
6. Plummer, M., et al., *Global burden of cancers attributable to infections in 2012: a synthetic analysis*. Lancet Glob Health, 2016. 4(9): p. e609-16.
7. McBride, A.A., *The papillomavirus E2 proteins*. Virology, 2013. 445(1-2): p. 57-79.
8. Bergvall, M., T. Melendy, and J. Archambault, *The E1 proteins*. Virology, 2013. 445(1-2): p. 35-56.
9. Hwang, E.S., T. Nottoli, and D. Dimaio, *The HPV16 E5 protein: expression, detection, and stable complex formation with transmembrane proteins in COS cells*. Virology, 1995. 211(1): p. 227-33.
10. Schwarz, E., et al., *Structure and transcription of human papillomavirus sequences in cervical carcinoma cells*. Nature, 1985. 314(6006): p. 111-4.
11. Doorbar, J., *The E4 protein; structure, function and patterns of expression*. Virology, 2013. 445(1-2): p. 80-98.
12. Hoppe-Seyler, K., et al., *The HPV E6/E7 Oncogenes: Key Factors for Viral Carcinogenesis and Therapeutic Targets*. Trends Microbiol., 2018. 26(2): p. 158-168.
13. Van Doorslaer, K., et al., *ICTV Virus Taxonomy Profile: Papillomaviridae*. J Gen Virol, 2018. 99(8): p. 989-990.
14. Schiller, J.T., P.M. Day, and R.C. Kines, *Current understanding of the mechanism of HPV infection*. Gynecol Oncol, 2010. 118(1 Suppl): p. S12-7.
15. Aksoy, P., E.Y. Gottschalk, and P.I. Meneses, *HPV entry into cells*. Mutat Res, 2017. 772: p. 13-22.
16. Pyeon, D., et al., *Establishment of human papillomavirus infection requires cell cycle progression*. PLoS Pathog, 2009. 5(2): p. e1000318.
17. zur Hausen, H., *Papillomaviruses and cancer: from basic studies to clinical application*. Nat Rev Cancer, 2002. 2(5): p. 342-50.
18. Arbyn, M., et al., *Estimates of incidence and mortality of cervical cancer in 2018: a worldwide analysis*. Lancet Glob Health, 2020. 8(2): p. e191-e203.
19. Smith, J.S., et al., *Human papillomavirus type distribution in invasive cervical cancer and high-grade cervical lesions: a meta-analysis update*. Int J Cancer, 2007. 121(3): p. 621-32.
20. Schiffman, M., et al., *Human papillomavirus and cervical cancer*. Lancet, 2007. 370(9590): p. 890-907.
21. McBride, A.A. and A. Warburton, *The role of integration in oncogenic progression of HPV-associated cancers*. PLoS Pathog, 2017. 13(4): p. e1006211.
22. Duensing, S. and K. Munger, *Mechanisms of genomic instability in human cancer: insights from studies with human papillomavirus oncoproteins*. Int J Cancer, 2004. 109(2): p. 157-62.
23. Goodwin, E.C., et al., *Rapid induction of senescence in human cervical carcinoma cells*. Proc Natl Acad Sci U S A, 2000. 97(20): p. 10978-83.
24. Scheffner, M., et al., *The HPV-16 E6 and E6-AP complex functions as a ubiquitin-protein ligase in the ubiquitination of p53*. Cell, 1993. 75(3): p. 495-505.

25. Huibregtse, J.M., M. Scheffner, and P.M. Howley, *A cellular protein mediates association of p53 with the E6 oncoprotein of human papillomavirus types 16 or 18*. EMBO J, 1991. 10(13): p. 4129-35.
26. Ganti, K., et al., *The Human Papillomavirus E6 PDZ Binding Motif: From Life Cycle to Malignancy*. Viruses, 2015. 7(7): p. 3530-51.
27. Thomas, M. and L. Banks, *Human papillomavirus (HPV) E6 interactions with Bak are conserved amongst E6 proteins from high and low risk HPV types*. J Gen Virol, 1999. 80 ( Pt 6): p. 1513-1517.
28. Filippova, M., et al., *The human papillomavirus 16 E6 protein binds to tumor necrosis factor (TNF) R1 and protects cells from TNF-induced apoptosis*. J Biol Chem, 2002. 277(24): p. 21730-9.
29. Garnett, T.O. and P.J. Duerksen-Hughes, *Modulation of apoptosis by human papillomavirus (HPV) oncoproteins*. Arch Virol, 2006. 151(12): p. 2321-35.
30. Katzenellenbogen, R.A., et al., *NFX1-123 and poly(A) binding proteins synergistically augment activation of telomerase in human papillomavirus type 16 E6-expressing cells*. J Virol, 2007. 81(8): p. 3786-96.
31. Huh, K., et al., *Human papillomavirus type 16 E7 oncoprotein associates with the cullin 2 ubiquitin ligase complex, which contributes to degradation of the retinoblastoma tumor suppressor*. J Virol, 2007. 81(18): p. 9737-47.
32. Munger, K., et al., *Complex formation of human papillomavirus E7 proteins with the retinoblastoma tumor suppressor gene product*. EMBO J, 1989. 8(13): p. 4099-105.
33. Boyer, S.N., D.E. Wazer, and V. Band, *E7 protein of human papilloma virus-16 induces degradation of retinoblastoma protein through the ubiquitin-proteasome pathway*. Cancer Res, 1996. 56(20): p. 4620-4.
34. Rashid, N.N., H.A. Rothan, and M.S. Yusoff, *The association of mammalian DREAM complex and HPV16 E7 proteins*. Am J Cancer Res, 2015. 5(12): p. 3525-33.
35. Münger, K. and P.M. Howley, *Human papillomavirus immortalization and transformation functions*. Virus Res, 2002. 89(2): p. 213-28.
36. Seavey, S.E., et al., *The E7 oncoprotein of human papillomavirus type 16 stabilizes p53 through a mechanism independent of p19(ARF)*. J Virol, 1999. 73(9): p. 7590-8.
37. Perea, S.E., P. Massimi, and L. Banks, *Human papillomavirus type 16 E7 impairs the activation of the interferon regulatory factor-1*. Int J Mol Med, 2000. 5(6): p. 661-6.
38. Hashida, T. and S. Yasumoto, *Induction of chromosome abnormalities in mouse and human epidermal keratinocytes by the human papillomavirus type 16 E7 oncogene*. J Gen Virol, 1991. 72 ( Pt 7): p. 1569-77.
39. Steenbergen, R.D., et al., *Non-random allelic losses at 3p, 11p and 13q during HPV-mediated immortalization and concomitant loss of terminal differentiation of human keratinocytes*. Int J Cancer, 1998. 76(3): p. 412-7.
40. Duensing, S. and K. Munger, *The human papillomavirus type 16 E6 and E7 oncoproteins independently induce numerical and structural chromosome instability*. Cancer Res, 2002. 62(23): p. 7075-82.
41. Nguyen, C.L., et al., *Human papillomavirus type 16 E7 oncoprotein associates with the centrosomal component gamma-tubulin*. J Virol, 2007. 81(24): p. 13533-43.
42. Mittal, S. and L. Banks, *Molecular mechanisms underlying human papillomavirus E6 and E7 oncoprotein-induced cell transformation*. Mutat Res Rev Mutat Res, 2017. 772: p. 23-35.
43. von Knebel Doeberitz, M., et al., *Inhibition of tumorigenicity of cervical cancer cells in nude mice by HPV E6-E7 anti-sense RNA*. Int J Cancer, 1992. 51(5): p. 831-4.
44. Butz, K., et al., *Induction of apoptosis in human papillomaviruspositive cancer cells by peptide aptamers targeting the viral E6 oncoprotein*. Proc Natl Acad Sci U S A, 2000. 97(12): p. 6693-7.
45. Butz, K., et al., *siRNA targeting of the viral E6 oncogene efficiently kills human papillomavirus-positive cancer cells*. Oncogene, 2003. 22(38): p. 5938-45.
46. Tan, S., et al., *Anticancer drugs aimed at E6 and E7 activity in HPV-positive cervical cancer*. Curr Cancer Drug Targets, 2012. 12(2): p. 170-84.

47. Bosch, F.X., et al., *Comprehensive control of human papillomavirus infections and related diseases*. Vaccine, 2013. 31 Suppl 7: p. H1-31.
48. Arbyn, M. and L. Xu, *Efficacy and safety of prophylactic HPV vaccines. A Cochrane review of randomized trials*. Expert Rev Vaccines, 2018. 17(12): p. 1085-1091.
49. Lei, J., et al., *HPV Vaccination and the Risk of Invasive Cervical Cancer*. N Engl J Med, 2020. 383(14): p. 1340-1348.
50. Harper, D.M. and L.R. DeMars, *HPV vaccines - A review of the first decade*. Gynecol Oncol, 2017.
51. Yang, A., et al., *Current state in the development of candidate therapeutic HPV vaccines*. Expert Rev Vaccines, 2016. 15(8): p. 989-1007.
52. (NCCN), N.C.C.N. *Clinical Practice Guidelines in Oncology. Cervical Cancer. Version 1.2021*. 2021 18.07.2021]; Available from: <https://www.nccn.org/guidelines/guidelines-detail?category=1&id=1426>.
53. Cohen, P.A., et al., *Cervical cancer*. Lancet, 2019. 393(10167): p. 169-182.
54. Borcoman, E. and C. Le Tourneau, *Keynote-158 study, FDA granted accelerated approval of pembrolizumab for the treatment of patients with advanced PD-L1-positive cervical cancer*. Ann Transl Med, 2020. 8(23): p. 1611.
55. Sirlin, C.B. and S.B. Reeder, *Magnetic resonance imaging quantification of liver iron*. Magn Reson Imaging Clin N Am, 2010. 18(3): p. 359-81, ix.
56. MacKenzie, E.L., K. Iwasaki, and Y. Tsuji, *Intracellular iron transport and storage: from molecular mechanisms to health implications*. Antioxid Redox Signal, 2008. 10(6): p. 997-1030.
57. Puig, S., et al., *The elemental role of iron in DNA synthesis and repair*. Metallomics, 2017. 9(11): p. 1483-1500.
58. Graslund, A., M. Sahlin, and B.M. Sjoberg, *The tyrosyl free radical in ribonucleotide reductase*. Environ Health Perspect, 1985. 64: p. 139-49.
59. Fenton, M., *Oxidation of tartaric acid in presence of iron*. Journal of the Chemical Society, Transactions, 1894. 65.
60. Park, C.H., et al., *Hepcidin, a urinary antimicrobial peptide synthesized in the liver*. J Biol Chem, 2001. 276(11): p. 7806-10.
61. Ganz, T. and E. Nemeth, *Regulation of iron acquisition and iron distribution in mammals*. Biochim Biophys Acta, 2006. 1763(7): p. 690-9.
62. Rishi, G., D.F. Wallace, and V.N. Subramaniam, *Hepcidin: regulation of the master iron regulator*. Biosci Rep, 2015. 35(3).
63. Cheng, Y., et al., *Structure of the human transferrin receptor-transferrin complex*. Cell, 2004. 116(4): p. 565-76.
64. Shindo, M., et al., *Functional role of DMT1 in transferrin-independent iron uptake by human hepatocyte and hepatocellular carcinoma cell, HLF*. Hepatol Res, 2006. 35(3): p. 152-62.
65. Lill, R., *Function and biogenesis of iron-sulphur proteins*. Nature, 2009. 460(7257): p. 831-8.
66. Ajioka, R.S., J.D. Phillips, and J.P. Kushner, *Biosynthesis of heme in mammals*. Biochim Biophys Acta, 2006. 1763(7): p. 723-36.
67. Harrison, P.M., *Ferritin: an iron-storage molecule*. Semin Hematol, 1977. 14(1): p. 55-70.
68. Arosio, P. and S. Levi, *Cytosolic and mitochondrial ferritins in the regulation of cellular iron homeostasis and oxidative damage*. Biochim Biophys Acta, 2010. 1800(8): p. 783-92.
69. Donovan, A., et al., *The iron exporter ferroportin/Slc40a1 is essential for iron homeostasis*. Cell Metab, 2005. 1(3): p. 191-200.
70. Vashchenko, G. and R.T. MacGillivray, *Multi-copper oxidases and human iron metabolism*. Nutrients, 2013. 5(7): p. 2289-313.
71. Muckenthaler, M.U., B. Galy, and M.W. Hentze, *Systemic iron homeostasis and the iron-responsive element/iron-regulatory protein (IRE/IRP) regulatory network*. Annu Rev Nutr, 2008. 28: p. 197-213.
72. Walden, W.E., et al., *Structure of dual function iron regulatory protein 1 complexed with ferritin IRE-RNA*. Science, 2006. 314(5807): p. 1903-8.

73. Salahudeen, A.A., et al., *An E3 ligase possessing an iron-responsive hemerythrin domain is a regulator of iron homeostasis*. Science, 2009. 326(5953): p. 722-6.
74. Muckenthaler, M., N.K. Gray, and M.W. Hentze, *IRP-1 binding to ferritin mRNA prevents the recruitment of the small ribosomal subunit by the cap-binding complex eIF4F*. Mol Cell, 1998. 2(3): p. 383-8.
75. Hentze, M.W., et al., *Identification of the iron-responsive element for the translational regulation of human ferritin mRNA*. Science, 1987. 238(4833): p. 1570-3.
76. Binder, R., et al., *Evidence that the pathway of transferrin receptor mRNA degradation involves an endonucleolytic cleavage within the 3' UTR and does not involve poly(A) tail shortening*. EMBO J, 1994. 13(8): p. 1969-80.
77. Fonseca-Nunes, A., P. Jakszyn, and A. Agudo, *Iron and cancer risk--a systematic review and meta-analysis of the epidemiological evidence*. Cancer Epidemiol Biomarkers Prev, 2014. 23(1): p. 12-31.
78. Wu, T., et al., *Serum iron, copper and zinc concentrations and risk of cancer mortality in US adults*. Ann Epidemiol, 2004. 14(3): p. 195-201.
79. Kowdley, K.V., *Iron, hemochromatosis, and hepatocellular carcinoma*. Gastroenterology, 2004. 127(5 Suppl 1): p. S79-86.
80. Fracanzani, A.L., et al., *Increased cancer risk in a cohort of 230 patients with hereditary hemochromatosis in comparison to matched control patients with non-iron-related chronic liver disease*. Hepatology, 2001. 33(3): p. 647-51.
81. Elmberg, M., et al., *Cancer risk in patients with hereditary hemochromatosis and in their first-degree relatives*. Gastroenterology, 2003. 125(6): p. 1733-41.
82. Okada, S., *Iron-induced tissue damage and cancer: the role of reactive oxygen species-free radicals*. Pathol Int, 1996. 46(5): p. 311-32.
83. Daniels, T.R., et al., *The transferrin receptor and the targeted delivery of therapeutic agents against cancer*. Biochim Biophys Acta, 2012. 1820(3): p. 291-317.
84. Mizuuchi, H., et al., *Identification of transferrin receptor in cervical and endometrial tissues*. Gynecol Oncol, 1988. 31(2): p. 292-300.
85. Hubert, R.S., et al., *STEAP: a prostate-specific cell-surface antigen highly expressed in human prostate tumors*. Proc Natl Acad Sci U S A, 1999. 96(25): p. 14523-8.
86. Brookes, M.J., et al., *Modulation of iron transport proteins in human colorectal carcinogenesis*. Gut, 2006. 55(10): p. 1449-60.
87. Isobe, T., et al., *Human STEAP3 maintains tumor growth under hypoferric condition*. Exp Cell Res, 2011. 317(18): p. 2582-91.
88. Leung, L., et al., *Lipocalin2 promotes invasion, tumorigenicity and gemcitabine resistance in pancreatic ductal adenocarcinoma*. PLoS One, 2012. 7(10): p. e46677.
89. Kakhlon, O., Y. Gruenbaum, and Z.I. Cabantchik, *Ferritin expression modulates cell cycle dynamics and cell responsiveness to H-ras-induced growth via expansion of the labile iron pool*. Biochem J, 2002. 363(Pt 3): p. 431-6.
90. Zhang, S., et al., *Disordered hepcidin-ferroportin signaling promotes breast cancer growth*. Cell Signal, 2014. 26(11): p. 2539-50.
91. Pinnix, Z.K., et al., *Ferroportin and iron regulation in breast cancer progression and prognosis*. Sci Transl Med, 2010. 2(43): p. 43ra56.
92. Mobarra, N., et al., *A Review on Iron Chelators in Treatment of Iron Overload Syndromes*. Int J Hematol Oncol Stem Cell Res, 2016. 10(4): p. 239-247.
93. Subissi, A., et al., *Ciclopirox: recent nonclinical and clinical data relevant to its use as a topical antimycotic agent*. Drugs, 2010. 70(16): p. 2133-52.
94. Kim, Y., et al., *Targeting the Wnt/beta-catenin pathway with the antifungal agent ciclopirox olamine in a murine myeloma model*. In Vivo, 2011. 25(6): p. 887-93.
95. Eberhard, Y., et al., *Chelation of intracellular iron with the antifungal agent ciclopirox olamine induces cell death in leukemia and myeloma cells*. Blood, 2009. 114(14): p. 3064-73.
96. Zhou, H., et al., *The antitumor activity of the fungicide ciclopirox*. Int J Cancer, 2010. 127(10): p. 2467-77.

97. Lui, G.Y.L., et al., *The Iron Chelator, Deferasirox, as a Novel Strategy for Cancer Treatment: Oral Activity Against Human Lung Tumor Xenografts and Molecular Mechanism of Action*. *Molecular Pharmacology*, 2013. 83(1): p. 179-190.
98. Fukushima, T., et al., *Iron chelation therapy with deferasirox induced complete remission in a patient with chemotherapy-resistant acute monocytic leukemia*. *Anticancer Res*, 2011. 31(5): p. 1741-4.
99. Donfrancesco, A., et al., *Deferoxamine, cyclophosphamide, etoposide, carboplatin, and thiotepa (D-CECaT): a new cytoreductive chelation-chemotherapy regimen in patients with advanced neuroblastoma*. *Am J Clin Oncol*, 1992. 15(4): p. 319-22.
100. Dayani, P.N., et al., *Desferoxamine (DFO)--mediated iron chelation: rationale for a novel approach to therapy for brain cancer*. *J Neurooncol*, 2004. 67(3): p. 367-77.
101. Donfrancesco, A., et al., *Role of deferoxamine in tumor therapy*. *Acta Haematol*, 1996. 95(1): p. 66-9.
102. Yuan, J., D.B. Lovejoy, and D.R. Richardson, *Novel di-2-pyridyl-derived iron chelators with marked and selective antitumor activity: in vitro and in vivo assessment*. *Blood*, 2004. 104(5): p. 1450-8.
103. Tian, J., et al., *Anti-tumor and radiosensitization activities of the iron chelator HDp44mT are mediated by effects on intracellular redox status*. *Cancer Lett*, 2010. 298(2): p. 231-7.
104. Zeidner, J.F., et al., *A phase II trial of sequential ribonucleotide reductase inhibition in aggressive myeloproliferative neoplasms*. *Haematologica*, 2014. 99(4): p. 672-8.
105. Traynor, A.M., et al., *A phase II trial of triapine (NSC# 663249) and gemcitabine as second line treatment of advanced non-small cell lung cancer: Eastern Cooperative Oncology Group Study 1503*. *Invest New Drugs*, 2010. 28(1): p. 91-7.
106. Attia, S., et al., *A phase 2 consortium (P2C) trial of 3-aminopyridine-2-carboxaldehyde thiosemicarbazone (3-AP) for advanced adenocarcinoma of the pancreas*. *Invest New Drugs*, 2008. 26(4): p. 369-79.
107. Feun, L., et al., *Phase I and pharmacokinetic study of 3-aminopyridine-2-carboxaldehyde thiosemicarbazone (3-AP) using a single intravenous dose schedule*. *Cancer Chemother Pharmacol*, 2002. 50(3): p. 223-9.
108. Fryknas, M., et al., *Iron chelators target both proliferating and quiescent cancer cells*. *Sci Rep*, 2016. 6: p. 38343.
109. Mody, K., et al., *A phase I study of the safety and tolerability of VLX600, an Iron Chelator, in patients with refractory advanced solid tumors*. *Invest New Drugs*, 2019. 37(4): p. 684-692.
110. Becton, D.L. and P. Bryles, *Deferoxamine inhibition of human neuroblastoma viability and proliferation*. *Cancer Res*, 1988. 48(24 Pt 1): p. 7189-92.
111. Kicic, A., A.C. Chua, and E. Baker, *Desferrithiocin is a more potent antineoplastic agent than desferrioxamine*. *Br J Pharmacol*, 2002. 135(6): p. 1393-402.
112. Choi, J.H., et al., *The potential of deferasirox as a novel therapeutic modality in gastric cancer*. *World Journal of Surgical Oncology*, 2016. 14.
113. Liu, M.C., T.S. Lin, and A.C. Sartorelli, *Synthesis and antitumor activity of amino derivatives of pyridine-2-carboxaldehyde thiosemicarbazone*. *J Med Chem*, 1992. 35(20): p. 3672-7.
114. Yu, Y., Z. Kovacevic, and D.R. Richardson, *Tuning cell cycle regulation with an iron key*. *Cell Cycle*, 2007. 6(16): p. 1982-94.
115. Whitnall, M., et al., *A class of iron chelators with a wide spectrum of potent antitumor activity that overcomes resistance to chemotherapeutics*. *Proc Natl Acad Sci U S A*, 2006. 103(40): p. 14901-6.
116. Lui, G.Y., et al., *Targeting cancer by binding iron: Dissecting cellular signaling pathways*. *Oncotarget*, 2015. 6(22): p. 18748-79.
117. Linden, T., et al., *The antimycotic ciclopirox olamine induces HIF-1alpha stability, VEGF expression, and angiogenesis*. *FASEB J*, 2003. 17(6): p. 761-3.
118. Tarawneh, R.T., et al., *Physicochemical studies on Ciclopirox olamine complexes with divalent metal ions*. *Int J Pharm*, 2005. 289(1-2): p. 179-87.
119. Neubert, R.H., et al., *Different physicochemical properties of antimycotic agents are relevant for penetration into and through human nails*. *Pharmazie*, 2006. 61(7): p. 604-7.

120. Niewerth, M., et al., *Ciclopirox olamine treatment affects the expression pattern of Candida albicans genes encoding virulence factors, iron metabolism proteins, and drug resistance factors*. Antimicrob Agents Chemother, 2003. 47(6): p. 1805-17.
121. Leem, S.H., et al., *The possible mechanism of action of ciclopirox olamine in the yeast Saccharomyces cerevisiae*. Mol Cells, 2003. 15(1): p. 55-61.
122. Sigle, H.C., et al., *Oxygen accessibility and iron levels are critical factors for the antifungal action of ciclopirox against Candida albicans*. J Antimicrob Chemother, 2005. 55(5): p. 663-73.
123. Shen, T. and S. Huang, *Repositioning the Old Fungicide Ciclopirox for New Medical Uses*. Curr Pharm Des, 2016. 22(28): p. 4443-50.
124. Huang, Z. and S. Huang, *Reposition of the Fungicide Ciclopirox for Cancer Treatment*. Recent Pat Anticancer Drug Discov, 2021.
125. Braun, J.A., et al., *Effects of the antifungal agent ciclopirox in HPV-positive cancer cells: Repression of viral E6/E7 oncogene expression and induction of senescence and apoptosis*. Int J Cancer, 2020. 146(2): p. 461-474.
126. Mihailidou, C., et al., *Superior efficacy of the antifungal agent ciclopirox olamine over gemcitabine in pancreatic cancer models*. Oncotarget, 2018. 9(12): p. 10360-10374.
127. Qi, J., et al., *Ciclopirox activates PERK-dependent endoplasmic reticulum stress to drive cell death in colorectal cancer*. Cell Death Dis, 2020. 11(7): p. 582.
128. Yang, J., et al., *Targeting Histone Demethylases in MYC-Driven Neuroblastomas with Ciclopirox*. Cancer Res, 2017. 77(17): p. 4626-4638.
129. Minden, M.D., et al., *Oral ciclopirox olamine displays biological activity in a phase I study in patients with advanced hematologic malignancies*. Am J Hematol, 2014. 89(4): p. 363-8.
130. Weir, S.J., et al., *Fosciclopirox suppresses growth of high-grade urothelial cancer by targeting the gamma-secretase complex*. Cell Death Dis, 2021. 12(6): p. 562.
131. Wu, J., et al., *Antileukemia Effect of Ciclopirox Olamine Is Mediated by Downregulation of Intracellular Ferritin and Inhibition beta-Catenin-c-Myc Signaling Pathway in Glucocorticoid Resistant T-ALL Cell Lines*. PLoS One, 2016. 11(8): p. e0161509.
132. Balabanov, S., et al., *Hypusination of eukaryotic initiation factor 5A (eIF5A): a novel therapeutic target in BCR-ABL-positive leukemias identified by a proteomics approach*. Blood, 2007. 109(4): p. 1701-11.
133. Su, Z., et al., *Ciclopirox and bortezomib synergistically inhibits glioblastoma multiforme growth via simultaneously enhancing JNK/p38 MAPK and NF-kappaB signaling*. Cell Death Dis, 2021. 12(3): p. 251.
134. Zhou, H., et al., *Ciclopirox induces autophagy through reactive oxygen species-mediated activation of JNK signaling pathway*. Oncotarget, 2014. 5(20): p. 10140-50.
135. Sen, S., et al., *Novel mTOR inhibitory activity of ciclopirox enhances parthenolide antileukemia activity*. Exp Hematol, 2013. 41(9): p. 799-807 e4.
136. Fortini, M.E., *Notch signaling: the core pathway and its posttranslational regulation*. Dev Cell, 2009. 16(5): p. 633-47.
137. Hansson, E.M., U. Lendahl, and G. Chapman, *Notch signaling in development and disease*. Semin Cancer Biol, 2004. 14(5): p. 320-8.
138. Logeat, F., et al., *The Notch1 receptor is cleaved constitutively by a furin-like convertase*. Proc Natl Acad Sci U S A, 1998. 95(14): p. 8108-12.
139. Kopan, R. and M.X. Ilagan, *The canonical Notch signaling pathway: unfolding the activation mechanism*. Cell, 2009. 137(2): p. 216-33.
140. Brou, C., et al., *A novel proteolytic cleavage involved in Notch signaling: the role of the disintegrin-metalloprotease TACE*. Mol Cell, 2000. 5(2): p. 207-16.
141. Struhl, G. and I. Greenwald, *Presenilin-mediated transmembrane cleavage is required for Notch signal transduction in Drosophila*. Proc Natl Acad Sci U S A, 2001. 98(1): p. 229-34.
142. Aster, J.C., W.S. Pear, and S.C. Blacklow, *The Varied Roles of Notch in Cancer*. Annu Rev Pathol, 2017. 12: p. 245-275.
143. Agrawal, N., et al., *Exome sequencing of head and neck squamous cell carcinoma reveals inactivating mutations in NOTCH1*. Science, 2011. 333(6046): p. 1154-7.

144. Rosati, E., et al., *Constitutively activated Notch signaling is involved in survival and apoptosis resistance of B-CLL cells*. *Blood*, 2009. 113(4): p. 856-65.
145. Stoeck, A., et al., *Discovery of biomarkers predictive of GSI response in triple-negative breast cancer and adenoid cystic carcinoma*. *Cancer Discov*, 2014. 4(10): p. 1154-67.
146. Palomero, T., et al., *Mutational loss of PTEN induces resistance to NOTCH1 inhibition in T-cell leukemia*. *Nat Med*, 2007. 13(10): p. 1203-10.
147. Leong, K.G., et al., *Jagged1-mediated Notch activation induces epithelial-to-mesenchymal transition through Slug-induced repression of E-cadherin*. *J Exp Med*, 2007. 204(12): p. 2935-48.
148. Sonoshita, M., et al., *Promotion of colorectal cancer invasion and metastasis through activation of NOTCH-DAB1-ABL-RHOGEF protein TRIO*. *Cancer Discov*, 2015. 5(2): p. 198-211.
149. Wang, Z., et al., *Targeting Notch signaling pathway to overcome drug resistance for cancer therapy*. *Biochim Biophys Acta*, 2010. 1806(2): p. 258-67.
150. Nowell, C.S. and F. Radtke, *Notch as a tumour suppressor*. *Nat Rev Cancer*, 2017. 17(3): p. 145-159.
151. Hayflick, L. and P.S. Moorhead, *The serial cultivation of human diploid cell strains*. *Exp Cell Res*, 1961. 25: p. 585-621.
152. Campisi, J. and F. d'Adda di Fagagna, *Cellular senescence: when bad things happen to good cells*. *Nat Rev Mol Cell Biol*, 2007. 8(9): p. 729-40.
153. Childs, B.G., et al., *Senescence and apoptosis: dueling or complementary cell fates?* *EMBO Rep*, 2014. 15(11): p. 1139-53.
154. Campisi, J., *Aging, cellular senescence, and cancer*. *Annu Rev Physiol*, 2013. 75: p. 685-705.
155. Coppe, J.P., et al., *The senescence-associated secretory phenotype: the dark side of tumor suppression*. *Annu Rev Pathol*, 2010. 5: p. 99-118.
156. Coppe, J.P., et al., *Senescence-associated secretory phenotypes reveal cell-nonautonomous functions of oncogenic RAS and the p53 tumor suppressor*. *PLoS Biol*, 2008. 6(12): p. 2853-68.
157. Shay, J.W. and I.B. Roninson, *Hallmarks of senescence in carcinogenesis and cancer therapy*. *Oncogene*, 2004. 23(16): p. 2919-33.
158. Blackburn, E.H., *Structure and function of telomeres*. *Nature*, 1991. 350(6319): p. 569-73.
159. Harley, C.B., A.B. Futcher, and C.W. Greider, *Telomeres shorten during ageing of human fibroblasts*. *Nature*, 1990. 345(6274): p. 458-60.
160. d'Adda di Fagagna, F., et al., *A DNA damage checkpoint response in telomere-initiated senescence*. *Nature*, 2003. 426(6963): p. 194-8.
161. Roninson, I.B., *Tumor cell senescence in cancer treatment*. *Cancer Res*, 2003. 63(11): p. 2705-15.
162. te Poele, R.H., et al., *DNA damage is able to induce senescence in tumor cells in vitro and in vivo*. *Cancer Res*, 2002. 62(6): p. 1876-83.
163. Sahin, E. and R.A. Depinho, *Linking functional decline of telomeres, mitochondria and stem cells during ageing*. *Nature*, 2010. 464(7288): p. 520-8.
164. Ziegler, D.V., C.D. Wiley, and M.C. Velarde, *Mitochondrial effectors of cellular senescence: beyond the free radical theory of aging*. *Aging Cell*, 2015. 14(1): p. 1-7.
165. Ben-Porath, I. and R.A. Weinberg, *The signals and pathways activating cellular senescence*. *Int J Biochem Cell Biol*, 2005. 37(5): p. 961-76.
166. el-Deiry, W.S., et al., *WAF1, a potential mediator of p53 tumor suppression*. *Cell*, 1993. 75(4): p. 817-25.
167. Dulic, V., et al., *p53-dependent inhibition of cyclin-dependent kinase activities in human fibroblasts during radiation-induced G1 arrest*. *Cell*, 1994. 76(6): p. 1013-23.
168. Narita, M., et al., *Rb-mediated heterochromatin formation and silencing of E2F target genes during cellular senescence*. *Cell*, 2003. 113(6): p. 703-16.
169. Gil, J. and G. Peters, *Regulation of the INK4b-ARF-INK4a tumour suppressor locus: all for one or one for all*. *Nat Rev Mol Cell Biol*, 2006. 7(9): p. 667-77.

170. Olsen, C.L., et al., *Raf-1-induced growth arrest in human mammary epithelial cells is p16-independent and is overcome in immortal cells during conversion*. *Oncogene*, 2002. 21(41): p. 6328-39.
171. Michaloglou, C., et al., *BRAF<sup>V600E</sup>-associated senescence-like cell cycle arrest of human naevi*. *Nature*, 2005. 436(7051): p. 720-4.
172. Abraham, R.T., *Cell cycle checkpoint signaling through the ATM and ATR kinases*. *Genes Dev*, 2001. 15(17): p. 2177-96.
173. Kang, C., et al., *The DNA damage response induces inflammation and senescence by inhibiting autophagy of GATA4*. *Science*, 2015. 349(6255): p. aaa5612.
174. Passos, J.F., et al., *Feedback between p21 and reactive oxygen production is necessary for cell senescence*. *Mol Syst Biol*, 2010. 6: p. 347.
175. Iwasa, H., J. Han, and F. Ishikawa, *Mitogen-activated protein kinase p38 defines the common senescence-signalling pathway*. *Genes Cells*, 2003. 8(2): p. 131-44.
176. Lin, A.W., et al., *Premature senescence involving p53 and p16 is activated in response to constitutive MEK/MAPK mitogenic signaling*. *Genes Dev*, 1998. 12(19): p. 3008-19.
177. Zhu, J., et al., *Senescence of human fibroblasts induced by oncogenic Raf*. *Genes Dev*, 1998. 12(19): p. 2997-3007.
178. Tam, S.W., J.W. Shay, and M. Pagano, *Differential expression and cell cycle regulation of the cyclin-dependent kinase 4 inhibitor p16<sup>Ink4</sup>*. *Cancer Res*, 1994. 54(22): p. 5816-20.
179. Mulvany, N.J., D.G. Allen, and S.M. Wilson, *Diagnostic utility of p16<sup>INK4a</sup>: a reappraisal of its use in cervical biopsies*. *Pathology*, 2008. 40(4): p. 335-44.
180. Hengstermann, A., et al., *Complete switch from Mdm2 to human papillomavirus E6-mediated degradation of p53 in cervical cancer cells*. *Proc Natl Acad Sci U S A*, 2001. 98(3): p. 1218-23.
181. Wells, S.I., et al., *Papillomavirus E2 induces senescence in HPV-positive cells via pRB- and p21(CIP)-dependent pathways*. *EMBO J*, 2000. 19(21): p. 5762-71.
182. Hall, A.H. and K.A. Alexander, *RNA interference of human papillomavirus type 18 E6 and E7 induces senescence in HeLa cells*. *J Virol*, 2003. 77(10): p. 6066-9.
183. Honegger, A., et al., *Dependence of intracellular and exosomal microRNAs on viral E6/E7 oncogene expression in HPV-positive tumor cells*. *PLoS Pathog*, 2015. 11(3): p. e1004712.
184. Ashkenazi, A. and G. Salvesen, *Regulated cell death: signaling and mechanisms*. *Annu Rev Cell Dev Biol*, 2014. 30: p. 337-56.
185. Thornberry, N.A. and Y. Lazebnik, *Caspases: enemies within*. *Science*, 1998. 281(5381): p. 1312-6.
186. Jin, Z. and W.S. El-Deiry, *Overview of cell death signaling pathways*. *Cancer Biol Ther*, 2005. 4(2): p. 139-63.
187. Kim, H., et al., *Stepwise activation of BAX and BAK by tBID, BIM, and PUMA initiates mitochondrial apoptosis*. *Mol Cell*, 2009. 36(3): p. 487-99.
188. Green, D.R. and J.C. Reed, *Mitochondria and apoptosis*. *Science*, 1998. 281(5381): p. 1309-12.
189. Martin, S.J. and D.R. Green, *Protease activation during apoptosis: death by a thousand cuts?* *Cell*, 1995. 82(3): p. 349-52.
190. Guicciardi, M.E. and G.J. Gores, *Life and death by death receptors*. *FASEB J*, 2009. 23(6): p. 1625-37.
191. Ozoren, N. and W.S. El-Deiry, *Defining characteristics of Types I and II apoptotic cells in response to TRAIL*. *Neoplasia*, 2002. 4(6): p. 551-7.
192. Plati, J., O. Bucur, and R. Khosravi-Far, *Dysregulation of apoptotic signaling in cancer: molecular mechanisms and therapeutic opportunities*. *J Cell Biochem*, 2008. 104(4): p. 1124-49.
193. Carneiro, B.A. and W.S. El-Deiry, *Targeting apoptosis in cancer therapy*. *Nat Rev Clin Oncol*, 2020. 17(7): p. 395-417.
194. Nelson, D.L.C., M. M., *Lehninger Principles of Biochemistry*. 2008, New York: W.H. Freeman and company.

195. Pfeiffer, T., S. Schuster, and S. Bonhoeffer, *Cooperation and competition in the evolution of ATP-producing pathways*. Science, 2001. 292(5516): p. 504-7.
196. Stincone, A., et al., *The return of metabolism: biochemistry and physiology of the pentose phosphate pathway*. Biol Rev Camb Philos Soc, 2015. 90(3): p. 927-63.
197. DeBerardinis, R.J., et al., *The biology of cancer: metabolic reprogramming fuels cell growth and proliferation*. Cell Metab, 2008. 7(1): p. 11-20.
198. Warburg, O., *On the origin of cancer cells*. Science, 1956. 123(3191): p. 309-14.
199. Racker, E., *History of the Pasteur effect and its pathobiology*. Mol Cell Biochem, 1974. 5(1-2): p. 17-23.
200. Graeber, T.G., et al., *Hypoxia-mediated selection of cells with diminished apoptotic potential in solid tumours*. Nature, 1996. 379(6560): p. 88-91.
201. Kroemer, G. and J. Pouyssegur, *Tumor cell metabolism: cancer's Achilles' heel*. Cancer Cell, 2008. 13(6): p. 472-82.
202. Brand, K.A. and U. Hermfisse, *Aerobic glycolysis by proliferating cells: a protective strategy against reactive oxygen species*. FASEB J, 1997. 11(5): p. 388-95.
203. Zu, X.L. and M. Guppy, *Cancer metabolism: facts, fantasy, and fiction*. Biochem Biophys Res Commun, 2004. 313(3): p. 459-65.
204. Ashton, T.M., et al., *Oxidative Phosphorylation as an Emerging Target in Cancer Therapy*. Clin Cancer Res, 2018. 24(11): p. 2482-2490.
205. Vaupel, P. and A. Mayer, *Availability, not respiratory capacity governs oxygen consumption of solid tumors*. Int J Biochem Cell Biol, 2012. 44(9): p. 1477-81.
206. Weinberg, S.E. and N.S. Chandel, *Targeting mitochondria metabolism for cancer therapy*. Nat Chem Biol, 2015. 11(1): p. 9-15.
207. Sica, V., et al., *Oxidative phosphorylation as a potential therapeutic target for cancer therapy*. Int J Cancer, 2020. 146(1): p. 10-17.
208. Foretz, M., B. Guigas, and B. Viollet, *Understanding the glucoregulatory mechanisms of metformin in type 2 diabetes mellitus*. Nat Rev Endocrinol, 2019. 15(10): p. 569-589.
209. Wheaton, W.W., et al., *Metformin inhibits mitochondrial complex I of cancer cells to reduce tumorigenesis*. Elife, 2014. 3: p. e02242.
210. Shackelford, D.B. and R.J. Shaw, *The LKB1-AMPK pathway: metabolism and growth control in tumour suppression*. Nat Rev Cancer, 2009. 9(8): p. 563-75.
211. Xia, C., et al., *Metformin inhibits cervical cancer cell proliferation by modulating PI3K/Akt-induced major histocompatibility complex class I-related chain A gene expression*. J Exp Clin Cancer Res, 2020. 39(1): p. 127.
212. Kalender, A., et al., *Metformin, independent of AMPK, inhibits mTORC1 in a rag GTPase-dependent manner*. Cell Metab, 2010. 11(5): p. 390-401.
213. Okoshi, R., et al., *Activation of AMP-activated protein kinase induces p53-dependent apoptotic cell death in response to energetic stress*. J Biol Chem, 2008. 283(7): p. 3979-87.
214. Han, K., et al., *Association between Metformin Use and Mortality after Cervical Cancer in Older Women with Diabetes*. Cancer Epidemiol Biomarkers Prev, 2016. 25(3): p. 507-12.
215. Takiuchi, T., et al., *Association of Metformin Use and Survival Outcome in Women With Cervical Cancer*. Int J Gynecol Cancer, 2017. 27(7): p. 1455-1463.
216. Dong, L.F., et al., *Suppression of tumor growth in vivo by the mitocan alpha-tocopheryl succinate requires respiratory complex II*. Clin Cancer Res, 2009. 15(5): p. 1593-600.
217. Fiorillo, M., et al., *Repurposing atovaquone: targeting mitochondrial complex III and OXPHOS to eradicate cancer stem cells*. Oncotarget, 2016. 7(23): p. 34084-99.
218. Diepart, C., et al., *Arsenic trioxide treatment decreases the oxygen consumption rate of tumor cells and radiosensitizes solid tumors*. Cancer Res, 2012. 72(2): p. 482-90.
219. Clementi, E., et al., *On the mechanism by which vascular endothelial cells regulate their oxygen consumption*. Proc Natl Acad Sci U S A, 1999. 96(4): p. 1559-62.
220. Wick, A.N., et al., *Localization of the primary metabolic block produced by 2-deoxyglucose*. J Biol Chem, 1957. 224(2): p. 963-9.
221. Guo, L., et al., *Inhibition of Mitochondrial Complex II by the Anticancer Agent Lonidamine*. J Biol Chem, 2016. 291(1): p. 42-57.

222. Ko, Y.H., et al., *Advanced cancers: eradication in all cases using 3-bromopyruvate therapy to deplete ATP*. *Biochem Biophys Res Commun*, 2004. 324(1): p. 269-75.
223. Vander Heiden, M.G. and R.J. DeBerardinis, *Understanding the Intersections between Metabolism and Cancer Biology*. *Cell*, 2017. 168(4): p. 657-669.
224. Price, G.S., et al., *Pharmacokinetics and toxicity of oral and intravenous lonidamine in dogs*. *Cancer Chemother Pharmacol*, 1996. 38(2): p. 129-35.
225. Maschek, G., et al., *2-deoxy-D-glucose increases the efficacy of adriamycin and paclitaxel in human osteosarcoma and non-small cell lung cancers in vivo*. *Cancer Res*, 2004. 64(1): p. 31-4.
226. De Lena, M., et al., *Paclitaxel, cisplatin and lonidamine in advanced ovarian cancer. A phase II study*. *Eur J Cancer*, 2001. 37(3): p. 364-8.
227. Braun, J.A., *The Effects of Iron Chelators on the Phenotype of HPV-Positive Cervical Cancer Cells*. Doctoral Thesis, Heidelberg University, 2018.
228. Herrmann, A.L., *Cooperative Effects of Iron Chelation with Chemo- and Radiotherapy in HPV-Positive Tumour Cells*. Master thesis, Heidelberg University, 2018.
229. Huang, Y.M., et al., *Gene Expression Signature-Based Approach Identifies Antifungal Drug Ciclopirox As a Novel Inhibitor of HMGA2 in Colorectal Cancer*. *Biomolecules*, 2019. 9(11).
230. Hoppe-Seyler, K., et al., *Effects of Metformin on the virus/host cell crosstalk in human papillomavirus-positive cancer cells*. *Int J Cancer*, 2021.
231. Stiban, J., M. So, and L.S. Kaguni, *Iron-Sulfur Clusters in Mitochondrial Metabolism: Multifaceted Roles of a Simple Cofactor*. *Biochemistry (Mosc)*, 2016. 81(10): p. 1066-1080.
232. Lee, S. and C.A. Schmitt, *The dynamic nature of senescence in cancer*. *Nat Cell Biol*, 2019. 21(1): p. 94-101.
233. Slaninova, V., et al., *Notch stimulates growth by direct regulation of genes involved in the control of glycolysis and the tricarboxylic acid cycle*. *Open Biol*, 2016. 6(2): p. 150155.
234. Yang, R., et al., *Combined Transcriptome and Proteome Analysis of Immortalized Human Keratinocytes Expressing Human Papillomavirus 16 (HPV16) Oncogenes Reveals Novel Key Factors and Networks in HPV-Induced Carcinogenesis*. *mSphere*, 2019. 4(2).
235. Chou, T.C. and P. Talalay, *Quantitative analysis of dose-effect relationships: the combined effects of multiple drugs or enzyme inhibitors*. *Adv Enzyme Regul*, 1984. 22: p. 27-55.
236. Bonnet, S., et al., *A mitochondria-K<sup>+</sup> channel axis is suppressed in cancer and its normalization promotes apoptosis and inhibits cancer growth*. *Cancer Cell*, 2007. 11(1): p. 37-51.
237. Hoppe-Seyler, K., et al., *The HPV E6/E7 Oncogenes: Key Factors for Viral Carcinogenesis and Therapeutic Targets*. *Trends Microbiol*, 2018. 26(2): p. 158-168.
238. Triantafyllou, A., et al., *Cobalt induces hypoxia-inducible factor-1 alpha (HIF-1 alpha) in HeLa cells by an iron-independent, but ROS-, PI-3K- and MAPK-dependent mechanism*. *Free Radical Research*, 2006. 40(8): p. 847-856.
239. Maxwell, P.H., et al., *The tumour suppressor protein VHL targets hypoxia-inducible factors for oxygen-dependent proteolysis*. *Nature*, 1999. 399(6733): p. 271-5.
240. Yu, F., et al., *HIF-1alpha binding to VHL is regulated by stimulus-sensitive proline hydroxylation*. *Proc Natl Acad Sci U S A*, 2001. 98(17): p. 9630-5.
241. Le, N.T. and D.R. Richardson, *Iron chelators with high antiproliferative activity up-regulate the expression of a growth inhibitory and metastasis suppressor gene: a link between iron metabolism and proliferation*. *Blood*, 2004. 104(9): p. 2967-75.
242. Coombs, G.S., et al., *Modulation of Wnt/beta-catenin signaling and proliferation by a ferrous iron chelator with therapeutic efficacy in genetically engineered mouse models of cancer*. *Oncogene*, 2012. 31(2): p. 213-225.
243. Chen, Z., et al., *Iron chelator-induced up-regulation of NdrG1 inhibits proliferation and EMT process by targeting Wnt/beta-catenin pathway in colon cancer cells*. *Biochem Biophys Res Commun*, 2018.
244. Chen, Z., et al., *The iron chelators Dp44mT and DFO inhibit TGF-beta-induced epithelial-mesenchymal transition via up-regulation of N-Myc downstream-regulated gene 1 (NDRG1)*. *J Biol Chem*, 2012. 287(21): p. 17016-28.

245. Rankin, E.B. and A.J. Giaccia, *Hypoxic control of metastasis*. Science, 2016. 352(6282): p. 175-80.
246. Zhou, X., et al., *Metformin suppresses hypoxia-induced stabilization of HIF-1alpha through reprogramming of oxygen metabolism in hepatocellular carcinoma*. Oncotarget, 2016. 7(1): p. 873-84.
247. Guimaraes, T.A., et al., *Metformin increases PDH and suppresses HIF-1alpha under hypoxic conditions and induces cell death in oral squamous cell carcinoma*. Oncotarget, 2016. 7(34): p. 55057-55068.
248. Gustafsson, M.V., et al., *Hypoxia requires notch signaling to maintain the undifferentiated cell state*. Dev Cell, 2005. 9(5): p. 617-28.
249. Lee, J.H., et al., *Notch signal activates hypoxia pathway through HES1-dependent SRC/signal transducers and activators of transcription 3 pathway*. Mol Cancer Res, 2009. 7(10): p. 1663-71.
250. Strobel, T., *STAT3 Downregulation in HPV-Positive Cervical Cancer Cells*. Master Thesis, University of Applied Sciences Mannheim, 2019.
251. Sahlgren, C., et al., *Notch signaling mediates hypoxia-induced tumor cell migration and invasion*. Proc Natl Acad Sci U S A, 2008. 105(17): p. 6392-7.
252. Wang, Y., et al., *Targeting HIF1alpha eliminates cancer stem cells in hematological malignancies*. Cell Stem Cell, 2011. 8(4): p. 399-411.
253. Franko-Tobin, L.G., et al., *Notch1-mediated tumor suppression in cervical cancer with the involvement of SST signaling and its application in enhanced SSTR-targeted therapeutics*. Oncologist, 2012. 17(2): p. 220-32.
254. Yao, J., et al., *Notch1 induces cell cycle arrest and apoptosis in human cervical cancer cells: involvement of nuclear factor kappa B inhibition*. Int J Gynecol Cancer, 2007. 17(2): p. 502-10.
255. Wang, L., et al., *Overexpressed active Notch1 induces cell growth arrest of HeLa cervical carcinoma cells*. Int J Gynecol Cancer, 2007. 17(6): p. 1283-92.
256. Yu, H., et al., *Blocking Notch1 signaling by RNA interference can induce growth inhibition in HeLa cells*. Int J Gynecol Cancer, 2007. 17(2): p. 511-6.
257. Weijzen, S., et al., *HPV16 E6 and E7 oncoproteins regulate Notch-1 expression and cooperate to induce transformation*. J Cell Physiol, 2003. 194(3): p. 356-62.
258. Talora, C., et al., *Specific down-modulation of Notch1 signaling in cervical cancer cells is required for sustained HPV-E6/E7 expression and late steps of malignant transformation*. Genes Dev, 2002. 16(17): p. 2252-63.
259. Yugawa, T., et al., *Regulation of Notch1 gene expression by p53 in epithelial cells*. Mol Cell Biol, 2007. 27(10): p. 3732-42.
260. Tan, M.J., et al., *Cutaneous beta-human papillomavirus E6 proteins bind Mastermind-like coactivators and repress Notch signaling*. Proc Natl Acad Sci U S A, 2012. 109(23): p. E1473-80.
261. Zagouras, P., et al., *Alterations in Notch signaling in neoplastic lesions of the human cervix*. Proc Natl Acad Sci U S A, 1995. 92(14): p. 6414-8.
262. Xia, Y., H.K. Choi, and K. Lee, *Recent advances in hypoxia-inducible factor (HIF)-1 inhibitors*. Eur J Med Chem, 2012. 49: p. 24-40.
263. Pavlova, N.N. and C.B. Thompson, *The Emerging Hallmarks of Cancer Metabolism*. Cell Metab, 2016. 23(1): p. 27-47.
264. Zeng, Q., et al., *LKB1 inhibits HPV-associated cancer progression by targeting cellular metabolism*. Oncogene, 2017. 36(9): p. 1245-1255.
265. Zwerschke, W., et al., *Modulation of type M2 pyruvate kinase activity by the human papillomavirus type 16 E7 oncoprotein*. Proc Natl Acad Sci U S A, 1999. 96(4): p. 1291-6.
266. Reitzer, L.J., B.M. Wice, and D. Kennell, *Evidence that glutamine, not sugar, is the major energy source for cultured HeLa cells*. J Biol Chem, 1979. 254(8): p. 2669-76.
267. Sonveaux, P., et al., *Targeting lactate-fueled respiration selectively kills hypoxic tumor cells in mice*. J Clin Invest, 2008. 118(12): p. 3930-42.

268. Perez-Escuredo, J., et al., *Lactate promotes glutamine uptake and metabolism in oxidative cancer cells*. Cell Cycle, 2016. 15(1): p. 72-83.
269. Yu, L., et al., *Modeling the Genetic Regulation of Cancer Metabolism: Interplay between Glycolysis and Oxidative Phosphorylation*. Cancer Res, 2017. 77(7): p. 1564-1574.
270. Rensvold, J.W., et al., *Complementary RNA and protein profiling identifies iron as a key regulator of mitochondrial biogenesis*. Cell Rep, 2013. 3(1): p. 237-45.
271. Rensvold, J.W., et al., *Iron Deprivation Induces Transcriptional Regulation of Mitochondrial Biogenesis*. J Biol Chem, 2016. 291(40): p. 20827-20837.
272. Oexle, H., E. Gnaiger, and G. Weiss, *Iron-dependent changes in cellular energy metabolism: influence on citric acid cycle and oxidative phosphorylation*. Biochim Biophys Acta, 1999. 1413(3): p. 99-107.
273. Yoon, Y.S., et al., *Mitochondrial dysfunction via disruption of complex II activity during iron chelation-induced senescence-like growth arrest of Chang cells*. Ann N Y Acad Sci, 2004. 1011: p. 123-32.
274. Berridge, M.V., P.M. Herst, and A.S. Tan, *Metabolic flexibility and cell hierarchy in metastatic cancer*. Mitochondrion, 2010. 10(6): p. 584-8.
275. Semenza, G.L., *Hypoxia-inducible factors in physiology and medicine*. Cell, 2012. 148(3): p. 399-408.
276. Riganti, C., et al., *The pentose phosphate pathway: an antioxidant defense and a crossroad in tumor cell fate*. Free Radic Biol Med, 2012. 53(3): p. 421-36.
277. Roberts, D.J. and S. Miyamoto, *Hexokinase II integrates energy metabolism and cellular protection: Aktting on mitochondria and TORCing to autophagy*. Cell Death Differ, 2015. 22(2): p. 248-57.
278. Wiley, C.D. and J. Campisi, *From Ancient Pathways to Aging Cells-Connecting Metabolism and Cellular Senescence*. Cell Metab, 2016. 23(6): p. 1013-1021.
279. Dorr, J.R., et al., *Synthetic lethal metabolic targeting of cellular senescence in cancer therapy*. Nature, 2013. 501(7467): p. 421-5.
280. Jackson, J.G., et al., *p53-mediated senescence impairs the apoptotic response to chemotherapy and clinical outcome in breast cancer*. Cancer Cell, 2012. 21(6): p. 793-806.
281. Tonnessen-Murray, C.A., G. Lozano, and J.G. Jackson, *The Regulation of Cellular Functions by the p53 Protein: Cellular Senescence*. Cold Spring Harb Perspect Med, 2017. 7(2).
282. Yao, G.D., et al., *Blocking the utilization of glucose induces the switch from senescence to apoptosis in pseudolaric acid B-treated human lung cancer cells in vitro*. Acta Pharmacol Sin, 2017. 38(10): p. 1401-1411.
283. Hayward, R.L., et al., *Antisense Bcl-xl down-regulation switches the response to topoisomerase I inhibition from senescence to apoptosis in colorectal cancer cells, enhancing global cytotoxicity*. Clin Cancer Res, 2003. 9(7): p. 2856-65.
284. Stevens, C. and N.B. La Thangue, *The emerging role of E2F-1 in the DNA damage response and checkpoint control*. DNA Repair (Amst), 2004. 3(8-9): p. 1071-9.
285. Dimri, G.P., et al., *Regulation of a senescence checkpoint response by the E2F1 transcription factor and p14(ARF) tumor suppressor*. Mol Cell Biol, 2000. 20(1): p. 273-85.
286. Xie, Q., et al., *E2F transcription factor 1 regulates cellular and organismal senescence by inhibiting Forkhead box O transcription factors*. J Biol Chem, 2014. 289(49): p. 34205-13.
287. DeGregori, J., et al., *Distinct roles for E2F proteins in cell growth control and apoptosis*. Proc Natl Acad Sci U S A, 1997. 94(14): p. 7245-50.
288. Ginsberg, D., *E2F1 pathways to apoptosis*. FEBS Lett, 2002. 529(1): p. 122-5.
289. Denechaud, P.D., L. Fajas, and A. Giralt, *E2F1, a Novel Regulator of Metabolism*. Front Endocrinol (Lausanne), 2017. 8: p. 311.
290. Jia, D., et al., *Elucidating cancer metabolic plasticity by coupling gene regulation with metabolic pathways*. Proc Natl Acad Sci U S A, 2019. 116(9): p. 3909-3918.
291. Welford, S.M. and A.J. Giaccia, *Hypoxia and senescence: the impact of oxygenation on tumor suppression*. Mol Cancer Res, 2011. 9(5): p. 538-44.
292. Welford, S.M., et al., *HIF1alpha delays premature senescence through the activation of MIF*. Genes Dev, 2006. 20(24): p. 3366-71.

293. Yoon, K.J., et al., *Exercise-induced AMPK activation is involved in delay of skeletal muscle senescence*. *Biochem Biophys Res Commun*, 2019. 512(3): p. 604-610.
294. Ido, Y., et al., *Acute activation of AMP-activated protein kinase prevents H2O2-induced premature senescence in primary human keratinocytes*. *PLoS One*, 2012. 7(4): p. e35092.
295. Xia, W., et al., *Macrophage migration inhibitory factor confers resistance to senescence through CD74-dependent AMPK-FOXO3a signaling in mesenchymal stem cells*. *Stem Cell Res Ther*, 2015. 6: p. 82.
296. Moiseeva, O., et al., *Mitochondrial dysfunction contributes to oncogene-induced senescence*. *Mol Cell Biol*, 2009. 29(16): p. 4495-507.
297. Wang, W., et al., *Increased AMP:ATP ratio and AMP-activated protein kinase activity during cellular senescence linked to reduced HuR function*. *J Biol Chem*, 2003. 278(29): p. 27016-23.
298. Wiley, C.D., et al., *Mitochondrial Dysfunction Induces Senescence with a Distinct Secretory Phenotype*. *Cell Metab*, 2016. 23(2): p. 303-14.
299. Saleh, T., L. Tyutyunyk-Massey, and D.A. Gewirtz, *Tumor Cell Escape from Therapy-Induced Senescence as a Model of Disease Recurrence after Dormancy*. *Cancer Res*, 2019. 79(6): p. 1044-1046.
300. Sun, X., et al., *Senescence-associated secretory factors induced by cisplatin in melanoma cells promote non-senescent melanoma cell growth through activation of the ERK1/2-RSK1 pathway*. *Cell Death Dis*, 2018. 9(3): p. 260.
301. Krtolica, A., et al., *Senescent fibroblasts promote epithelial cell growth and tumorigenesis: a link between cancer and aging*. *Proc Natl Acad Sci U S A*, 2001. 98(21): p. 12072-7.
302. Kim, Y.H., et al., *Senescent tumor cells lead the collective invasion in thyroid cancer*. *Nat Commun*, 2017. 8: p. 15208.
303. Angelini, P.D., et al., *Constitutive HER2 signaling promotes breast cancer metastasis through cellular senescence*. *Cancer Res*, 2013. 73(1): p. 450-8.
304. Soto-Gamez, A., W.J. Quax, and M. Demaria, *Regulation of Survival Networks in Senescent Cells: From Mechanisms to Interventions*. *J Mol Biol*, 2019. 431(15): p. 2629-2643.
305. Canino, C., et al., *SASP mediates chemoresistance and tumor-initiating-activity of mesothelioma cells*. *Oncogene*, 2012. 31(26): p. 3148-63.
306. Laberge, R.M., et al., *MTOR regulates the pro-tumorigenic senescence-associated secretory phenotype by promoting IL1A translation*. *Nat Cell Biol*, 2015. 17(8): p. 1049-61.
307. Hoppe-Seyler, K., et al., *Induction of dormancy in hypoxic human papillomavirus-positive cancer cells*. *Proc Natl Acad Sci U S A*, 2017. 114(6): p. E990-E998.
308. Sagiv, A. and V. Krizhanovsky, *Immunosurveillance of senescent cells: the bright side of the senescence program*. *Biogerontology*, 2013. 14(6): p. 617-28.
309. Acosta, J.C., et al., *Chemokine signaling via the CXCR2 receptor reinforces senescence*. *Cell*, 2008. 133(6): p. 1006-18.
310. Williams, G.C., *Pleiotropy, Natural Selection, and the Evolution of Senescence*. *Evolution*, 1957. 11(4): p. 398-411.
311. Campisi, J., *Cancer and ageing: rival demons?* *Nat Rev Cancer*, 2003. 3(5): p. 339-49.
312. Kirkland, J.L. and T. Tchkonja, *Clinical strategies and animal models for developing senolytic agents*. *Exp Gerontol*, 2015. 68: p. 19-25.
313. Demaria, M., et al., *Cellular Senescence Promotes Adverse Effects of Chemotherapy and Cancer Relapse*. *Cancer Discov*, 2017. 7(2): p. 165-176.
314. Vasileiou, P.V.S., et al., *Mitochondrial Homeostasis and Cellular Senescence*. *Cells*, 2019. 8(7).
315. Shen, T., et al., *Ciclopirox activates ATR-Chk1 signaling pathway leading to Cdc25A protein degradation*. *Genes Cancer*, 2018. 9(1-2): p. 39-52.
316. Aird, K.M., et al., *Identification of ribonucleotide reductase M2 as a potential target for pro-senescence therapy in epithelial ovarian cancer*. *Cell Cycle*, 2014. 13(2): p. 199-207.
317. Moiseeva, O., et al., *Metformin inhibits the senescence-associated secretory phenotype by interfering with IKK/NF-kappaB activation*. *Aging Cell*, 2013. 12(3): p. 489-98.

318. Maehama, T., et al., *Selective down-regulation of human papillomavirus transcription by 2-deoxyglucose*. Int J Cancer, 1998. 76(5): p. 639-46.
319. Bossler, F., et al., *Repression of Human Papillomavirus Oncogene Expression under Hypoxia Is Mediated by PI3K/mTORC2/AKT Signaling*. mBio, 2019. 10(1).
320. Hoppe-Seyler, F. and K. Butz, *Cellular control of human papillomavirus oncogene transcription*. Mol Carcinog, 1994. 10(3): p. 134-41.
321. Torti, S.V. and F.M. Torti, *Iron and cancer: more ore to be mined*. Nat Rev Cancer, 2013. 13(5): p. 342-55.
322. Dancey, J.E. and H.X. Chen, *Strategies for optimizing combinations of molecularly targeted anticancer agents*. Nat Rev Drug Discov, 2006. 5(8): p. 649-59.
323. Harrison, L.B., et al., *Impact of tumor hypoxia and anemia on radiation therapy outcomes*. Oncologist, 2002. 7(6): p. 492-508.
324. Kuo, M.L. and T.J. Kinsella, *Expression of ribonucleotide reductase after ionizing radiation in human cervical carcinoma cells*. Cancer Res, 1998. 58(10): p. 2245-52.
325. Kunos, C.A., et al., *Ribonucleotide reductase inhibition enhances chemoradiosensitivity of human cervical cancers*. Radiat Res, 2010. 174(5): p. 574-81.
326. Hreshchyshyn, M.M., et al., *Hydroxyurea or placebo combined with radiation to treat stages IIIB and IV cervical cancer confined to the pelvis*. Int J Radiat Oncol Biol Phys, 1979. 5(3): p. 317-22.
327. Chevalier, B., et al., *Metformin: (future) best friend of the radiation oncologist?* Radiother Oncol, 2020. 151: p. 95-105.
328. Gong, Y., et al., *Rapamycin-induced autophagy plays a pro-survival role by enhancing up-regulation of intracellular ferritin expression in acute lymphoblastic leukemia*. Exp Oncol, 2020. 42(1): p. 11-15.
329. Martinez-Outschoorn, U.E., et al., *Cancer metabolism: a therapeutic perspective*. Nat Rev Clin Oncol, 2017. 14(1): p. 11-31.
330. Zecchini, V. and C. Frezza, *Metabolic synthetic lethality in cancer therapy*. Biochim Biophys Acta Bioenerg, 2017. 1858(8): p. 723-731.
331. Pelicano, H., et al., *Glycolysis inhibition for anticancer treatment*. Oncogene, 2006. 25(34): p. 4633-46.
332. Palorini, R., et al., *Mitochondrial Complex I Inhibitors and Forced Oxidative Phosphorylation Synergize in Inducing Cancer Cell Death*. International Journal of Cell Biology, 2013. 2013: p. 243876.
333. Liu, H., et al., *Hypersensitization of tumor cells to glycolytic inhibitors*. Biochemistry, 2001. 40(18): p. 5542-7.
334. Fath, M.A., et al., *Mitochondrial electron transport chain blockers enhance 2-deoxy-D-glucose induced oxidative stress and cell killing in human colon carcinoma cells*. Cancer Biol Ther, 2009. 8(13): p. 1228-36.
335. Ben Sahra, I., et al., *Targeting cancer cell metabolism: the combination of metformin and 2-deoxyglucose induces p53-dependent apoptosis in prostate cancer cells*. Cancer Res, 2010. 70(6): p. 2465-75.
336. Sun, R.C., P.G. Board, and A.C. Blackburn, *Targeting metabolism with arsenic trioxide and dichloroacetate in breast cancer cells*. Mol Cancer, 2011. 10: p. 142.
337. Stacpoole, P.W., et al., *Controlled clinical trial of dichloroacetate for treatment of congenital lactic acidosis in children*. Pediatrics, 2006. 117(5): p. 1519-31.
338. Stacpoole, P.W., et al., *Dichloroacetate in the treatment of lactic acidosis*. Ann Intern Med, 1988. 108(1): p. 58-63.
339. Sun, R.C., et al., *Reversal of the glycolytic phenotype by dichloroacetate inhibits metastatic breast cancer cell growth in vitro and in vivo*. Breast Cancer Res Treat, 2010. 120(1): p. 253-60.
340. Tataranni, T. and C. Piccoli, *Dichloroacetate (DCA) and Cancer: An Overview towards Clinical Applications*. Oxid Med Cell Longev, 2019. 2019: p. 8201079.
341. Wong, J.Y., et al., *Dichloroacetate induces apoptosis in endometrial cancer cells*. Gynecol Oncol, 2008. 109(3): p. 394-402.

342. Zhou, L., et al., *Dichloroacetic acid upregulates apoptosis of ovarian cancer cells by regulating mitochondrial function*. *Onco Targets Ther*, 2019. 12: p. 1729-1739.
343. Hirayama, A., et al., *Quantitative metabolome profiling of colon and stomach cancer microenvironment by capillary electrophoresis time-of-flight mass spectrometry*. *Cancer Res*, 2009. 69(11): p. 4918-25.
344. Cignarelli, A., et al., *Diabetes and cancer: Pathophysiological fundamentals of a 'dangerous affair'*. *Diabetes Res Clin Pract*, 2018. 143: p. 378-388.
345. Reinfeld, B.I., et al., *Cell-programmed nutrient partitioning in the tumour microenvironment*. *Nature*, 2021. 593(7858): p. 282-288.
346. Varghese, E., et al., *Targeting Glucose Metabolism to Overcome Resistance to Anticancer Chemotherapy in Breast Cancer*. *Cancers (Basel)*, 2020. 12(8).
347. Varghese, S., et al., *High Glucose Represses the Anti-Proliferative and Pro-Apoptotic Effect of Metformin in Triple Negative Breast Cancer Cells*. *Biomolecules*, 2019. 9(1).
348. Huang, C.Y., et al., *Glucose Metabolites Exert Opposing Roles in Tumor Chemoresistance*. *Front Oncol*, 2019. 9: p. 1282.
349. Zhao, W., et al., *High glucose promotes gastric cancer chemoresistance in vivo and in vitro*. *Mol Med Rep*, 2015. 12(1): p. 843-50.
350. Bergandi, L., et al., *Hyperglycemia Promotes Chemoresistance Through the Reduction of the Mitochondrial DNA Damage, the Bax/Bcl-2 and Bax/Bcl-XL Ratio, and the Cells in Sub-G1 Phase Due to Antitumoral Drugs Induced-Cytotoxicity in Human Colon Adenocarcinoma Cells*. *Front Pharmacol*, 2018. 9: p. 866.
351. Clement, P.M., et al., *The antifungal drug ciclopirox inhibits deoxyhypusine and proline hydroxylation, endothelial cell growth and angiogenesis in vitro*. *Int J Cancer*, 2002. 100(4): p. 491-8.
352. Kellner, H.M., et al., *[Pharmacokinetics and biotransformation of the antimycotic drug ciclopiroxolamine in animals and man after topical and systemic administration]*. *Arzneimittelforschung*, 1981. 31(8A): p. 1337-53.
353. Ceschin-Roques, C.G., et al., *Ciclopiroxolamine cream 1%: in vitro and in vivo penetration into the stratum corneum*. *Skin Pharmacol*, 1991. 4(2): p. 95-9.
354. Engelmann, L., et al., *Organotypic Co-Cultures as a Novel 3D Model for Head and Neck Squamous Cell Carcinoma*. *Cancers (Basel)*, 2020. 12(8).
355. O'Neill, H.S., et al., *A stimuli responsive liposome loaded hydrogel provides flexible on-demand release of therapeutic agents*. *Acta Biomater*, 2017. 48: p. 110-119.
356. Weir, S.J., et al., *Preclinical Pharmacokinetics of Fosciclopirox, a Novel Treatment for Urothelial Cancers in Rats and Dogs*. *J Pharmacol Exp Ther*, 2019.
357. Dimri, G.P., et al., *A biomarker that identifies senescent human cells in culture and in aging skin in vivo*. *Proc Natl Acad Sci U S A*, 1995. 92(20): p. 9363-7.
358. Lee, B.Y., et al., *Senescence-associated beta-galactosidase is lysosomal beta-galactosidase*. *Aging Cell*, 2006. 5(2): p. 187-95.
359. Perez-Riverol, Y., et al., *The PRIDE database and related tools and resources in 2019: improving support for quantification data*. *Nucleic Acids Res*, 2019. 47(D1): p. D442-D450.
360. Livak, K.J. and T.D. Schmittgen, *Analysis of relative gene expression data using real-time quantitative PCR and the 2(-Delta Delta C(T)) Method*. *Methods*, 2001. 25(4): p. 402-8.